Stony Brook University

Plasmin-Mediated Cleavage of Monocyte Chemoattractant Protein-1 (MCP1) Affects Its Biological Activities

A Dissertation Presented

By

Yao Yao

to

The Graduate School

in Partial Fulfillment of the Requirements

for the Degree of

DOCTOR OF PHILOSOPHY

in

Molecular and Cellular Pharmacology

Stony Brook University

May 2011

Stony Brook University
The Graduate School

Yao Yao

We, the dissertation committee for the above candidate for the degree of Doctor of Philosophy, hereby recommend acceptance of this dissertation.

Styliani-Anna E. Tsirka, Ph.D.
Dissertation Advisor
Professor
Department of Pharmacological Sciences

William E. Van Nostrand, Ph.D.
Chairperson of Defense
Professor
Department of Medicine

Joav Prives, Ph.D.
Professor
Department of Pharmacological Sciences

Sanford R. Simon, Ph.D.
Professor
Department of Biochemistry

This dissertation is accepted by the Graduate School

Lawrence Martin
Dean of the Graduate School

Abstract of the Dissertation

Plasmin-Mediated Cleavage of Monocyte Chemoattractant Protein-1 (MCP1) Affects Its Biological Activities

by

Yao Yao

Doctor of Philosophy

in

Molecular and Cellular Pharmacology

Stony Brook University

2011

Monocyte chemoattractant protein-1 (MCP1) is a potent chemokine for monocytes and microglia. Previous studies in our lab showed that plasmin cleaved mouse MCP1 at lysine (K) 104 and the truncated MCP1 (N terminal fragment 1-104) had a higher chemotactic potency. Here we reported the mechanisms underlying the enhanced activity. Plasmin-mediated truncation of mouse MCP1 increased MCP1-CCR2 interaction, promoted Rac1 activation and lamellipodia formation on microglia.

Besides chemotactic activity, MCP1 also functions to disrupt the integrity of the Blood-Brain Barrier (BBB). We also showed here that plasmin-mediated truncation of MCP1 is indispensable for its BBB-compromising activity. Binding of MCP1 to CCR2 leads to activation of Ezrin-Radixin-Moesin (ERM) proteins, which link ZO-1 to actin cytoskeleton. MCP1 also induces phosphorylation of myosin light chain, resulting in

reorganization of actin cytoskeleton. The acto-myosin machinery then generates the force to pull ZO-1 away from tight junctions, disrupting the integrity of BBB.

Furthermore, we found the mouse MCP1 C-terminal fragment (105-148) is inhibitory to human MCP1, which lacks the C-terminal tail. Fusion of the C-terminal tail to human MCP1 decreased its chemotactic potency and abrogated its BBB-compromising activity.

Because MCP1-CCR2 axis is the major signaling system to recruit monocyte and microglia, and microglia are one of the key players during central nervous system (CNS) injury, we investigated the role of MCP1-CCR2 system in vivo using the collagenase-induced intracerebral hemorrhage (ICH) model. We found that $MCP1^{-/-}$ or $CCR2^{-/-}$ mice have smaller hematoma early after injury but the recovery is delayed. The hematoma size is paralleled by the water content in the ipsilateral hemisphere, neuronal death at peri-hematoma region, and neurobehavioral deficit. It should be noted that we found accumulation of activated microglia in mice deficient for MCP1 or CCR2 at later time points, probably because of the activation of other chemokines. Thus, it is still unclear whether microglia activation at later time is neuroprotective or neurotoxic, although early inhibition seems beneficial. Therefore, we propose that early inhibition of microglia activation/accumulation (through antagonists of MCP1-CCR2 axis or plasmin) might be of clinical utility in treating diseases with inflammation in the CNS.

Table of Contents

List of Abbreviations

Ab	Antibody
AJ	Adherens Junctions
BBB	Blood-Brain Barrier
BMEC	Brain Microvascular Endothelial Cells
CCL2	CC-Chemokine Ligand-2
CCR2	CC-Chemokine Receptor-2
cDNA	Complementary Deoxyribonucleic Acid
CNS	Central Nervous System
DAB	Diaminobenzidine
DMEM	Dulbecco's Modified Eagle's Medium
DNA	Deoxyribonucleic Acid
ECL	Enhanced Chemiluminescence
EDTA	Ethylene Diamine Tetraacetic Acid
FBS	Fetal Bovine Serum
FITC	Fluorescein Isothiocyanate
GAG	Glycosaminoglycans
HBMEC	Human Brain Microvascular Endothelial Cells
HBSS	Hank's Buffered Salt Solution
ICH	Intracerebral Hemorrhage
IP	Immunoprecipitation
IPTG	Isopropyl-β-D-Thiogalactopyranoside

kDa	Kilodaltons
LB	Lysogeny Broth
LDH	Lactose Dehydrogenase
MCP1	Monocyte Chemoattractant Protein-1
mRNA	Messenger Ribonucleic Acid
PBMC	Peripheral Blood Mononuclear Cells
PBS	Phosphate Buffered Saline
plg	Plasminogen
pln	Plasmin
RIPA	Radioimmunoprecipitation Assay
RT-PCR	Reverse Transcription Polymerase Chain Reaction
SDS-PAGE	Sodium Dodecyl Sulfate-Polyacrylamide Gel Electrophoresis
TEER	Transendothelial Electrical Resistance
TJ	Tight Junction
TJP	Tight Junction Proteins
TNFα	Tumor Necrosis Factor-Alpha
tPA	Tissue-Type Plasminogen Activator
uPA	Urokinase-Type Plasminogen Activator

List of Figures

Acknowledgments

First and foremost, I would like to thank my advisor, Dr. Stella Tsirka. She is the best advisor I have ever known in the world. She is very patient to her students and would like to do anything she could to help them. She is knowledgeable and smart. Under her guidance, I have learnt to read (check all the controls and inconsistency within the papers) and think (with a bigger picture in mind) critically. Additionally, she also taught me how to write a good paper and grant. You can always learn “new” techniques from her. I still remember how exciting I was when she told me to make a brain powder to clear the dirty antibody. Of course, she is humorous, because she told me not to put the brain powder into the (my or her?) tea cup.

Next, I want to thank my committee members, Dr. William van Nostrand, Dr. Joav Prives, Dr. Sanford Simon for their stimulating discussions on the blood-brain barrier and nice comments and suggestions.

I would also like to thank Dr. Michael Frohman, Dr. Holly Colognato, Dr. Howard Crawford, Dr. Joav Prives, Dr. Miguel Garcia-Diaz and their lab members. I always went to their labs to borrow reagents, use their equipment, and ask for instruction.

In addition, I also want to thank the Tsirka Lab members for their support and ideas, especially when my experiments did not work out. They made the lab a nice place to be. Special thanks to Dr. Noreen Bukhari, who accompanied me when I came to the lab at 2AM and Dr. Jaime Emmetsberger, who taught me those curse words when I first came here.

Last but not least, I would like to thank my family, especially my parents. They did everything you could to support me. When grandpa passed away, my parents and grandma did not tell me because I was taking the qualifying exam. When they were lying in the hospital (no matter it was car accident or by the robber), they told me they were fine and asked me not to worry. As the only child, I know how hard it was. Thank you very much for your love and support, I really appreciate it.

Chapter 1

Introduction

1. Blood-Brain Barrier (BBB)

The BBB is a specific structure that prevents the infiltration of components in the systemic circulation into the central nervous system (CNS). The BBB was first described by Paul Ehrlich in 1885. He found that the brain and spinal cord failed to be stained by dyes injected into the systematic circulation (Ehrlich, 1885). These organs, however, were stained by trypan blue injected into the cerebrospinal fluid (Goldmann, 1913), suggesting there was a barrier between the CNS and the systematic circulation. The term 'blood-brain barrier' was first used by Lewandowsky in 1900 (Lewandowsky, 1900). Anatomically, BBB is comprised of brain microvascular endothelial cells (BMEC), astrocytes, pericytes, neurons, and microglia (Guillemin and Brew, 2004), as shown in Figure 1-1.

1.1 Brain Microvascular Endothelial Cells (BMEC)

BMEC are characterized by the presence of many mitochondria, lack of fenestrations, low pinocytotic activity, and the presence of tight junctions (TJ) (Oldendorf et al., 1977, Fenstermacher et al., 1988, Sedlakova et al., 1999, Kniesel and Wolburg, 2000). BMEC connect to each other forming an impermeable monolayer. In the interendothelial space specific structures, including adherens junctions (AJ) and TJ, are

present (Schulze and Firth, 1993, Kniesel and Wolburg, 2000, Wolburg and Lippoldt, 2002, Vorbrodt and Dobrogowska, 2003). Both AJ and TJ act to limit the transendothelial permeability (Bazzoni and Dejana, 2004).

Although disruption of AJ results in enhanced BBB permeability, TJ form the primary structure that maintains the impermeability of BBB (Romero et al., 2003). In the TJ, many tight junction proteins (TJP) are expressed. There are two types of TJP: transmembrane proteins, such as occludin and claudin-1, 5, 11, and cytoplasmic accessory proteins, such as zonula occludens-1, 2, 3 (ZO-1, 2, 3) and cingulin (Citi and Cordenonsi, 1998, Huber et al., 2001). The transmembrane proteins, especially occludin, function to seal gaps between adjacent cells (Mitic and Anderson, 1998, Michel and Curry, 1999, Ogunrinade et al., 2002, Forster, 2008). Accumulating evidence suggests that occludin contributes to the integrity of BBB (McCarthy et al., 1996, Bolton et al., 1998, Huber et al., 2002, Brown and Davis, 2005). Occludin, a 60-65kD transmembrane protein with its amino- and carboxyl-terminus in the cytoplasm, has several serine and threonine residues that can be phosphorylated. It has been shown that the phosphorylation state of occludin plays a role in its membrane association (Sakakibara et al., 1997, Wachtel et al., 1999, Clarke et al., 2000b, Andreeva et al., 2001, Hirase et al., 2001, Rao et al., 2002, Kale et al., 2003). The molecular mechanisms, however, are not yet known. Cytoplasmic accessory proteins, on the other hand, link transmembrane proteins to cortical actin-based cytoskeleton (Mitic and Anderson, 1998, Michel and Curry, 1999, Ogunrinade et al., 2002, Forster, 2008). ZO-1, the first identified accessory protein that associates with occludin, is a 220kD phosphoprotein (Stevenson et al., 1986). By linking occludin to the actin

cytoskeleton (Fanning et al., 1998), ZO-1 plays a critical role in regulating the permeability of BBB. Dissociation of ZO-1 from the TJ has been shown to accompany the disruption of BBB (Abbruscato et al., 2002, Fischer et al., 2002, Mark and Davis, 2002). In addition, ZO-1 is found to be in the nucleus and co-localized with transcription factors in some conditions (Gottardi et al., 1996, Balda and Matter, 2000, Riesen et al., 2002, Hawkins et al., 2004), suggesting its potential role as a signaling molecule.

Unlike BMEC, peripheral endothelial cells have few mitochondria, many pinocytic vesicles and absence of TJ (Oldendorf et al., 1977, Fenstermacher et al., 1988, Sedlakova et al., 1999, Kniesel and Wolburg, 2000), suggesting that these properties are unique to BMEC. Are the differences due to intrinsic characteristics of BMEC or the microenvironment in the brain? Stewart and Wiley elegantly demonstrated that non-vascularized brain tissue grafted into coelomic cavity developed capillaries with BMEC properties (Stewart and Wiley, 1981). Somite tissue grafted into cerebral ventricles, on the contrary, showed the opposite: low mitochondria density, many pinocytic vesicles and less TJ (Stewart and Wiley, 1981). This study strongly suggests that interaction between vascular tissue and CNS tissue contributes to the properties of BMEC.

1.2 Astrocytes

Astrocytes are star-shaped glial cells in the brain. They play many roles in the brain, such as supporting neurons, providing nutrients to nervous tissue, maintaining ion homeostasis, repairing damaged tissues, and modulate BBB integrity. In the brain, astrocytic endfeet cover more than 99% of the vascular surface facing BMEC or pericytes (Kacem et al., 1998, Simard et al., 2003), suggesting that by interacting with

BMEC, astrocytes may confer BMEC these unique properties and thus contribute to the impermeability of BBB. By injecting neonatal astrocytes into the eye, Janzer and Raff found that the astrocyte aggregates were vascularized and the vessels were impermeable to Evan blue dye injected intravenously (Janzer and Raff, 1987), suggesting that astrocytes do confer impermeability to BBB. Consistent with this, a BMEC-astrocyte co-culture system showed a higher transendothelial electrical resistance (TEER) and less infiltration of tracers across the *in vitro* BBB than BMEC alone (Tao-Cheng et al., 1987, Neuhaus et al., 1991). Additionally, it has been reported that the temporary focal loss of astrocytes parallels the compromise of BBB integrity *in vivo* (Willis et al., 2004). These data support the idea that astrocytes contribute to the impermeability of BBB. The effect of astrocytes in BBB integrity, however, only takes place in adulthood, not in development, because astrocyte development starts after birth (Daneman et al., 2010). It should be noted that there is also evidence suggesting that astrocytes may not contribute to the BBB integrity (Krum et al., 1997). This inconsistence may be due to different experimental conditions or methodology.

1.3 Pericytes

A group of cells that reside on capillary walls were first described by Rouget in 1873 (Rouget, 1873, 1874, 1879). These cells were named as pericytes by Zimmermann in 1923 (Zimmermann 1923). Pericytes cover 22-32% of the capillaries (Kim et al., 2006) and the degree of coverage correlates with the tightness of TJ (Lai and Kuo, 2005). Although anatomically localized between BMEC and astrocytic endfeet,

the role of pericytes in BBB integrity had not been addressed for a long time. Only recently, it was reported that addition of pericytes to BMEC-astrocyte co-culture system significantly enhances TEER (Dente et al., 2001, Nakagawa et al., 2009), suggesting that pericytes are a key player in the regulation of BBB integrity. In addition, pericytes have been shown to up-regulate P-glycoprotein activity in endothelial cells and control blood flow, as well as regulate TJ permeability (Dohgu et al., 2005, Edelman et al., 2006, Peppiatt et al., 2006), suggesting that the interaction between endothelial cells and pericytes may play an important role on BBB integrity. Using mice deficient in pericyte generation, Daneman and colleagues have demonstrated that the pericyte coverage determines the BBB permeability and this is due to the inhibition of expression of molecules that enhance BBB permeability and peripheral immune cell infiltration into the brain (Daneman et al., 2010). Consistently, Armulik and colleagues showed that loss of pericytes elevated BBB permeability. It also affected the mechanisms involved in the regulation of BBB-specific gene expression in endothelial cells, and induced polarization of astrocytic endfeet (Armulik et al., 2010). In pathological conditions, such as hypoxia or traumatic brain injury (Dore-Duffy et al., 2000, Gonul et al., 2002), which lead to the disruption of BBB, pericytes have been found to migrate away from the micro-vasculature, but the relationship between migration of pericytes and compromise of BBB has not yet been studied.

1.4 Neurons

The contribution of neurons to BBB integrity is less well studied. However, anatomical studies have shown that the BMEC and astrocytic processes are in direct contact with noradrenergic, serotonergic, cholinergic, and GABA-ergic neurons (Ben-Menachem et al., 1982, Vaucher and Hamel, 1995, Cohen et al., 1996, Cohen et al., 1997, Tong and Hamel, 1999, Vaucher et al., 2000, Hawkins and Davis, 2005). In addition, neurons have been shown to regulate blood flow by promoting expression of specific enzymes on BMEC (Persidsky et al., 2006). These data suggest that neurons may play a critical role in the development and maintenance of BBB.

1.5 Microglia

Microglia are the immune competent cells in the brain, an immune privileged organ. Blood cells do not get access to the brain in physiological conditions, so microglia constitute the resident sensor of immune compromise. The number of microglial cells (100 to 200 billion cells depending on the condition) in the brain is comparable to that of neurons. Microglia account for 10-20% of glial cells. It had long been reported that microglia originate from myeloid progenitors in the born marrow (Ling, 1979, Hailer et al., 1997, Ono et al., 1999, Wu et al., 2000, Chan et al., 2007) and these macrophage-like cells migrated into the brain during early development (before the formation of BBB). Until recently, microglia have been shown to originate from the primitive myeloid progenitors that arise before embryonic day 8 (Ginhoux et al., 2010). Microglia exist in two states: a resting state with ramified morphology and an activated state with amoeboid morphology. Compared with the amoeboid morphology, the

ramified cell has a smaller cell body surrounded by many long, thin, and highly dynamic processes. In the brain parenchyma, ramified microglia extend and retract their processes continually to sense changes in the surrounding microenvironment (Nimmerjahn et al., 2005). It is estimated that microglia can survey the entire brain in a few hours (Nimmerjahn et al., 2005). When there is an injury or disturbance of homeostasis in the CNS, microglia become activated. The activation involves change of morphology and gene expression. The activated microglia migrate to the injury site and proliferate locally. In addition, these cells can also function as antigen presenting cells, secrete both pro- and anti-inflammatory cytokines, and phagocytose cellular debris (Giulian and Baker, 1986, Suzumura et al., 1987, Abromson-Leeman et al., 1993, Ulvestad et al., 1994, Aloisi, 2001, Nakajima and Kohsaka, 2004, Kim and de Vellis, 2005, Hanisch and Kettenmann, 2007). Whether microglia play a beneficial role or a detrimental role in CNS injury is highly controversial. It has been shown that microglia play neuroprotective roles by clearing neuronal debris and secreting factors promoting neurite growth and neuronal survival, such as neurotrophin-3, brain-derived neutrophic factor (Elkabes et al., 1996, Rabchevsky and Streit, 1997, Nakajima et al., 2002). On the contrary, microglia have also been shown to produce pro-inflammatory cytokines, such as TNF-α and IL1β, which are cytotoxic. These data suggest that microglia have dual roles during injury. Given that microglia are found in the perivascular space, it is speculated that microglia may play a critical role in the regulation of BBB properties by interacting with BMEC, astrocyte endfeet, or pericytes (Choi and Kim, 2008). However, to answer the question “how” they regulate these properties, further investigation is necessary.

2. **Chemokines**

Chemokines are a superfamily of structurally related small basic proteins with strong chemotactic activity. They function to induce cell-specific migration and activation of cells, especially immune cells, in response to insult (Hulkower et al., 1993, Glabinski et al., 1996, Lahrtz et al., 1998, Miller and Meucci, 1999). The first chemokine was identified by Wu and colleagues in 1977 (Wu et al., 1977). Since then, many chemokines and chemokine receptors have been reported (Ruffini et al., 2007). Based on the number and position of conserved cysteines on the chemokine primary sequences, they are divided into 4 sub-types: C, CC, CXC, and CXXXC (Murphy, 1994, Rollins, 1997, Yoshie et al., 1997). The function of CC type chemokines is to recruit other leukyocytes, such as monocytes and microglia (Tran and Miller, 2003). The function of CXC type chemokines, on the other hand, is to recruit neutrophils, short-lived but fast responding leukocytes. The biological effects of chemokines are mediated through G-protein-coupled receptors (Ransohoff, 2002). Studies on chemokines and their receptors reveal promiscuity: one receptor may have more than one ligands and one ligand may have more than one receptors, which makes the chemokine-receptor system very complex.

2.1 Monocyte Chemoattractant Protein-1 (MCP1)

During inflammation, one of the most highly and transiently expressed chemokines is MCP1. MCP1 is a member of CC family of chemokines, and is also called CCL2. The N-terminus of MCP1 is highly homologous among species, but the C-teminus is not. Human MCP1 has 76 amino acids, whereas the mouse and rat proteins are much longer: the mouse MCP1 has a C-terminal extension with about 50 amino acids. It has been shown that the C-terminal extension of mouse MCP1 is heavily O-glycosylated (Ernst et al., 1994).

MCP1 has only one receptor CCR2, but CCR2 has more than one ligands, including CCL2, CCL7, CCL8, CCL12, and CCL13 (Gong et al., 1997, Wain et al., 2002, Gouwy et al., 2004). In rodents, only one form of CCR2 is found, whereas there are two alternatively spliced forms of CCR2 in human, denoted CCR2A and CCR2B. The difference between CCR2A and CCR2B is in the C-terminal tail of the receptor (Charo et al., 1994). For monocytes and activated NK cells, CCR2B is the major isoform, whereas mononuclear cells and vascular smooth muscle cells predominately express CCR2A (Bartoli et al., 2001).

In the brain, MCP1 is expressed by neurons, astrocytes, microglia and BMEC (Ransohoff et al., 1993, Horuk et al., 1997, Andjelkovic et al., 1999a, Andjelkovic et al., 1999b, Boddeke et al., 1999, Mennicken et al., 1999, Andjelkovic and Pachter, 2000, Mahad and Ransohoff, 2003, Dicou et al., 2004, Kalehua et al., 2004, Wittendorp et al., 2004, Banisadr et al., 2005, Mahajan et al., 2005, Meeuwsen et al., 2005, Storer et al., 2005, Zeng et al., 2005) and CCR2 is expressed by microglia, astrocytes and BMEC (Banisadr et al., 2002, Ge et al., 2008). MCP1 is synthesized with a signal peptide in its N-terminus, which is removed during secretion (Yoshimura et al., 1989). The secreted

MCP1 protein binds to soluble glycosaminoglycans (GAG) and GAG immobilized on cell surface and the extracellular matrix (Rot, 1992, 1993, Hoogewerf et al., 1997, Middleton et al., 1997, Wagner et al., 1998, Kuschert et al., 1999, Middleton et al., 2002). This interaction is predicted to induce dimerization/oligomerization of MCP1, increase its local concentration and promote formation of chemokine gradients (Hoogewerf et al., 1997, Lau et al., 2004, Wang et al., 2005).

It has been shown that human MCP1 forms dimers in physiological concentrations and the residues involved in the dimerization are amino acids 6-16 (Zhang and Rollins, 1995). Supporting this report, two mutant forms of human MCP1, carrying the P8A and Y13A mutations, have been reported to be unable to dimerize (Paavola et al., 1998).

The ability to form a dimer does not necessary mean that MCP1 functions as a dimer. Whether MCP1 functions as a monomer or dimer has been controversial. Zhang and Rollins showed that chemically-crosslinked human MCP1 dimer was functional in attracting monocytes *in vitro* (Zhang and Rollins, 1995). Furthermore, a mutant form of MCP1, 7ND, which lacks residues 2-8, has been shown to inhibit the function of wt MCP1, but did not crosslink to MCP1 (Zhang and Rollins, 1995), suggesting that 7ND is a dominant-negative mutant and MCP1 functions as a dimer. P8A mutant MCP1, on the other hand, has wild-type binding affinity for CCR2, induces calcium influx and chemotaxis at the same level as wild-type MCP1 (Paavola et al., 1998). 7ND MCP1 has also been shown to function as a competitive inhibitor of monomeric MCP1 (Paavola et al., 1998), suggesting that MCP1 works as a monomer. As mouse MCP1 has a heavily

glycosylated C-terminus, how this C-terminal tail affects the dimerization/oligomerization of mouse MCP1 is still not clear.

2.2 Activation of MCP1

A very important function of MCP1 is to induce chemotaxis of monocytes and microglia in many CNS injuries, including ischemia, excitotoxicity and hemorrhage (Dimitrijevic et al., 2006, Frangogiannis et al., 2007, Hanisch and Kettenmann, 2007, Sheehan et al., 2007, Yan et al., 2007, Capoccia et al., 2008, Kim et al., 2008, Morimoto et al., 2008). The trafficking of microglia and leukocytes, however, is impaired in mice lacking CCR2, suggesting that the chemotaxis ability of MCP1 depends on CCR2 activation (Chen et al., 2001, El Khoury et al., 2007). Our lab has shown that microglial migration and the neurodegeneration induced by excitotoxic injury are attenuated in $MCP1^{-/-}$ mice (Sheehan et al., 2007). Similar results were found in rats or mice injected with MCP1 blocking antibody (Galasso et al., 2000, Sheehan et al., 2007). Interestingly, like $MCP1^{-/-}$ mice, the excitotoxicity-induced microglial activation/migration and neurodegeneration are decreased in mice lacking plasminogen (plg) or tissue plasminogen activator (tPA), a protease which converts plg to active plasmin (Tsirka et al., 1995, Tsirka et al., 1997). These results suggest that the functions of mouse MCP1 and the plg activation system may proceed with pathways that converge regarding the outcomes of excitotoxic injuries. Further studies in our lab revealed that plasmin, generated by the action of tPA on plg in the mouse CNS (or urokinase plasminogen activator in other systems), cleaves MCP1 at K104 (Sheehan et al., 2007). This

cleavage removes the highly glycosylated C-terminal extension and generates an N-terminal fragment that is highly homologous to human MCP1. The chemotactic potency of plasmin-cleaved MCP1 is higher than that of intact MCP1 and comparable to human MCP1 (Sheehan et al., 2007, Yao and Tsirka, 2010), suggesting that plasmin is an activator of mouse MCP1. In accordance with this, infusion of plasmin-cleaved MCP1 into the CNS restored excitotoxicity-induced microglial activation/migration and subsequent neuronal death in $plg^{-/-}$ mice, whereas infusion of FL-MCP1 failed to do so. These data indicate that plasmin-mediated cleavage may be a mechanism used by cells to activate MCP1 and initiate downstream signaling cascades. What is the potential mechanism responsible for the enhanced chemotactic potency of truncated MCP1 is unknown. It is also interesting to investigate whether the C-terminus of mouse MCP1 is also inhibitory for human MCP1, which lacks this fragment in nature.

Although human MCP1 does not have a highly glycosylated C-terminus, it can also be truncated at the C-terminus. A fragment with 69 amino acids (1-69) has been detected and this fragment has the same activity as the wild-type MCP1 (Proost et al., 1998). Which enzyme(s) is responsible for this cleavage, however, is not clear.

In the N-terminus, human MCP1 has been reported to be cleaved by matrix metalloproteinases-1, -3, -8, and -12 between aminoacid 4 and 5 (McQuibban et al., 2002, Dean et al., 2008). This cleavage generates a fragment (5-76) that functions as an antagonist for ligand binding to CCR2 (Gong and Clark-Lewis, 1995, Proost et al., 1998, McQuibban et al., 2002, Dean et al., 2008). Consistently, the MCP1 mutant (7ND) lacking amino acids 2-8 has been shown to inhibit MCP1-CCR2 signaling both *in vitro* and *in vivo* (Zhang and Rollins, 1995, Ni et al., 2001, Kitamoto and Egashira, 2003).

There is no report on whether these matrix metalloproteinases cleave mouse MCP1. However, it would be reasonable to assume that they do, based on the primary sequence of human and mouse MCP1. The first eight amino acids are QPDAINAP and QPDAVNAP for human and mouse MCP1, respectively.

3. MCP1 and BBB

The BBB becomes compromised in many CNS injuries, including stroke, hemorrhage, neuroinflammation, Alzheimer's disease, and Parkinson's disease. A large number of molecules have been reported to disrupt the integrity of BBB, such as MCP1, TNF-α, IL1β, IL-10, and IFN-γ (Wojciak-Stothard et al., 1998b, Yang et al., 1999b, Blamire et al., 2000b, Oshima et al., 2001, Stamatovic et al., 2003, Stamatovic et al., 2005, Stamatovic et al., 2006). Here we focus on the effect of MCP1 on BBB integrity. It has been shown that injection of recombinant mouse MCP1 into the brain disrupts BBB integrity (Stamatovic et al., 2003, Stamatovic et al., 2005, Dimitrijevic et al., 2006, Stamatovic et al., 2006). Chronic expression of MCP1 in astrocytes has also been shown to induce BBB compromise *in vivo* (Huang et al., 2005). Additionally, tPA, as it generates plasmin, has been shown to promote BBB disruption and subsequent peripheral blood mononuclear cell (PBMC) infiltration (Reijerkerk et al., 2008). BBB compromise and PBMC infiltration have also been observed in mice deficient for plasminogen activator inhibitor (PAI)-1 (Kataoka et al., 2000). These data suggest again that the plasminogen activation system and MCP1-CCR2 axis may use the same signaling pathway, and that plasmin-mediated truncation of MCP1 may be a necessary

step in MCP1-induced BBB compromise. Further studies using $CCR2^{-/-}$ mice showed that MCP1-induced BBB disruption is dependent on CCR2. Using BMEC-astrocyte co-culture system, Stamatovic et al elegantly demonstrated that lack of CCR2 expressed in BMEC was sufficient to prevent BBB leakage upon MCP1 treatment, whereas lack of CCR2 expressed in astrocytes did not affect the effect of MCP1 on BBB (Stamatovic et al., 2005). These data suggest that MCP1 induces BBB compromise via interaction with CCR2 on BMEC, not astrocytes.

BMEC as the major cell type forming the BBB barrier have been extensively studied. Accumulating evidence shows that MCP1 compromises BBB integrity via redistribution of TJP from the cell-cell border (probably via endocytosis) and reorganization of actin cytoskeleton in the BMEC (Stamatovic et al., 2003, Stamatovic et al., 2005, Dimitrijevic et al., 2006, Stamatovic et al., 2006). Mechanistic studies reveal that phosphorylation of TJP regulates their functions and localization (Farshori and Kachar, 1999, Clarke et al., 2000a, Clarke et al., 2000b, Hirase et al., 2001, Ward et al., 2002). Stamatovic and colleagues further demonstrated that the binding of MCP1 to CCR2 activated PKC (specifically PKCα and PKCζ) and Rho kinase, resulting in shift of TJP from the cell border to intracellular compartments (Stamatovic et al., 2003, Stamatovic et al., 2006). Additionally, this phosphorylation event also promoted the interaction between TJP and the actin cytoskeleton, resulting in a shift of TJP from Triton X-100 soluble fractions to Triton X-100 insoluble fractions (Tsukamoto and Nigam, 1997b, 1999b, Stamatovic et al., 2003, Stamatovic et al., 2005, Stamatovic et al., 2006). These changes are not limited to MCP1, because growth factors (PDGF and VEGF) also induce phosphorylation and redistribution of TJP (Harhaj et al., 2002, Pedram et al.,

2002), suggesting that phosphorylation of TJP may be a common mechanism to transport TJP to different cellular compartments. In addition to TJP phosphorylation, the activated kinases, especially Rho Kinase, also phosphorylate myosin light chain phosphatase (MLCP) and inhibit its activity. The inhibition of MLCP results in enhanced phosphorylation of myosin light chain, leading to increased actin-myosin interaction and thus increased cortical force in the endothelial cells (Stephan and Brock, 1996, van Nieuw Amerongen et al., 2000, Stamatovic et al., 2003, Hicks et al., 2010). These data underscore the role of actin cytoskeleton in the regulation of TJ structures, however, how exactly reorganization of actin cytoskeleton leads to redistribution of TJP is still elusive.

4. Intracerebral Hemorrhage (ICH)

ICH accounts for 10-20% of all strokes, which is a leading course of death and disability (Qureshi et al., 2001, Ribo and Grotta, 2006). The prognosis of ICH is poor (Donnan et al., 2010). Although the pathophysiology of ICH is still elusive, strong evidence suggests that inflammation (Castillo et al., 2002, Wang et al., 2003, Aronowski and Hall, 2005, Xi et al., 2006, Wang, 2010) and apoptosis (Matsushita et al., 2000, Gong et al., 2001, Qureshi et al., 2003) contribute to the cell death in the brain. When ICH occurs, microglia are activated and migrate to site of injury. In addition, the BBB becomes compromised and blood leukocytes infiltrate into the brain parenchyma. The infiltrated leukocytes or microglia then secrete chemotactic cytokines, such as MCP1, to induce migration of more cells towards the site of injury. These cells may either promote

the progress of ICH by secreting cytotoxic cytokines, including TNF-α and IL-1β (Aloisi, 2001, Kim and de Vellis, 2005, Hanisch and Kettenmann, 2007), or play a beneficial role by cleaning up cell debris (Elkabes et al., 1996, Rabchevsky and Streit, 1997, Nakajima et al., 2002, Nakajima and Kohsaka, 2004).

Collagenase-induced hemorrhage is an established model of ICH. After injection into the brain, collagenase degrades collagen, which is an important component of blood vessel wall, leading to bleeding at the site of injection. For wt mice, 24 hours after injection, the injury peaks and the injury site is full of necrotic tissue and erythrocytes. 7 days after injection, the injury resolves. At this time point, a lot of phagocytic cells (activated microglia, monocytes, and lymphocytes) can be seen at the injury site.

Figure 1-1. Structure of BBB. BMEC form impermeable monolayer via TJ. Pericytes attach to endothelial cells. Astrocyte endfeet wrap pericytes and endothelial cells. Neurons and microglia have direct contact with astrocyte endfeet. Adapted from Abbott et al, 2006 (Abbott et al., 2006).

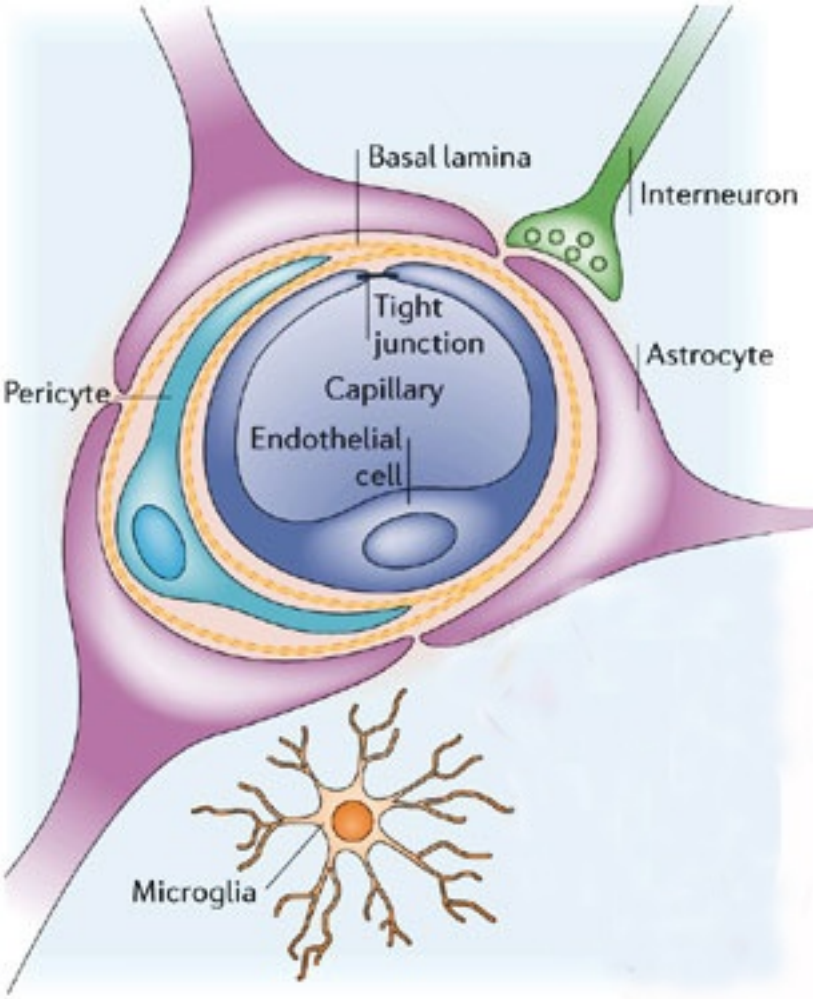

Chapter 2

MCP1 C-Terminus Mediates Its Dimerization While Blocking Its Chemotactic Potency

INTRODUCTION

Microglia, the immune cells normally present in the brain, enter the CNS early during development and reside in the parenchyma in a resting state characterized by ramified morphology. In the healthy brain, they extend and retract their processes continually to sense changes in the surrounding microenvironment (Nimmerjahn et al., 2005). However, when there is an injury in the CNS, microglia switch to an activated state characterized by changes in gene expression, morphology and proliferation (Giulian and Baker, 1986, Suzumura et al., 1987, Andersson et al., 1991, Abromson-Leeman et al., 1993, Ulvestad et al., 1994, Aloisi, 2001, Nakajima and Kohsaka, 2004, Davalos et al., 2005, Kim and de Vellis, 2005, Nimmerjahn et al., 2005, Hanisch and Kettenmann, 2007). The activated microglia then migrate to the site of injury and modify the injury outcome.

The migration of microglia to the site of injury is stimulated by the local release of chemokines. As a potent chemoattractant for monocytes/microglia (Van Der Voorn et al., 1999), MCP1 is upregulated in many types of CNS injury, including ischemia, hemorrhage, trauma, infection, hypoxia, and peripheral nerve axotomy (Mahad and Ransohoff, 2003, Dimitrijevic et al., 2006, Frangogiannis et al., 2007, Yan et al., 2007, Capoccia et al., 2008, Kim et al., 2008, Morimoto et al., 2008). The MCP1 protein is

highly conserved in the N-terminus among different species, while the C-terminus is much more variable. The rodent MCP1 C-terminus is decorated extensively with O-linked carbohydrates (Zhang et al., 1996), which bind both soluble GAG and GAG immobilized on cell surface. Soluble GAG inhibit the binding of MCP1 to its high-affinity receptor CCR2 (Kushhert et al 1999), which is expressed by microglia, astrocytes and microvascular endothelial cells in the brain (Banisadr et al., 2002, Ge et al., 2008). Cell surface GAG, on the other hand, have been reported to concentrate MCP1 locally, promote MCP1 oligomerization, and thus facilitate the binding of MCP1 to CCR2 (Hoogewerf et al., 1997, Kuschert et al., 1999, Lau et al., 2004, Handel et al., 2005). Whether MCP1 functions as a monomer or homodimer, however, is still under debate. Although it is believed that MCP1 exerts its function as a homodimer (Zhang and Rollins, 1995, Zhang et al., 1996), it has also been suggested that MCP1 can bind to CCR2 and induce downstream signaling as a monomer (Paolini et al., 1994, Paavola et al., 1998). It should be noted, however, that these experiments were conducted using human MCP1, not rodent MCP1, which contains a heavily glycosylated C-terminal tail.

Previous studies in our lab have shown that: (1) the highly glycosylated C-terminal extension of mouse MCP1 is removed by plasmin, the active protease of plg, and (2) the C-terminus-truncated mouse MCP1 has a higher chemotactic potency than the full-length mouse MCP1 (Sheehan et al., 2007). Additionally, the fact that infusion of C-terminus-deleted mouse MCP1 into plg-deficient mice, which are more resistant to excitotoxic injury, restored microglial migration and neuronal loss, unlike the intact mouse MCP1, further suggests that the C-terminal extension negatively regulates the chemotactic ability of mouse MCP1 (Sheehan et al., 2007). How exactly the highly

glycosylated C-terminus regulates mouse MCP1 function, however, remains to be elucidated. Herein, we investigated several potential mechanisms: dimerization/oligomerization of mouse MCP1, interaction of MCP1 with CCR2, and intracellular signaling. We find that the C-terminus of mouse MCP1 is required for MCP1 dimerization, inhibitis MCP1-CCR2 interaction, and suppresses MCP1-induced Rac activation and subsequent microglial migration.

MATERIALS AND METHODS

Cell Culture

N9 cells were originally provided by Drs. S. Barger (University of Arkansas, Fayetteville, AR) and P. Ricciardi-Castagnoli (University of Milano-Bicocca, Milan, Italy). The cells were maintained in modified Eagle's medium (MEM) supplemented with 10% fetal bovine serum (FBS), 100 U/ml penicillin and 100 μg/ml streptomycin at 37℃ with 5% CO_2.

Primary microglia were prepared from mixed cortical cultures as described previously with minor modifications (Giulian and Baker, 1986). Briefly, brains of 1-day-old pups from wild-type or CCR2$^{-/-}$ mice were collected. After removing meninges and hippocampi, the cortical tissue was digested with trypsin (0.25% in Hanks balanced saline solution, HBSS) for 15 minutes at 37℃. The tissu e was mechanically dissociated by trituration and filtered through a 70μm nylon mesh. The cell suspensions were plated onto poly-D-lysine-coated tissue culture dishes. Cultures were maintained in Dulbecco's MEM (DMEM) supplemented with 10% FBS. The medium was changed on day 3 and 14, and the microglia collected through addition of 15 mM lidocaine for 10 minutes at room temperature followed by centrifugation. The microglia were used for migration assay immediately or maintained in DMEM with 1% FBS for 2 days before use in other experiments.

Human embryonic kidney 293 (HEK293) cells were maintained in DMEM supplemented with 10% FBS, 100 U/ml of penicillin and 100 μg/ml of streptomycin.

Cell Treatment

N9 cells or primary microglia were treated with 10nM recombinant MCP1 proteins.

Generation of 6His-tagged MCP1 Proteins

FL-, K104A-, and K104Stop-MCP1 were subcloned without the signal peptide into pET vectors with an N-terminal 6xHis tag. CT-MCP1 was subcloned into a pTYB1 vector with an N-terminal 6xHis tag. BL21 cells were transformed with these constructs and expression of the target proteins was induced for 5 hours using isopropyl-beta-D-thiogalactopyranoside (IPTG). Recombinant proteins were purified using cobalt affinity resins (Clontech, Cambridge, UK) according to the manufacturer's instructions. The fractions were analyzed on 16% Tris-Tricine sodium dodecyl sulfate polyacrylamide gel electrophoresis (SDS-PAGE) by coommassie blue staining. The purified proteins were confirmed by immunoblotting using 1:1000 anti-MCP1 antibody (Serotec and Cell Sciences) or 1:1000 anti-6xHis antibody (Santa Cruz Biotechnology).

Transient Transfection

FL-, K104A-, and K104Stop-MCP1 subcloned into pcDNA3.1 vectors with N-terminal c-myc or HA tags were transfected into HEK293 cells using lipofectamine (Invitrogen Life Technologies) according to the manufacturer’s protocol. Two days later, cell lysates were collected and used for co-immunoprecipitation.

Co-Immunoprecipitation (CoIP)

Mixtures of lysates of cells expressing c-myc- and HA-tagged MCP1 proteins were precleared with protein A/G agarose beads, incubated with rabbit anti-c-myc (Sigma) or rat anti-HA (Roche) antibody overnight at 4℃, and the immunocomplexes pulled down using protein A/G-agarose beads (Santa Cruz) for 2 hours at 4℃ and centrifugation. Pelleted proteins were subjected to immunoblot analysis with the anti-c-myc and -HA antibodies to demonstrate equal expression and assess coIP.

***In vitro* Pull-Down Assay**

Purified recombinant 6xHis-MCP1 and c-myc-MCP1 proteins were mixed and coIP'd as above, using anti-c-myc and rabbit anti-6xHis antibody (Roche).

Western Blot Analysis and Immunoblotting

Cells were lysed in RIPA buffer (50mM Tris-HCl pH 7.4, 150mM NaCl, 1% NP40, 0.25% sodium deoxycholate, 1mM PMSF, 1x protease inhibitor cocktail, 1x Na_3VO_4). Protein concentrations were determined by DC (Bio-Rad) protein assay. Lysates containing equal amounts of protein were resolved in 10% or 15% Tris-Glycine SDS-PAGE, transferred to Immobilon-P transfer membranes (Millipore), blocked in 5% nonfat milk or Odyssey blocking buffer for 1 hour at room temperature, incubated with primary antibodies overnight at 4℃, washed, incubated with 1 :5000 HRP-conjugated secondary antibodies (Jackson Immunoresearch Lab) or IRDye secondary antibodies (LI-COR) for 1 hour at room temperature washed, and developed using ECL (Pierce) or scanned using Odyssey infrared imaging (LI-COR).

Rac Activity Assay

Activated Rac was quantified through specific interaction with its downstream effector p21-activated kinase (PAK) (del Pozo et al., 2000). PAK p21-binding domain (PBD) purified as a GST fusion protein was immobilized to glutathione beads (generously provided by Dr. J. Prives, Stony Brook University). Microglia stimulated with 10nM MCP-1 proteins for varied times were lysed in RIPA buffer and the activated Rac pulled down using the GST-PBD beads and detected by immunoblotting using mouse anti-Rac1 antibody. Total Rac1 was determined by immunoblotting samples of the cell lysates. Band intensities were quantified using Scion Image (Scion, Frederick, MD) or Odyssey Infrared Imaging. Rac activation in stimulated cells was normalized to the amount of activated Rac in control microglia.

Membrane Sheet Assay

This was performed as previously described with minor modifications (Robinson et al., 1992). Briefly, primary microglia were plated on coverslips and activated with 100ng/ml LPS overnight. The cells were then treated with 10nM recombinant MCP1 for 1 hour at 37℃, followed by swelling in hypotonic buf fer (25mM KCl, 10mM Hepes, 2mM MgCl2, 1mM EGTA, 1mM PMSF, 1x protease inhibitor cocktail, pH 7.5) for 20 minutes. After PBS washing, the cells were fixed with 4% paraformaldehyde, permeabilized and stained with 1:1000 rat-anti-Mac2 antibody (BD Pharmingen) and 1:500 rabbit anti-CCR2 antibody (Epitomics), followed by 1:1000 fluorescence-conjugated secondary antibodies (Invitrogen). The cells were then imaged using Zeiss LSM510 confocal microscopy.

Immunofluorescent imaging of the F-actin cytoskeleton

To mimic endogenous chemoattractant gradient, 12-well plates were spotted at the edges of the wells with heparin, which avidly binds MCP1. 15μl of recombinant MCP1 proteins were then added directly onto the dried heparin spot to create an MCP1 point source. 1h later, primary microglia attached to coverslips were placed in the well and cultured for varied periods of time, washed, and fixed with 4% paraformaldehyde for 15 minutes at room temperature. After PBS washing, the cells were incubated with 1:20 Alexa-647 phalloidin (Invitrogen) overnight at room temperature, washed, mounted using FluorMount with DAPI, and imaged using confocal microscopy.

Migration Assay

Migration assays were performed using chemotactic chambers (Boyden; NeuroProbe). Recombinant mouse MCP1 proteins or human MCP1 suspended in MEM with or without the Rac inhibitor, NSC23766 were added to the bottom wells of the chamber. Wild-type or $CCR2^{-/-}$ primary microglia suspended in MEM (5×10^5/ml) with or without the Rac inhibitor were added to the top wells, with 5.0μm filter inserted between the chemoattactants and microglial cells. Migration was allowed to proceed for 2 h at 37℃. Cells that did not migrate into the membrane were wiped off, and cells that migrated into or through the membrane fixed and stained with hematoxylin for 10 minutes at room temperature. The membranes were photographed at 100X magnification. Total migration was quantified by counting stained cells. The background for random cell movement (cells responding to MEM only) was subtracted.

Statistics

Statistics were performed using the two-tailed t test. *$p<0.05$ was considered significant. Error bars indicate the SEM.

RESULTS

The C-terminus of MCP1 enables multimerization.

GAG modifications can enhance the local concentration of chemokines and facilitate their homodimerization/ oligomerization (Hoogewerf et al., 1997, Kuschert et al., 1999, Lau et al., 2004). Mouse MCP1 has a highly GAG-glycosylated C-terminal extension (Zhang et al., 1996). Since plasmin removes the C-terminus of mouse MCP1 (Sheehan et al., 2007), this processing event could affect homodimerization/ oligomerization for MCP1. To examine the role of MCP1 C-terminal extension in this context, co-IPs were performed using HEK293 cells transfected with HA- and c-myc-tagged full length MCP1 (FL), or a full length mutant that can not be processed by plasmid (K104A) (Figure 2-1), or a C-terminally truncated mutant that terminates at the plasmin cleavage site (K104Stop). We observed that the full length protein and the plasmin-resistant mutant K104A both readily form stable homodimers/oligomers (Figure 2-2A). In contrast, however, homodimers/oligomers were not observed for the K104Stop.

To determine whether MCP1 forms homodimers or whether individual MCP1 proteins associate indirectly through forming complexes with other proteins, the co-IP was performed using purified recombinant proteins. FL-MCP1 and K104A-MCP1 exhibited the ability to form stable homodimers/oligomers, and as expected, K104Stop-MCP1 failed to do so (Figure 2-2B). Similar results were observed regardless of which anti-epitope antibody was used for the co-IP (data not shown). However, the isolated C-terminal extension fragment (CT-MCP1) did not co-IP with FL-, K104A-, or K104Stop-

MCP1 (data not shown), suggesting that the C-terminal extension is necessary but not sufficient for the interaction.

These data indicate that full length MCP1 dimerizes / oligomerizes and that the plasmin cleavage event converts it to a monomeric form. A number of studies have reported that MCP1, like most other chemokines, binds to its receptor, CCR2, and exerts its function as a homodimer (Zhang and Rollins, 1995, Zhang et al., 1996). However, there is also evidence supporting that it functions as a monomer (Paolini et al., 1994, Paavola et al., 1998). To address whether MCP1 functions as a monomer or homodimer, we further investigated MCP1-CCR2 interaction and intracellular signaling using these recombinant proteins.

N-terminus-containing MCP1 proteins reduce membrane-bound CCR2.

CCR2 is a critical receptor for MCP1 (Paavola et al., 1998, Terashima et al., 2005), since CCR2-deficient microglia and macrophages fail to migrate in response to MCP1 stimulation (Chen et al., 2001, El Khoury et al., 2007). CCR2 is expressed in the mouse CNS by microglia, astrocytes and microvascular endothelial cells (Banisadr et al., 2002, Ge et al., 2008). We next used microglia to assess how modulation of the MCP1 protein structure affects CCR2 responses. Microglia were stimulated with human MCP1 (Hu) or mouse wild-type and modified forms of MCP1 and assessed for changes in CCR2 amount and subcellular distribution. To undertake this study, we employed a commercial anti-CCR2 antiserum (Biovision), which detects an immunoreactive band present in brain lysates prepared from wild-type mice but not in ones prepared from $CCR2^{-/-}$ mice (Figure 2-3). Treatment of the microglia with wild-type and modified forms

of MCP1 did not alter the total levels of CCR2 over a two-hour period, indicating that stimulation-induced receptor down-regulation and degradation does not occur within this time frame (Figure 2-4). To examine changes in subcellular localization, the amount of CCR2 at the plasma membrane was assessed using a membrane sheet assay (Robinson et al., 1992). In non-stimulated cells, CCR2 is observed in a punctate distribution on the plasma membrane (Ctr, Figure 2-5). Stimulation of the microglia with full-length MCP1 (FL) greatly decreased the amount of plasma membrane-associated CCR2, presumably via receptor endocytosis. Similar findings were observed for K104Stop-MCP1, indicating the lack of requirement for the C-terminal extension for receptor engagement. The C-terminal extension by itself (CT) did not cause plasma membrane-associated CCR2 to decrease. Nor did the forced dimers (FL-FL and K104S-K104S) change the membrane bound CCR2 level, suggesting that MCP1 functions as a monomer. Moreover, the decrease in plasma-membrane associated CCR2 was much less substantial for K104A-MCP1, suggesting that the presence of the C-terminal extension interferes with receptor engagement. Finally, human MCP1, which lacks a C-terminal extension, also significantly decreased plasma membrane-associated CCR2 and this effect was comparable with K104Stop-MCP1. These findings are consistent with a previous report that MCP1 binds to CCR2 via its N-terminus (Hemmerich et al., 1999), and newly suggest that the C-terminal extension of mouse MCP1 interferes with the interaction between the MCP1 N-terminus and CCR2.

Plasmin-truncated MCP1 exhibits increased chemotactic activity.

Migration of microglia in response to stimulation by the modified MCP1 proteins was next examined, using a chemotaxis Boyden chamber assay. Wild-type MCP1 (FL) elicited a modest migratory response (140 ± 20 cells, Figure 2-6). In contrast, K104A provoked a weaker response (60 ± 15 cells), again suggesting that the presence of the C-terminal extension interferes with receptor engagement / stimulation. Conversely, K104Stop triggered a much stronger response (460 ± 28 cells) than wild-type MCP-1, and the C-terminal extension by itself (CT) caused no response, both confirming the lack of requirement for the C-terminal extension, and suggesting that processing to remove the C-terminal extension is a key step in efficient CCR2 stimulation. The MCP1 forced dimers (FL-FL and K104S-K104S) were unable to attract microglia, again suggesting that MCP1 functions as a monomer. Of note, the chemotactic activity of mouse K104Stop-MCP1 was comparable to that of human MCP1. $CCR2^{-/-}$ primary microglia failed to migrate in response to MCP1 recombinant proteins in this assay, confirming the indispensable role of the CCR2 receptor in MCP1-induced microglial migration.

Plasmin-mediated cleavage of MCP1 promotes Rac1 activation.

MCP1 engagement of CCR2 activates intracellular signaling cascades that differ depending on the cell type (Terashima et al., 2005, Stamatovic et al., 2006). In microglia, one of these signaling pathways involves activation (GTP-loading) of Rac, a member of the Rho family of small GTPases (Maghazachi, 2000, Terashima et al., 2005). The activated Rac then promotes protrusion of lamellipodia and cell migration (Rickert et al., 2000, Ridley et al., 2003, Terashima et al., 2005). As a molecular switch, Rac1 needs to

be activated transiently and then deactivated. We assessed over time the activation of Rac using N9 microglial cells. FL-MCP1 induced a moderate level of Rac1 activation over the 90-minute time course of the assay (Figure 2-7A), and this increase was dependent on CCR2 stimulation since no Rac activation was seen in CCR2$^{-/-}$ primary microglia. In contrast, K104Stop-MCP1 provoked a rapid and dramatic increase in Rac1 activation in 5 minutes that was also extinguished rapidly, while K104A-MCP1 prompted a very weak response. These data again support the earlier findings that the C-terminal extension inhibits receptor engagement and mobilization.

As expected, the C-terminal extension by itself (CT) and two forced dimers (FL-FL and K104S-K104S), did not cause Rac activation (Figure 2-7B). Surprisingly, unlike K104Stop-MCP1, human MCP1 induced a much lower and delayed Rac1 activation: it induced a two-fold change at 15 minutes after treatment. This effect, however, was deactivated rapidly. These data suggest that the transient activation of Rac1 plays an important role in cell migration.

To assess whether activation of Rac1 is necessary for the stimulation of microglial migration, NSC23766, a Rac1 specific inhibitor, was employed. NSC23766 fully blocked microglial migration in response to MCP1 (Figure 2-6).

Plasmin-mediated cleavage of MCP1 promotes the formation of lamellipodia.

Lamellipodia, which are cytoskeletal actin projections at the leading edges of cells observed during cell migration, are induced by the activation of Rac1 (Maghazachi, 2000, Pankov et al., 2005, Terashima et al., 2005). We thus investigated whether MCP1 truncation by plasmin induced lamellipodia formation. After incubation of primary

microglia in the presence of localized source of MCP1 to create a chemotatic gradient for different periods of time, the microglia were fixed and stained with phalloidin. Most of the control cells cultured in the absence of MCP1 exhibited actin cytoskeletal projections, but did so in a uniform, non-polarized manner (Ctr, Figure 2-8). Only 5-8% of the control cells exhibited lamellipodia (polarized actin cytoskeletal projections). In contrast, 20% of cells stimulated with a gradient of FL-MCP1 exhibited polarized actin cytoskseletal reorganization, and 50% of cells stimulated with K104Stop-MCP1 displayed lamellipodia, which were exaggerated in appearance. Similar to K104Stop-MCP1, 40% of human MCP1-treated cells showed unipolar lamellipodia. K104A-MCP1, CT-MCP1, and two forced dimers (FL-FL and K104S-K104S), however, did not promote cellular polarization, suggesting that plasmin-mediated cleavage of MCP1 is critical for cell migration and the formation of lamellipodia and that MCP1 functions as a monoer.

The cleavage of MCP1 by plasmin activates ERK1/2 slightly.

During microglial activation and migration, changes in gene expression and morphology also occur (Andersson et al., 1991, Davalos et al., 2005, Nimmerjahn et al., 2005). To investigate whether MCP1 may affect characteristics of microglia activation such as proliferation and differentiation, we explored other signaling pathways that could be involved. Mitogen-activated protein kinase (MAPK) has been implicated in many cellular processes including proliferation, differentiation and apoptosis (Jimenez-Sainz et al., 2003). Many factors acting through GPCRs lead to the activation of MAPK cascades and finally activate extracellular signal-regulated Kinases 1 and 2 (ERK1/2) (Marinissen and Gutkind, 2001).

N9 cells were cultured with or without human MCP1 and recombinant mouse MCP1 proteins and the levels of phosphorylated and total ERK1/2 analyzed by western blotting (Figure 2-9). FL- and K104A-MCP1 promoted low-level and prolonged ERK1/2 activation (1.2-1.4 fold change over the course of 120 minutes). Although K104Stop-MCP1 and human MCP1 also induced ERK1/2 phosphorylation, the activation was detectable as early as in 5 minutes and returned to base line in 30 minutes, indicating a higher potency. CT- MCP1, on the other hand, failed to activate ERK1/2. The forced MCP1 dimers (FL-FL and K104S-K104S), slightly induced activation of ERK1/2, but it should be noticed that the activation was not found at early time point (5 min). As a positive control, LPS dramatically enhanced phosphorylated ERK1/2 (data not shown). These data suggest that K104Stop-MCP1 is more active than the FL- or K104A-MCP1 in activation of the MAPK cascade and its effect was comparable with human MCP1, but the major and more dramatic effect was evident on Rac activation.

DISCUSSION

MCP1 is a potent chemoattractant for monocytes and microglia. It has been reported to be involved in many diseases, including asthma (Lamkhioued et al., 2000, Tillie-Leblond et al., 2000), rheumatoid arthritis (Koch et al., 1992, Kunkel et al., 1996) and atherosclerosis (Chen et al., 1999, Kowala et al., 2000). In addition, MCP1 plays a very important role in excitotoxic injury. It has been shown that kainate injection induces excitotoxic injury, leading to microglial migration and neuronal death in wild-type mice. Previous studies in our lab reported that the kainate-induced microglial activation/migration and neuronal death were attenuated in mice deficient for MCP1 or plasminogen, the inactive precursor of plasmin (Tsirka et al., 1997, Rogove et al., 1999, Sheehan et al., 2007). Further studies in our lab show that plasmin removes the highly glycosylated C-terminus of mouse MCP1 and it is the truncated MCP1, not the intact MCP1, that is responsible for microglial migration and neuronal loss (Sheehan et al., 2007), thus identifying plasmin as an activator of MCP1 and offering an explanation for the diminished microglial recruitment in $plg^{-/-}$ mice. However, the mechanisms underlying the enhanced biological functions of plasmin-cleaved MCP1 are not known. The data presented in this study argue that (1) plasmin-mediated cleavage of mouse MCP1 abrogates its potential for dimerization/ oligomerization, (2) the C-terminus of mouse MCP1 alone can not bind to CCR2, 3) Plasmin cleavage is required to engage the CCR2 receptor, 4) the monomer form is needed to cause engaged receptor to initiate signaling to Rac 5) the Rac pathway is activated and critical 6) ERK is also activated, but less dramatically.

GAG have been reported to increase local chemokine concentration and promote the oligomerization of chemokines both *in vitro* and *in vivo* (Hoogewerf et al., 1997, Kuschert et al., 1999, Lau et al., 2004, Handel et al., 2005). The C-terminus of MCP1 is heavily O-glycosylated and has many GAG modifications (Zhang et al., 1996). Thus, the C-terminus of MCP1 has been speculated to promote the formation of MCP1 dimerization/oligomerization or stabilize the dimerization/oligomerization (Zhang et al., 1996, Handel et al., 2005). Consistent with this speculation, K104Stop-MCP1, which does not have the highly glycosylated C-terminal extension, did not homodimerize/oligomerize, thus supporting the hypothesis that the C-terminal extension of mouse MCP1 is necessary for its dimerization/oligomerization. Since the C-terminal fragment alone failed to form stable dimer/oligomer with FL-, K104A-, or K104Stop-MCP1, it appears that both N-terminus and C-terminus contribute to the formation of stable homodimers.

Upon ligand binding, many receptors, such as the interleukin-8 receptor, the mu opioid receptor, and pattern recognition receptor, undergo internalization (Ray and Samanta, 1996, Minnis et al., 2003, Robatzek et al., 2006). Like these receptors, CCR2 is also expected to translocate from the plasma membrane to intracellular vesicles upon MCP1 binding (Favre et al., 2008). Recently, by using GFP-CCR2 transfected cells or GFP-CCR2 transgenic mice, Jung et al have shown that upon MCP1 binding, CCR2 undergoes endocytosis (Jung et al., 2009). Consistent with this report, we showed that those N-terminus-containing MCP1 proteins (FL-, K104A-, and K104Stop-MCP1) induced a significant reduction of membrane CCR2. CT-MCP1, as it does not have the N-terminus region of the MCP1 protein failed to decrease membrane bound CCR2.

Significant decrease of plasma CCR2 was also accomplished with human MCP1, which lacks the heavily glycosylated C-terminal extension, suggesting the C-terminus of mouse MCP1 hinders MCP1-CCR2 interaction.

Our data indicated that the binding of monomeric N-terminal domains of MCP1 to CCR2 activated Rac and induced the protrusion of lamellipodia, leading to microglial migration. We therefore propose a model to describe how mouse MCP1 may interact with CCR2 in the CNS. Upon secretion, mouse MCP1 binds via its glycosylated C-terminus to neuronal cell membranes, an event that increases local MCP1 concentration. This increase in local MCP1 promotes the formation of dimers or higher order aggregates, which thus generate a point source for a potential chemokine gradient. Upon neuronal injury or exaggerated stimulation, the neurons form and secrete plasmin, which then cleaves and removes the C-terminal, GAG-glycosylated extension of mouse MCP1, thus abrogating MCP1 dimers. These truncated MCP1 monomers are more easily diffusible and able to form potent chemotactic gradients, bind to CCR2 on microglia and initiate microglial intracellular signaling pathways. The pathways include activation of Rac1, rearrangement of the actin cytoskeleton with protrusion of lamellipodia, and eventual promotion of microglial migration along the MCP1 chemokine gradient.

It should be noted that: (1) unlike the mouse MCP1, human MCP1 does not have a heavily glycosylated C-terminus, and (2) human MCP1 and plasmin-truncated mouse MCP1 (K104Stop-MCP1) are highly homologous. Then a few questions need to be answered: What is the function of mouse MCP1 C-terminal extension? Do humans have an unknown protein that functions like the C-terminal extension of mouse MCP1? Do

human and mouse MCP1 use different mechanisms to activate CCR2? Understanding of the functions of carbohydrate on mouse MCP1 will provide important clues for these questions.

Figure 2-1. Plasmin does not cleave K104A-MCP1. Recombinant FL- and K104A-MCP1 were treated with plasmin, then the integrity of these proteins were assessed by western blotting. Experiments were performed in triplicate. Representative experiment shown.

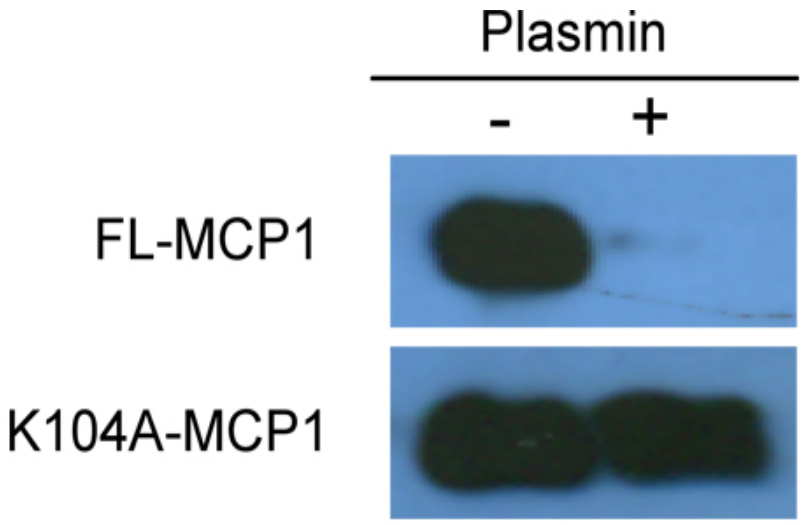

Figure 2-2. Homodimerization of recombinant mouse MCP1 proteins. A. HEK293 cells transfected with HA- and c-myc- tagged FL-, K104A-, or K104Stop-MCP1 were lysed, immunoprecipitated with anti-c-myc antibody, and immunoblotted using anti-HA antibody. Note that the 25 kDa IgG light chain runs just above the 23 kDa epitope-tagged FL and K104A MCP1 proteins but is well separable from K104Stop MCP1, which is 6 kDa smaller than FL-MCP1. Lysate lane shows the equal levels of expression of the HA-tagged version of the 3 forms of MCP1. **B.** Purified recombinant 6xHis- and c-myc-tagged MCP1 proteins were immunoprecipitated with anti-6xHis antibody and immunoblotted with anti-c-myc antibody. Shown is an experiment representative of four performed with similar results.

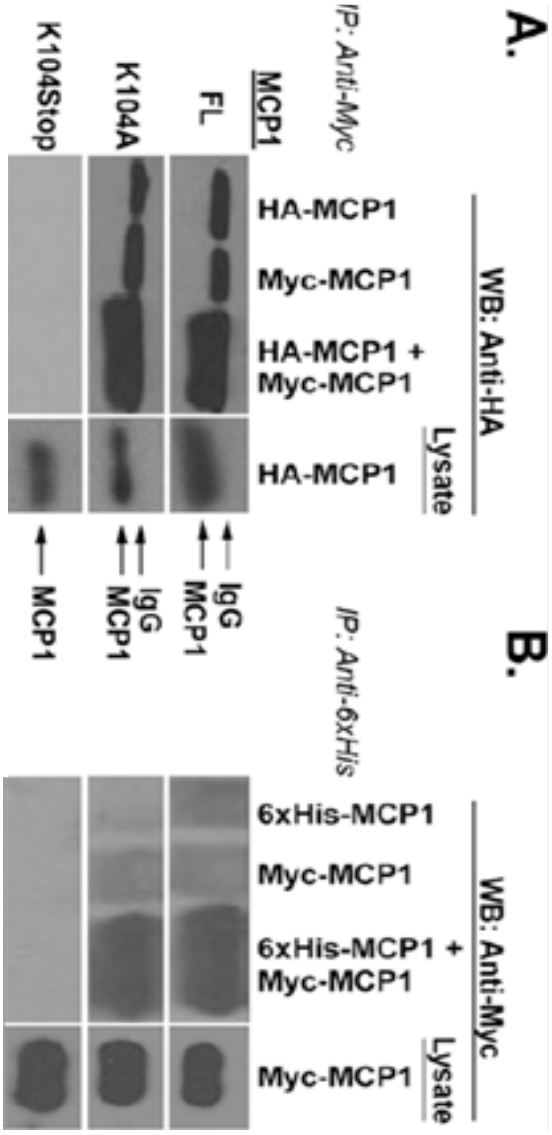

Figure 2-3. The anti-CCR2 antiserum employed detects a CCR2-specific immunoreactive band by western blotting. Brain lysates from wild-type and CCR2$^{-/-}$ mice were western-blotted using anti-CCR2 antisera. Anti-tubulin antiserum was used as a loading control.

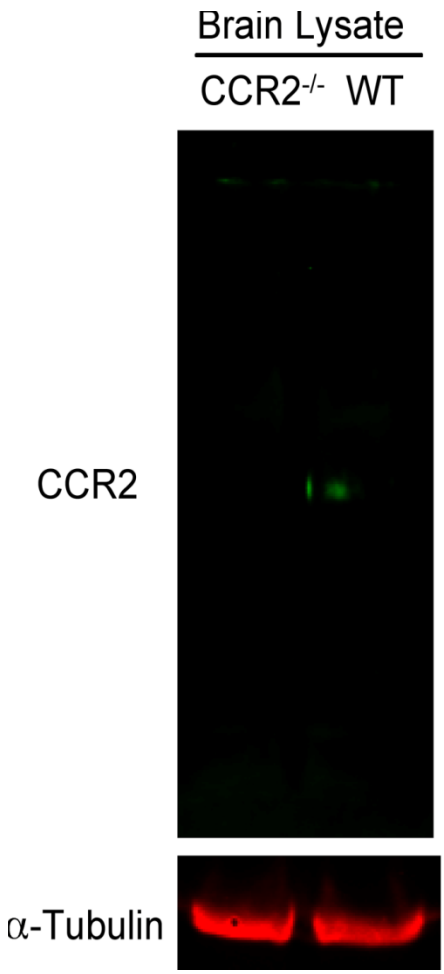

Figure 2-4. Ligand binding to CCR2 does not alter total levels of receptor expression in primary microglia over short time periods. Primary microglia were treated with recombinant MCP1 proteins for different periods of time at which cell lysates were collected and assessed for CCR2 and α-tubulin by western blotting. Experiments were performed in triplicate. Representative experiment shown.

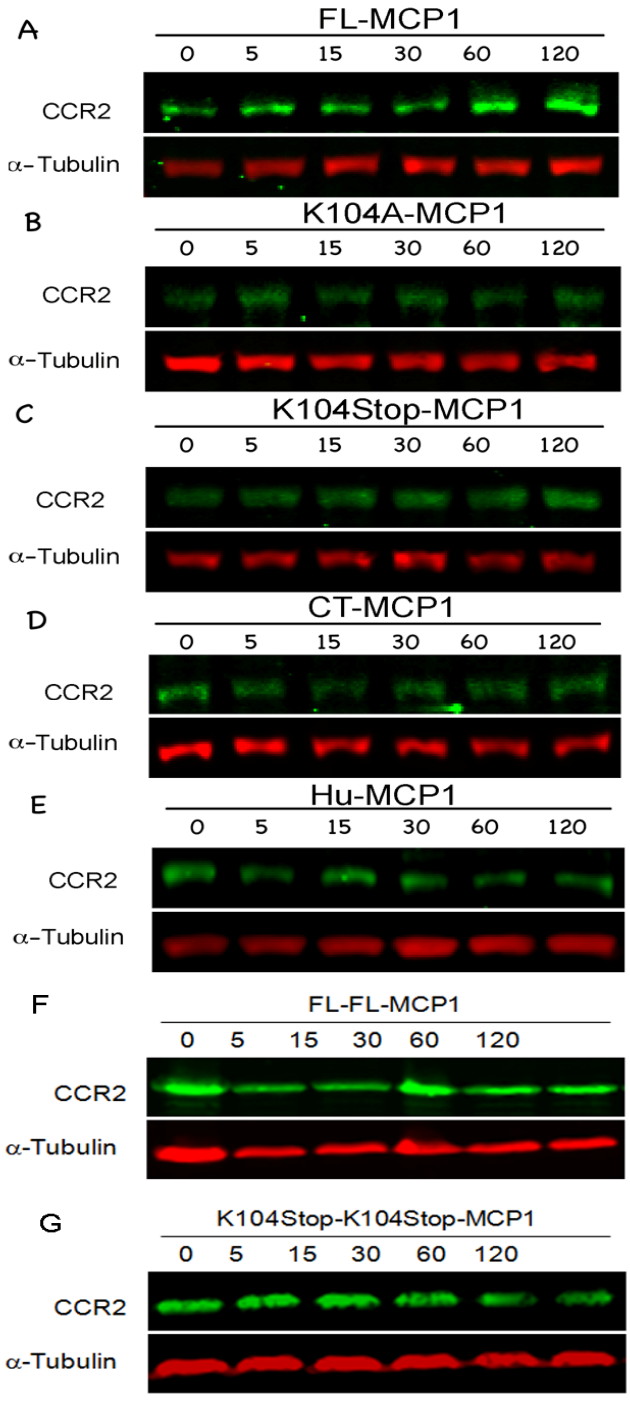

Figure 2-5. Stimulation of microglia by N-terminus-containing MCP1 proteins triggers CCR2 internalization. Primary microglia from wild-type mice activated overnight with 100ng/ml LPS were treated with saline (Ctr) or 10nM recombinant MCP1 proteins for 1 h and then swelled in hypotonic buffer for 20 min to cause cell lysis. The plasma membrane sheets that remained adhered to the coverslips were stained for Mac-2 (Green) to visualize the membrane sheets and CCR2 (Red). $CCR2^{-/-}$ microglia serve as a control for the CCR2 antibody. Microglia immunostained with secondary antibodies only exhibited no fluorescence. *Scale bar* = 10 μm. The fluorescence intensity was quantified in 20 cells per condition in 3 separate experiments. The results were analyzed with one-Way ANOVA plus Dunn's Test: *p<0.05.

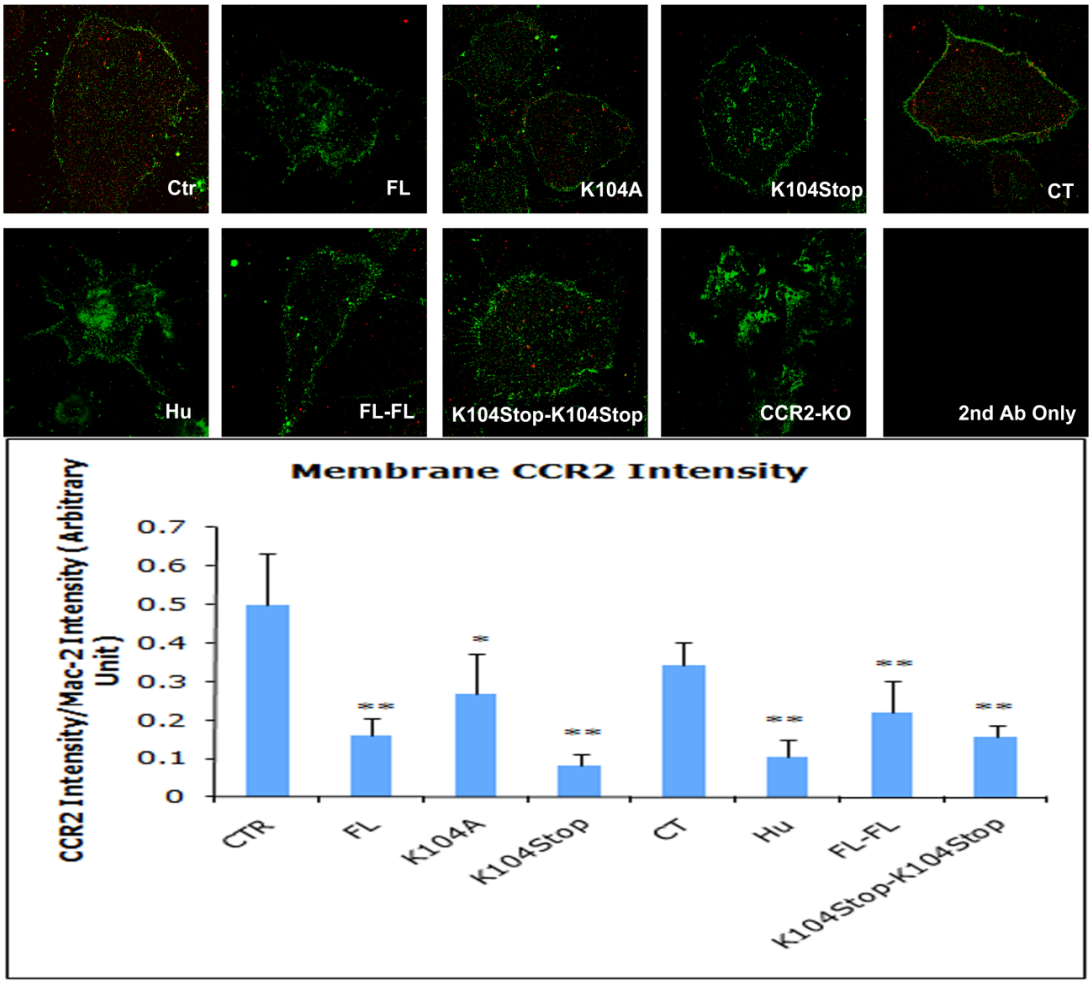

Figure 2-6. Plasmin-truncated MCP1 has much higher chemotactic potency and the chemotactic activity depends on Rac1. Primary microglia from wild-type or CCR2$^{-/-}$ mice were plated and evaluated for chemotaxis in response to recombinant MCP1 proteins, in the presence or absence of the Rac1 inhibitor NSC23766. Each experimental condition was assayed in triplicate. Data are expressed as Mean ± SD. **, p<0.01.

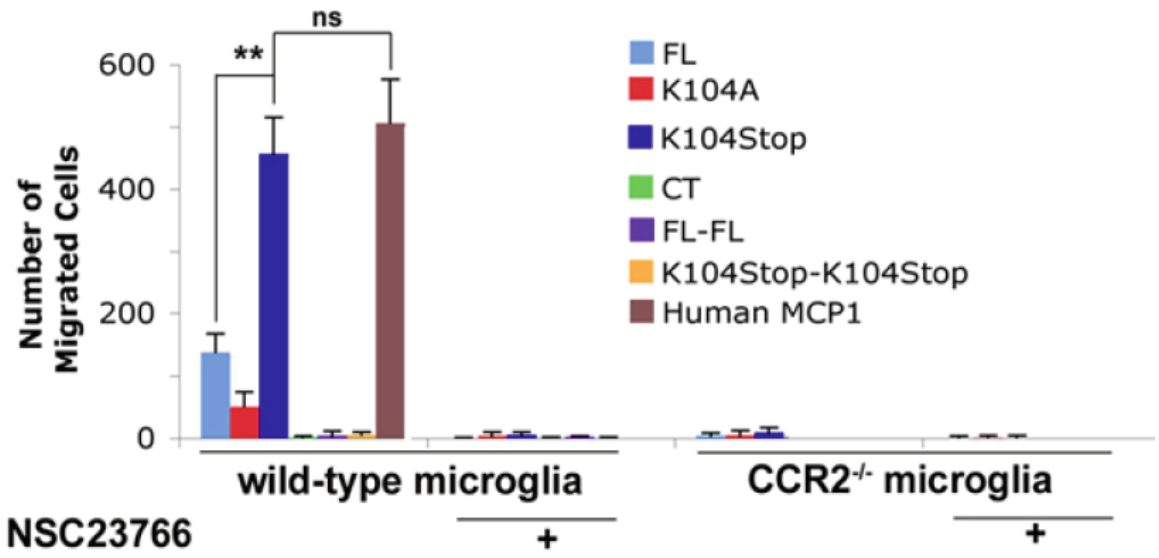

Figure 2-7. Plasmin-truncated MCP1 activates Rac1. N9 microglial cells were treated with 10nM MCP1 over time. The activated Rac1 was immunoprecipitated using GST-PBD beads. At each time point, the activated and total Rac1 were detected by western blotting. **A.** Representative western blots of activated and total Rac1 (both wild-type and CCR2$^{-/-}$ cells). **B.** Quantification of western blots. For FL-, K104A- and K104Stop-MCP1, the blots were normalized to the 0 time point. Each experimental condition was assayed in triplicate and the data were expressed as Mean ± SD. *, p<0.05, **, p<0.01.

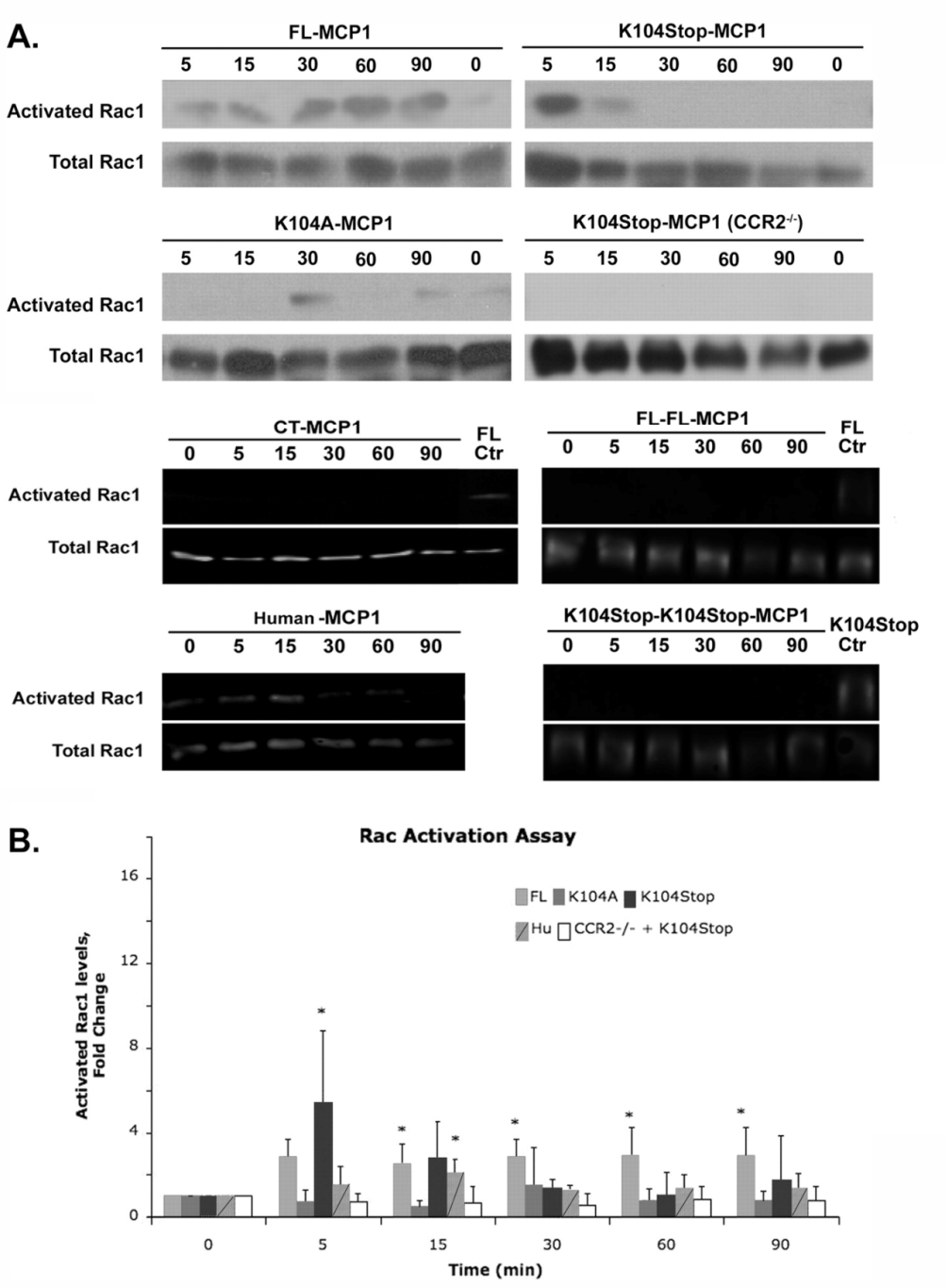

Figure 2-8. Plasmin-truncated MCP1 promotes the formation of lamellipodia. Primary microglia plated on coverslips were incubated with a point source of recombinant MCP1 protein for different periods of time. At each time point, the cells were washed, fixed, and stained for actin cytoskeleton using Alexa-Phalloidin. *Scale bar* = 20 μm. The percentage of unipolar cells (migrating towards the focal point of MCP1 protein, arrows) was quantified. Data are expressed as Mean ± SD. N=8. **p*<0.05.

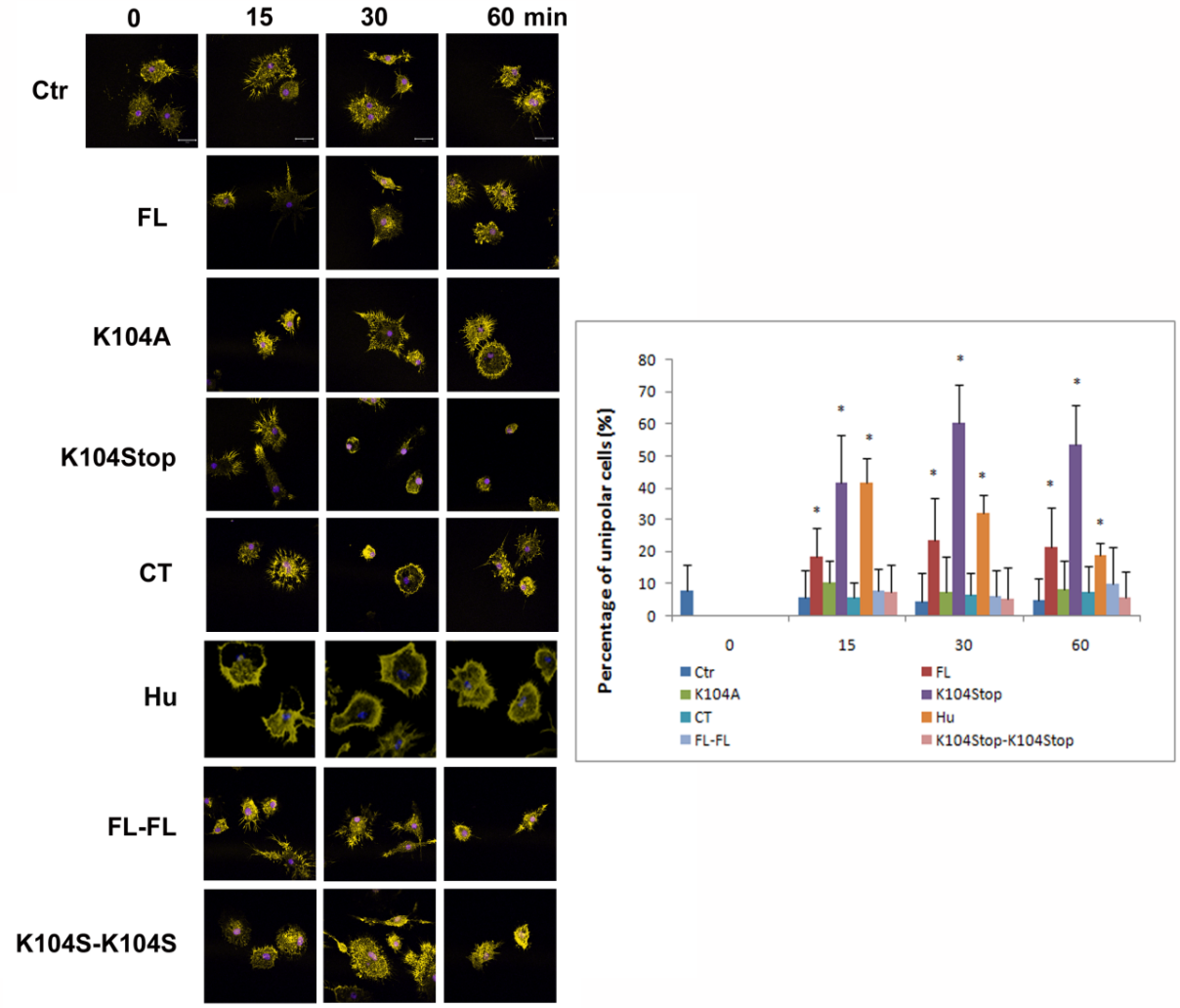

Figure 2-9. Plasmin-truncated MCP1 more potently activates MAPK pathways. Microglial cells were treated with human MCP1 or recombinant mouse MCP1 proteins. At the indicated time points, the cells were lysed and analyzed for phosphorylated and total ERK1/2 by western blotting.

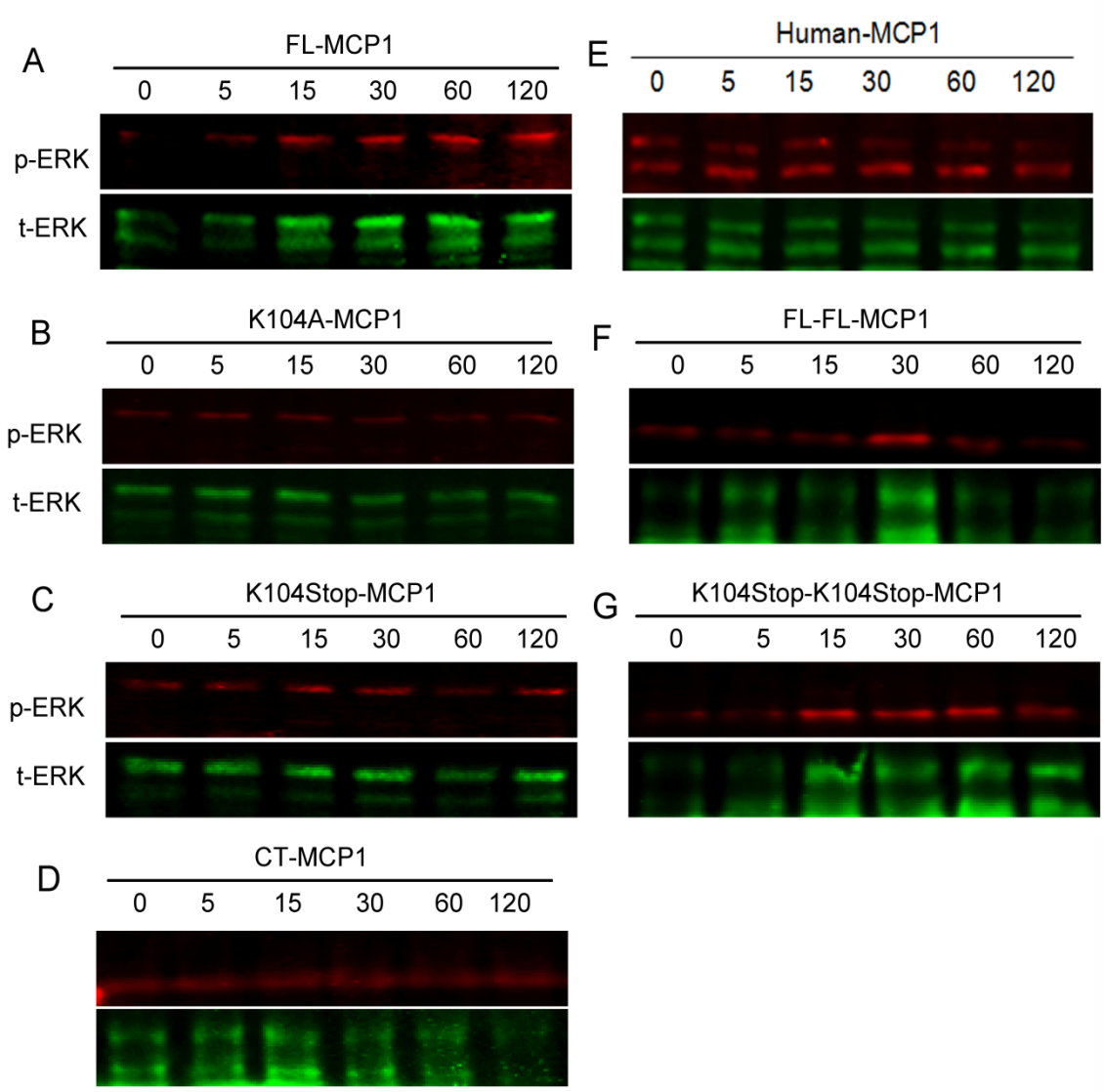

Chapter 3

Truncation of MCP1 By Plasmin Promotes BBB Disruption

INTRODUCTION

Chemokines are a superfamily of structurally related small proteins with strong chemotactic activity. By binding to their specific G-protein-coupled receptors, chemokines induce cell-specific migration and activation of immune cells (Hulkower et al., 1993, Glabinski et al., 1996, Lahrtz et al., 1998, Miller and Meucci, 1999).

MCP1 is highly and transiently expressed in many CNS injuries, including ischemia, hemorrhage and excitotoxic injury (Hanisch, 2002, Dimitrijevic et al., 2006, Frangogiannis et al., 2007, Sheehan et al., 2007, Yan et al., 2007, Capoccia et al., 2008, Kim et al., 2008, Morimoto et al., 2008). We have previously shown that mouse MCP1 can be cleaved by plasmin at Lysine 104 and the truncated MCP1 is more potent than the full-length MCP1 in inducing microglial migration (Sheehan et al., 2007, Yao and Tsirka, 2010) through its receptor CCR2 (Chapter 2).

Besides chemotaxis, MCP1 is also involved in BBB compromise (Stamatovic et al., 2003, Stamatovic et al., 2005, Dimitrijevic et al., 2006, Stamatovic et al., 2006). In this set of experiments we investigated whether plasmin-mediated cleavage regulates MCP1-induced BBB breakdown. It has been reported that components of the plasmin(ogen) system can regulate BBB integrity. Specifically, tPA, which converts inactive plg to active plasmin, promotes BBB disruption and subsequent PBMC infiltration (Reijerkerk et al., 2008), suggesting that plasmin-mediated cleavage of MCP1 may play a role in BBB disruption.

Accumulating evidence shows that MCP1 increases BBB permeability via redistribution of TJP and reorganization of actin cytoskeleton in a CCR2 dependent manner (Stamatovic et al., 2003, Stamatovic et al., 2005, Dimitrijevic et al., 2006, Stamatovic et al., 2006). The molecular mechanisms underlying TJP redistribution, however, are still elusive.

In this study, we show that plasmin-mediated cleavage is critical for fast MCP1-induced BBB compromise. Further mechanistic studies reveal that MCP1-induced redistribution of ZO-1 is mediated by Erzin-Radixin-Moesin (ERM) proteins and reorganization of actin cytoskeleton.

MATERIALS AND METHODS

Generation of 6xHis-tagged MCP1 proteins

FL-, K104A-, and K104Stop-MCP1 were subcloned without the signal peptide into pET vectors with an N-terminal 6xHis tag (Sheehan et al., 2007). CT-MCP1 was subcloned into a pTYB1 vector with an N-terminal 6xHis tag (Yao and Tsirka, 2010). BL21 cells were transformed with these constructs and expression of the target proteins was induced for 5 hours using isopropyl-beta-D-thiogalactopyranoside. Recombinant proteins were purified using a cobalt affinity resin (Clontech, Cambridge, UK) according to the manufacturer's instructions. The column fractions were analyzed on 16% Tris-Tricine SDS-PAGE by coomassie blue staining. The purified proteins were confirmed by immunoblotting using 1:1000 anti-MCP1 antibodies (Serotec and Cell Sciences) or 1:1000 anti-6xHis antibody (Santa Cruz Biotechnology).

Cell Culture

Human BMEC (HBMEC) were kindly provided by Dr. M. Stins (John Hopkins University). The cells were cultured in Dulbecco's modified Eagle's medium (DMEM) supplemented with 10% fetal bovine serum (FBS), 10% NuSerum, 1X Sodium Pyruvate, 1X Nonessential Amino Acid, 1X Vitamin mixtures, 15U/ml Heparin, 30μg/ml ECGS, 100U/ml penicillin and 100μg/ml streptomycin at 37℃ with 5% CO_2.

Mouse BMEC (CRL2299) and mouse astrocyte (CRL2541) cell lines were purchased from ATCC and cultured in DMEM supplemented with 10% FBS, 100U/ml penicillin and 100μg/ml streptomycin at 37℃ with 5% CO_2.

Primary mouse BMEC were isolated and cultured as previously described with minor modifications (Deli et al., 2003, Calabria et al., 2006). Briefly, brains were removed and cut into two hemispheres. The meninges were removed by rolling the hemispheres on sterile Whatman chromatography paper. The cortices were minced and triturated, followed by collagenase (0.7mg/ml) and DNase I (39U/ml) digestion at 37℃ for 1 h. Then the solution was diluted with DMEM and centrifuged at 1000 g for 8 min at 4℃. The pellet was re-suspended in 20% bovine serum albumin and centrifuged at 1000 g for 20 min at 4℃. The pellet was further digested with collagenase/dispase (1 mg/ml), DNase I (39U/ml) at 37℃ for 1 h. Then the solution was diluted with DMEM and centrifuged at 700g at 4℃ for 7 min. The pellet was re-suspended and layered over a 33% continuous Percoll gradient and centrifuged at 1000g for 10 min at 4℃. The microvessel layer was collected using an 18 gauge needle and diluted into DMEM. After centrifuging at 700g for 10 min at 4℃, the pellet was re-suspended in complete culture medium (DMEM supplemented with 20% bovine pletelet-poor plasma-derived serum (Biomedical Technologies Inc.), 100μg/ml heparin, 1ng/ml basic fibroblast growth factor, 4μg/ml puromycin, 100U/ml penicillin and 100μg/ml streptomycin) and plated on type IV collagen (400μg/ml) and fibronectin (100μg/ml) pre-coated plates. The culture medium was changed every 24 h after initial plating. From day 3 after the initial plating, complete culture medium without puromycin was used.

Cytotoxicity Assay

Cytotoxicity was performed using the LDH Detection Kit (Roche) according to manufacturer's instructions. Briefly, mouse BMEC or HBMEC were seeded into 96-well

plate at the density of 1 X 10^4/well and maintained in DMEM with 1%FBS. The next day, the medium was replaced with fresh DMEM+1%FBS and the cells were treated with 100nM FL-, K104A-, K104Stop-, CT-, or human MCP1 overnight. The medium was collected and used to determine LDH levels. Cells treated with 2% Triton X-100 were used as control to determine the maximal LDH release. The data were converted to percentage of maximal LDH release.

TEER Assay

For a simple BBB model, HBMEC were plated in the upper chamber of 0.4μm Transwell inserts. For the co-culture system, mouse astrocytes were plated on the lower side of the 0.4μm Transwell inserts. After 4h, the inserts were inverted and mouse BMEC were seeded in the upper chamber as described (Stamatovic et al., 2005, Dimitrijevic et al., 2006). When the cells reached confluence, 100nM FL-, K104A-, K104Stop-, and CT-MCP1 were added to the lower chambers. After different periods of time, TEER values were measured using the EVOM Epithelial Volt-ohm-meter (World Precision Instruments). The resistance of empty inserts were also measured and subtracted for calculation of final TEER values ($\Omega \bullet cm^2$).

***In vitro* Permeability Assay**

The permeability of BBB was assessed *in vitro* as described previously (Eugenin, 2006). Briefly, HBMEC or the co-culture system was prepared as described above. Sterile Evans blue or FITC-Dextran was added into the upper chamber and 100nM FL-, K104A-, K104Stop-, and CT-MCP1 were added to the lower chambers. At different time

points, 100ul samples from the lower chamber were collected and 100µl fresh medium with 100nM MCP1 was added back to the lower chamber. The collected samples were read at 620nm (for Evans blue dye) or 488nm (for FITC-Dextran) to quantify the concentrations of infiltrated tracers. Empty inserts were used to measure the maximal OD reading, which signifies the complete disruption of the BBB. The OD values were converted to percentage of permeability (%) with respect to the maximal OD reading.

In vivo permeability assay

In vivo permeability assays were performed as described previously with minor modifications (Ohno et al., 1980, Yepes et al., 2003, Parathath et al., 2006, Wu and Tsirka, 2009). Briefly, wild-type (C57BL6, wt), MCP1$^{-/-}$, CCR2$^{-/-}$, and tPA$^{-/-}$ mice were anesthetized by injecting atropine (0.6µg/g of body weight) and avertin (0.02ml/g of body weight) intraperitoneally. A burr hole was then drilled for hippocampal injection at stereotaxic coordinates: -2.5mm posterior to bregma, 1.7mm lateral from midline, and 1.6mm in depth. 1µg FL-, K104A-, K104Stop-, and CT-MCP1 were delivered in 2.5µl saline over 2 minutes. The needle was kept in place for 2 minutes to prevent reflux. 2.5µl saline was injected as a control. 2% Evans Blue was injected into the systematic circulation via the eye. 12 hours after MCP1 injection, the mice were anesthetized again, followed by transcardiac perfusion with PBS to remove the blood from the vessels. Brains were removed, divided into ipsilateral and contralateral hemispheres, and weighed. Each hemisphere was homogenized in PBS supplemented with 0.5% TritonX-100, and centrifuged at 21,000g. Evans blue in the supernatant was calculated as follows: Evans blue= $OD_{620\ ipsi}/W_{ipsi}$-$OD_{620\ cont}/W_{cont}$

Immunofluorescent Staining

HBMEC or Primary BMEC were plated on coverslips and treated with MCP1 as above. After fixed in -20℃ methanol for 10min or in 4% paraformaldehyde for 20 min, the cells were incubated overnight with 1:300 mouse anti-occludin antibody (ZYMED) and 1:300 rabbit anti-ZO-1 antibody (ZYMED) followed by 1:1000 fluorescent anti-mouse or anti-rabbit antibodies (Invitrogen). Next, the cells were washed and mounted on slides using Fluoromount with DAPI. For phalloidin staining, the cells were fixed with 4% paraformaldehyde and stained with 1:30 Alexa-647 phalloidin overnight at 4℃. The stained samples were examined using Zeiss LSM510 confocal microscopy.

Triton X-100 Fractionation

Triton X-100 fractionation was performed as described previously with minor modifications (Fey et al., 1984, Stamatovic et al., 2003, Stamatovic et al., 2005, Stamatovic et al., 2006). Briefly, extracting buffer (10mM Tris pH 7.4, 100mM NaCl, 300mM sucrose, 0.5% Triton X-100 and protease inhibitor cocktail) was added on top of confluent monolayer of HBMEC. Extraction was performed by gently rocking at 4℃ for 20 min. Collected supernatants were defined as the Triton X-100 soluble fraction. The residue of cells, which still adheres to the culture dishes, was washed twice with PBS supplemented with protease inhibitor cocktail, and lysed with radioimmunoprecipitation assay buffer (RIPA buffer, 10mM Tris pH 7.4, 140mM NaCl, 1% sodium deoxycholate, 0.1% SDS, 1% Triton X-100 and protease inhibitor cocktail). Collected supernatants were defined as the Triton X-100 insoluble fraction. Both Triton X-100 soluble and

insoluble fractions were prepared by adding 4X SDS sample loading buffer and heating at 95℃ for 10 min.

Western Blotting

The samples were resolved on SDS-PAGE and transferred to PVDF membranes. Target proteins were visualized using 1:1000 mouse anti-occludin, 1:1000 rabbit anti-ZO-1, 1:1000 rabbit anti-actin antibodies, and 1:500 rabbit anti-phospho-ERM antibody (Santa Cruz), and the densities of the bands were measured using the NIH Image 1.63 software or the LICOR odyssey program.

Coimmunoprecipitation

Cells treated with or without K104Stop-MCP1 were lysed with RIPA buffer. The lysates were incubated with anti-phospho-ERM antibody, anti-ZO-1 antibody, or anti-occludin antibody for 2 hours at 4℃. Then, 25 μl protein A/G agarose beads (Santa Cruz) were added to pull down the immunocomplexes. After incubating at 4℃ for 2 hours, the beads were collected by centrifugation and washed 4 times with PBS. After last wash, 20μl 2X sample loading buffer was added and the resulting protein complexes were immunoblotted with these antibodies and visualized using LICOR odyssey scanner. Total Rac was determined similarly using cell lysates.

Statistics

Results are shown as Mean ± SD. The one way ANOVA followed by Newman-Keuls Multiple Comparison Test was used to analyze difference between two groups.

* indicates $p<0.05$ and ** indicates $p<0.01$.

RESULTS

Truncation by plasmin promotes MCP1-induced BBB compromise

It has been shown that mouse MCP1 increases BBB permeability *in vitro* and *in vivo* (Stamatovic et al., 2005, Dimitrijevic et al., 2006). However it is not known whether plasmin mediated cleavage of MCP1 at K104, which enhances its chemotactic activity (Sheehan et al, 2007), affects MCP1-induced BBB compromise. To address this question, we used four recombinant MCP1 proteins, full length MCP1 (FL), plasmin-noncleavable MCP1 (K104A), constitutively-cleaved MCP1 (K104Stop), and MCP1 C-terminal extension (CT), that we previously characterized (Yao and Tsirka, 2010). First, we evaluated the cytotoxicity of these MCP1 mutants to mouse or human BMEC using LDH cytotoxicity assays. None of the MCP1 mutants was cytotoxic to BMEC (Figure 3-1). Then, we investigated the function of these MCP1 proteins on BBB permeability in a simple *in vitro* BBB model, which only involved HBMEC (Glynn and Yazdanian, 1998, Alter et al., 2003). Although both FL- and K104Stop-MCP1 were found to decrease TEER values significantly, the effect of K104Stop-MCP1 was more dramatic than that of FL-MCP1 (Figure 3-2A) at all timepoints. Consistent with these data, an *in vitro* permeability assay revealed similar results: both FL- and K104Stop-MCP1 increased the permeabilization of Evans blue across the monolayer of HBMEC (Figure 3-2B), indicating a decreased BBB integrity. Since HBMEC have endogenous plasmin expression and activity, we explored the possibility that the decrease in TEER values observed with FL-MCP1 was due to the truncation of MCP1 by endogenous plasmin. To block the endogenous plasmin generated by HBMEC, α_2-antiplasmin (A2AP), a specific

plasmin inhibitor, was used. In the presence of A2AP, addition of FL-MCP1 did not decrease TEER values (Figure 3-2A) and was unable to promote infiltration of Evans blue (Figure 3-2B), suggesting that the effect of FL-MCP1 observed in the initial experiments was due to HBMEC endogenous plasmin activity. Evans blue can cross the BMEC monolayer by both transcellular and paracellular pathways (Hart et al., 1987, Kawedia et al., 2007). The addition of A2AP alone appeared to modify BBB permeability to Evans blue, but not the TEER values. This result suggested that A2AP may affect the transcellular diffusion of Evans blue, although it is not at this point clear why A2AP would have this effect. When we performed the *in vitro* permeability experiment using another tracer, FITC-Dextran (Sigma, MW: 4000 Dalton), which only uses paracellular pathways to go across BMEC monolayer (Kacem et al., 1998, Simard et al., 2003), in the presence of A2AP, only K104Stop-MCP1 was able to enhance significantly the leakage of the tracer across the co-culture system (Figure 3-3), suggesting an important role of plasmin activity in MCP1-induced BBB disruption. Next, we investigated whether there is dose-dependency of the effect of FL- and K104Stop-MCP1 on BBB permeability. As shown in Figure 3-4, the activity of FL-MCP1 increased in a dose-dependent manner reaching a plateau at 100nM. K104Stop-MCP1, on the other hand, was full active even at lower concentrations (50nM). These data suggest that K104Stop-MCP1 is more "active" than FL-MCP1 in this permeability assay.

To better replicate the *in vivo* BBB conditions, we used a mouse BMEC-astrocyte co-culture system, since astrocytes contribute to the impermeability of BBB by covering more than 99% of the microvessels (Kacem et al., 1998, Simard et al., 2003). Consistent with previous data, in the absence of A2AP, FL- and K104Stop-MCP1

reduced TEER values and increased Evans blue infiltration significantly (data not shown), whereas in the presence of A2AP, only K104Stop-MCP1 was effectively compromising the integrity of this *in vitro* BBB (Figs 3-5A,B). These data further support the hypothesis that plasmin-mediated truncation of MCP1 plays a vital role in MCP1-induced BBB compromise.

We investigated the integrity of BBB in wt, $tPA^{-/-}$, $MCP1^{-/-}$, and $CCR2^{-/-}$ mice as *in vivo* the shearing stress effects on BBB are also present. In wt or $MCP1^{-/-}$ mice, both FL- and K104Stop-MCP1 enhanced the diffusion of Evans blue into the brain parenchyma. In the tPA-deficient mice the FL-MCP1 was not as efficient as the K104Stop-MCP1 in driving BBB permeability. Since the absence of tPA results in virtual absence of plasmin activity, the decreased efficiency of FL-MCP1 to compromise the BBB suggests that MCP1-induced disruption of BBB depends on the activity of plasmin. While $MCP1^{-/-}$ mice showed virtually no compromise of the BBB, adding back recombinant MCP1 to them (Figure 3-5C) resulted in significant BBB compromise by both FL- and K104Stop-MCP1. In $CCR2^{-/-}$ mice, on the contrary, none of these MCP1 proteins was able to increase the diffusion of Evans blue from the blood to the brain parenchyma (Figure 3-5C), indicating an indispensable role of CCR2 in MCP1-induced BBB leakage.

Plasmin-mediated truncation of MCP1 promotes redistribution of TJP

Redistribution of TJP has been reported in MCP1-treated BMEC (Stamatovic et al., 2003, Stamatovic et al., 2005, Stamatovic et al., 2006). We further studied whether plasmin-mediated cleavage of MCP1 is involved in this process. Using HBMEC, we

found that FL- and K104Stop-MCP1 disrupted the integrity of occludin distribution on the cell membrane. K104Stop-MCP1 was more potent, in that disruption of BBB was evident from the 30 min time point on (Figures 3-6A, 3-6B showing the 120min timepoint). K104A- and CT-MCP1, on the contrary, did not change the staining pattern of occludin. Similarly, FL- and K104Stop-MCP1 treatment led to punctate ZO-1 staining in the cell border, whereas K104A- and CT-MCP1 treatment minimally affected ZO-1 staining (Figure 3-6A). We also investigated the redistribution of ZO-1 and occludin in primary BMEC and the results were the same as those from HBMEC (Figure 3-6C at the 120 min timepoint).

Next, we quantified the redistribution of TJP via semi-quantitative western blot using Triton X-100 fractions. Consistent with previous reports (Tsukamoto and Nigam, 1997a, 1999a, Stamatovic et al., 2003, Stamatovic et al., 2005, Stamatovic et al., 2006), FL-MCP1 shifted occludin and ZO-1 from the Triton X-100 soluble fraction to Triton X-100 insoluble fraction. K104Stop-MCP1, however, dramatically amplified the changes induced by FL-MCP1. On the contrary, K104A- and CT-MCP1 failed to induce the shift of the TJP (Figure 3-7). Since the effect of K104Stop-MCP1 was more dramatic than that of FL-MCP1, we tested again the possibility that endogenous plasmin generated by BMEC may truncate MCP1, as described for Figure 3-2. In the presence of A2AP the shift of the TJP induced by FL-MCP1 was abrogated, whereas A2AP alone did not affect their distribution (Figure 3-7).

Plasmin-mediated truncation of MCP1 changes actin cytoskeleton

Since MCP1 treatment leads to the redistribution of TJP, which are connected to the actin cytoskeleton directly or indirectly, we examined the reorganization of F-actin in HBMEC over time. FL-MCP1 increased F-actin over time (Figure 3-8A). It peaked at 1 h after treatment and remained stable until the 2 h time point tested. K104Stop-MCP1 treatment led to a significant enhancement of F-actin as early as 15 min after treatment. This effect was even more dramatic at 2-h after treatment. Although K104A- and CT-MCP1 elevated F-actin slightly at early time points, its distribution remained mainly at the cell border. F-actin levels went back to baseline 2-h after treatment (Figure 3-8A). We also treated primary BMEC with various MCP1 proteins for 2 h. Consistently, FL-MCP1 increased F-actin expression in the cells, compared with that in untreated cells. K104Stop-MCP1 treatment resulted in a dramatic enhancement of the intensity of F-actin (Figure 3-8B). K104A-MCP1 only elevated F-actin staining slightly in the cell border (indicative of the presence of cortical actin), whereas CT-MCP1 had no effect on F-actin levels or distribution (Figure 3-8B). Quantification of the intensity of F-actin fluorescence is shown in Figure 5C. Although K104A also significantly increased F-actin intensity, the effect was limited to the cell border (see Figure 3-8B). Compared with FL-MCP1, K104Stop-MCP1 more efficiently enhanced F-actin (Figure 3-8C). These results further support the hypothesis that plasmin-mediated truncation is necessary for MCP1-induced BBB compromise.

Plasmin-truncated MCP1 induces phosphorylation of ERM proteins

In an effort to understand how TJP are redistributed during BBB compromise, we focused on the ERM proteins (ezrin/radixin/moesin), a family of highly conserved

proteins that serve as a linker between plasma membrane and the actin cytoskeleton (Louvet-Vallee, 2000). These proteins have two states: a dormant state (located in cytoplasm) and an active state (located just beneath the plasma membrane) (Louvet-Vallee, 2000). The activation process involves post-translational and conformational changes. It has been shown that phosphorylation on a conserved threonine residue (Thr567 for ezrin, Thr564 for radixin, and Thr558 for moesin) suppresses the intramolecular interaction between N-terminus and C-terminus of ERMs and promotes their subsequent conformation change (Bretscher et al., 1995, Louvet-Vallee, 2000, Pearson et al., 2000), such as the N-terminus interacts with membrane proteins, e.g. CD44, (Tsukita et al., 1994), CD43 (Yonemura et al., 1993), and ICAM-2 (Helander et al., 1996), ICAM-3 (Serrador et al., 1997), and the C-terminus interacts with actin cytoskeleton (Turunen et al., 1994, Nakamura et al., 1995, Pestonjamasp et al., 1995, Matsui et al., 1998). Here, we investigated whether activation of ERM proteins is involved in MCP1-induced BBB disruption. Using a phospho-specific antibody, we found that FL- and K104Stop-MCP1 significantly enhanced phosphorylation of ERM proteins over time (Figure 3-9), suggesting that phosphorylation of ERM proteins is involved in the MCP1-induced BBB compromise. In the presence of A2AP, however, FL-MCP1 failed to induce phosphorylation of ERM proteins, suggesting that plasmin-mediated truncation of MCP1 plays a crucial role.

Plasmin-truncated MCP1 promotes interaction between phosphorylated ERM proteins and ZO-1

Since K104Stop-MCP1 induced phosphorylation of ERM proteins, we next asked

whether the N-termini of ERM proteins interact with TJP. By performing coimmunoprecipitation experiments we found that in the absence of MCP1, phosphorylated ERM proteins did not interact with ZO-1 (Figure 3-10). Treatment of endothelial cells with K104Stop-MCP1 for 1 hour, however, promoted interaction between phosphorylated ERM proteins and ZO-1 (Figure 3-10). Occludin, on the other hand, failed to interact with phosphorylated ERM proteins, suggesting the redistribution of occludin may not regulated through ERM proteins.

DISCUSSION

BBB is a unique structure that separates the CNS from the peripheral nervous system. It is mainly comprised of BMEC, pericytes and astrocytes (Guillemin and Brew, 2004). BMEC, which connect to each other by TJP, form the primary barrier. Astrocytes, which cover more than 99% of the microvessels via their endfeet, confer a secondary barrier to BBB (Kacem et al., 1998, Simard et al., 2003). Here we used two different *in vitro* BBB models to assess the effect of plasmin on MCP1-induced BBB compromise. In both models, we found that the constitutively active K104Stop-MCP1 was functional in increasing BBB permeability, suggesting that the activation of MCP1 by plasmin is indispensable for MCP1-induced BBB compromise.

Although the *in vitro* systems replicate some of the anatomical structures of BBB, they lack the shear stress, which plays an important role in maintaining the dynamic properties and integrity of BBB. Similar results were obtained *in vivo*, when the Evans Blue permeability assay was performed in wt and $MCP1^{-/-}$ mice. However, the effect was more potent in $MCP1^{-/-}$ mice than in wt mice. It has been shown that MCP1 binds to and reduces membrane CCR2 levels (probably via endocytosis) (Jung et al., 2009) (Yao and Tsirka, 2010). The dramatic change observed in $MCP1^{-/-}$ mice could be due to higher membrane CCR2 density, as in the absence of MCP1 there would be no recycling of CCR2 off the plasma membrane. To examine whether plasmin activity is indispensable, we also conducted experiments in mice deficient for tPA ($tPA^{-/-}$). As expected, only K104Stop-MCP1 was functional in $tPA^{-/-}$ mice. $CCR2^{-/-}$ mice were used as negative controls. Consistent with previous reports that $CCR2^{-/-}$ mice were resistant

to MCP1-induced BBB compromise, none of these MCP1 disrupted BBB integrity in these mice, suggesting that MCP1 exerts its BBB-compromising effect solely via CCR2.

Stamatovic and colleagues showed that loss of CCR2 on astrocytes did not affect MCP1-induced BBB disruption in the BMEC-astrocyte co-culture system, whereas loss of CCR2 on BMEC significantly decreased BBB permeability (Stamatovic et al., 2005), suggesting that MCP1 exerts its function by binding to CCR2 on BMEC. To maintain the stability of the microenvironment in the brain, BMEC connect to each other via TJ, where a lot of adhesion molecules, such as TJP, bind to each other, sealing the intercellular gaps. This structure makes the permeability highly dependent on the expression and localization of TJP. Our immunofluorescence data showed that plasmin-truncated MCP1 disrupted occludin and ZO-1 staining in the borders of HBMEC, suggesting a disruption of TJ structure. Since TJ disassembly involves formation of large protein complexes and increased association of TJP with actin cytoskeleton, which is Triton X-100 insoluble, we utilized detergent extractability to analyze the integrity of BBB biochemically. Semi-quantitative western blot revealed a shift of occludin and ZO-1 from Triton X-100 soluble fraction to insoluble fraction. Although connected to the actin cytoskeleton directly or indirectly, TJP are not normally affixed to it, which allows them to be extracted mostly in a Triton X-100 soluble fraction. The translocation from Triton X-100 soluble fraction to insoluble fraction supports the compromise of TJ structures, suggesting that truncated MCP1 induces BBB disruption via redistribution of TJP. Consistently, we found that K104Stop-MCP1 significantly enhanced stress fiber formation in endothelial cells, suggesting reorganization of actin skeleton. These data suggest that upon MCP-1 binding to endothelial CCR2, a property

that all MCP-1 mutants (that retain the N-terminal portion of the protein) exhibit, an increase in cortical actin is observed. However, the next step of the process, which is the internalization of CCR2 and re-arrangements of actin cytoskeleton to allow the cells to retract/reorganize the TJP is taking place only in the FL- and K104Stop MCP-1 active mutants (Stamatovic et al., 2005).

The redistribution of TJP, which leads to gap formation between endothelial cells, and the reorganization of actin cytoskeleton, which promotes the formation of contractile forces, have been shown to cause the compromise of BBB integrity, the mechanisms underlying the shift of TJP are not clear. It is thought that a phosphorylation event contributes to the translocation of TJP (Farshori and Kachar, 1999, Clarke et al., 2000a, Hirase et al., 2001, Ward et al., 2002, Stamatovic et al., 2003, Stamatovic et al., 2006). The kinases responsible for the phosphorylation involve members of PKC family and Rho (Stamatovic et al., 2003, Stamatovic et al., 2006), although it is not clear how phosphorylation of TJP leads to their subcellular redistribution. MCP1 has been shown to activate Rho associated kinase via Rho A in endothelial cells (Stamatovic et al., 2006). A substrate for Rho associated kinase is myosin light chain phosphatase (MLCP), whose function opposes that of myosin light chain kinase (MLCK) (Hicks et al., 2010), which phosphorylates myosin light chain (MLC) and promotes actin-myosin contraction, (Stephan and Brock, 1996, van Nieuw Amerongen et al., 2000, Stamatovic et al., 2003, Hicks et al., 2010). Our data clearly show that the presence of MCP1 leads to increased phosphorylation of ERM proteins, which subsequently bind to ZO-1 and the actin cytoskeleton (Figure 3-11). We think that by binding to CCR2, MCP1 activates intracellular kinases, which induce phosphorylation of ERM proteins, leading to their

conformation change. The phosphorylated ERM proteins then bind to ZO-1 and actin cytoskeleton. In addition, MCP1 also activates RhoA, which further activates Rho associated kinase (Stamatovic et al., 2006). The kinase is expected to phosphorylate the regulatory subunits of MLCP, and inhibit phosphatase activity. The effect of MLCK would outweigh that of MLCP, resulting in increased phosphorylation of MLC, which would cause enhanced and prolonged actin-myosin contraction. The contraction pulls ZO-1 away from TJ and leads to disruption of BBB integrity. It should be noted, however, that the phosphorylated ERM proteins do not interact with occludin upon MCP1 treatment, suggesting the translocation of occludin is not mediated by ERM proteins. Whether there is another ERM-like protein that mediates shift of occludin or if the redistribution of occludin is mediated by other mechanisms is unclear.

Besides MCP1, many other cytokines, including IL-1, IL-4, IL-8, IL-10, IL-13, TNF-α, IFN-γ (Ross and Joyner, 1997, Wojciak-Stothard et al., 1998a, Yang et al., 1999a, Youakim and Ahdieh, 1999, Blamire et al., 2000a, Ahdieh et al., 2001, Coyne et al., 2002, Paul et al., 2003) have been shown to change the structure of TJ and promote the formation of stress fibers in epithelial and endothelial cells. Whether these molecules induce BBB compromise using the same signaling pathways is not clear, however, based on the conserved function and high expression level of ERM proteins in epithelial and endothelial cells, we would assume the same signaling pathways are activated upon the cytokine treatment.

Our work suggests that: 1. Plasmin-mediated truncation of MCP1 is indispensable for MCP1-induced BBB compromise. 2. The mechanisms involve reorganization of actin cytoskeleton and redistribution of TJP. 3. The redistribution of

ZO-1 is mediated by ERM proteins. However, which kinase(s) phosphorylates ERM proteins and what mediates the redistribution of occludin need further investigation.

Figure 3-1. MCP1 mutants were non-toxic to mouse BMEC or HBMEC. Mouse BMEC or HBMEC were treated with MCP1 mutants or saline for 24 hours. Media were collected and used for LDH assays. **A.** Cytotoxicity of MCP1 mutants to mouse BMEC. **B.** Cytotoxicity of MCP1 mutants to HBMEC. Data are shown as mean ± SD (n=3).

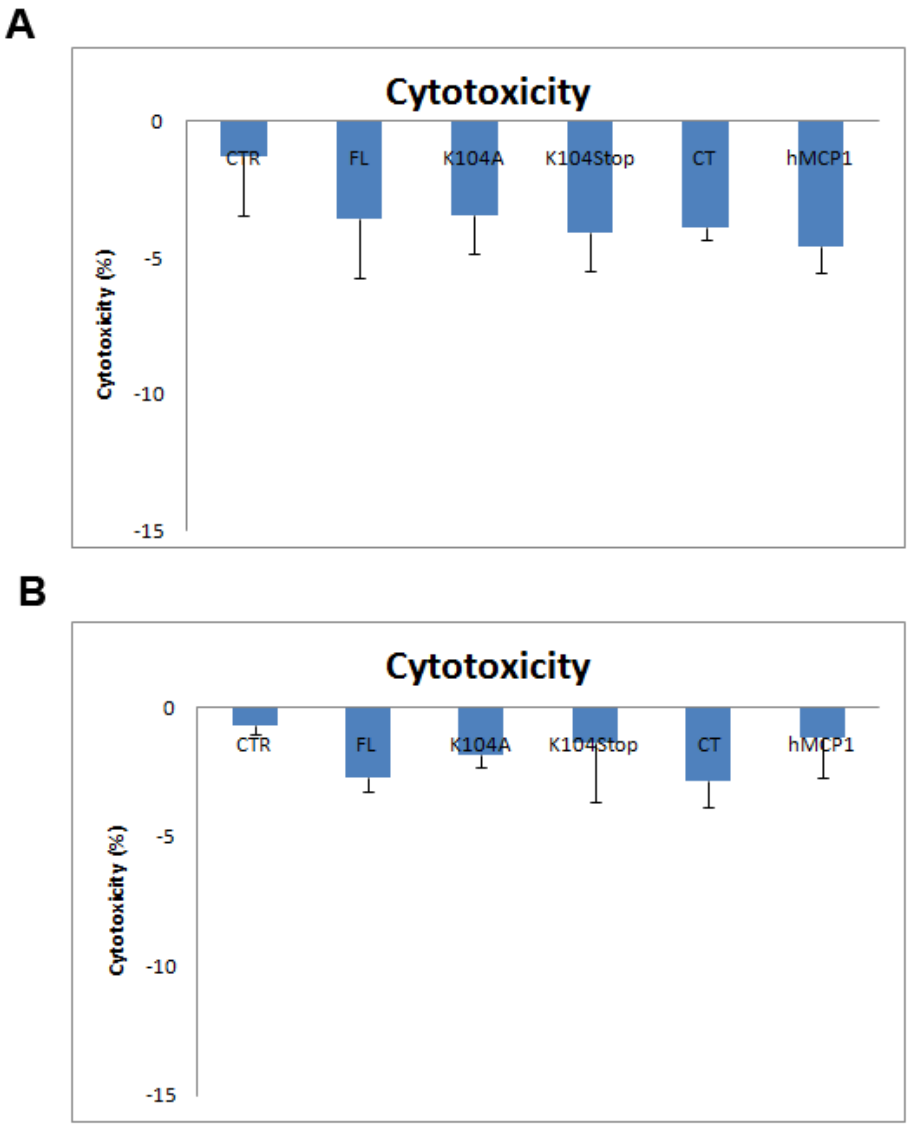

Figure 3-2. Truncated MCP1 compromises the integrity of the HBMEC monolayer. HBMEC seeded in Transwell inserts were treated with the indicated form of MCP1 (100 nM; in the lower chamber, abluminal side) in the presence or absence of A2AP. Ctr, control (saline). **A.** Changes in the TEER over time. Results are means ± s.d. (*n*=3). **P*<0.05 (analyzed using one-way ANOVA followed by Newman–Keuls multiple comparison test) compared with results with FL-MCP1 without A2AP. **B**. Changes in the permeability of Evan Blue over time. Results are means ± s.d. (*n*=6). **P*<0.05 (comparison with Ctr).

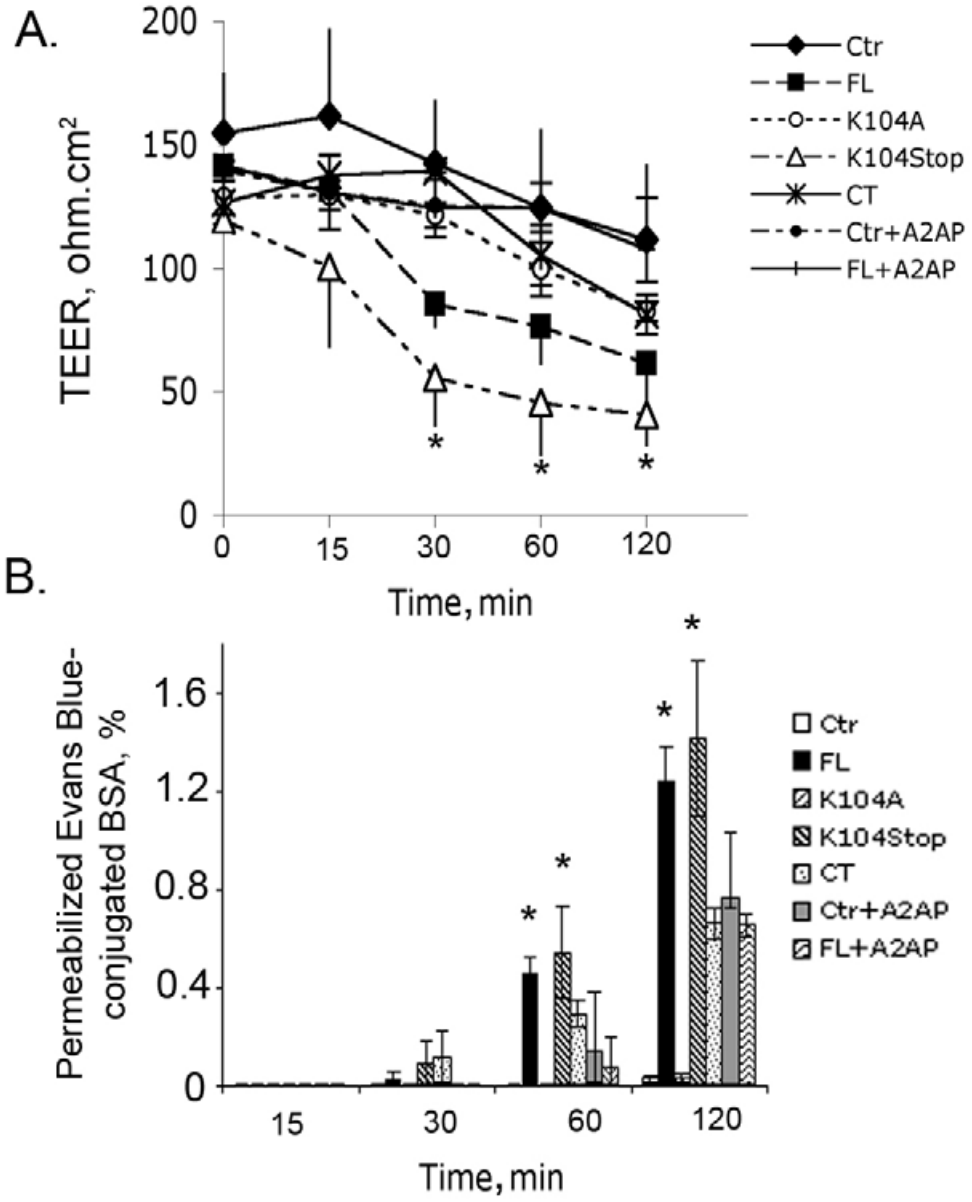

Figure 3-3. Truncated MCP1 compromises BBB integrity. 100 nM MCP1 was added to the lower chamber of the BMEC-astrocyte co-culture system. FITC-Dextran was added to the upper chamber of the co-culture system. In the presence of A2AP, the leakage of FITC-Dextran across the co-culture system was determined by quantifying the fluorescence intensity in the lower chamber. Values are mean ± SD (n=3). Analysis was done by using student's t-test. Compared with FL, *p<0.05.

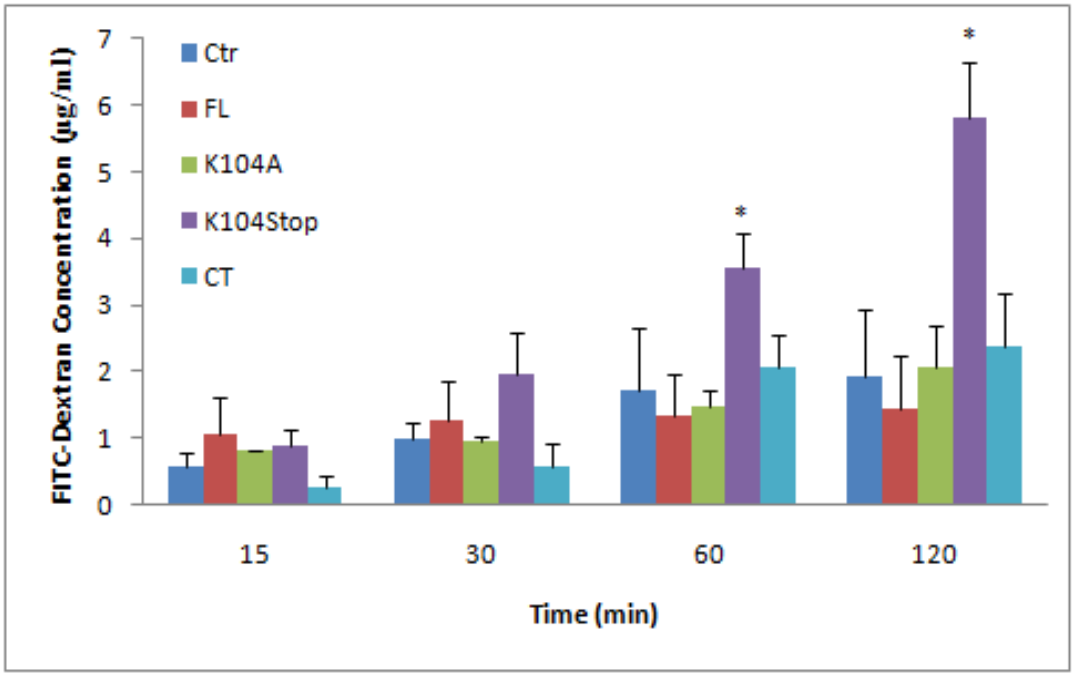

Figure 3-4. Dose-dependent effect of FL- and K104Stop-MCP1. 10, 50, 100nM FL- and K104Stop-MCP1 were added to the lower chamber of the BMEC-Astrocyte co-culture system. FITC-Dextran was added to the upper chamber of the co-culture system. After 1 hour, the leakage of FITC-Dextran across the co-culture system was determined by quantifying the fluorescence intensity in the lower chamber. Values are mean ± SD (n=3). Analysis was done using Student's t-test. Compared with FL, *p<0.05.

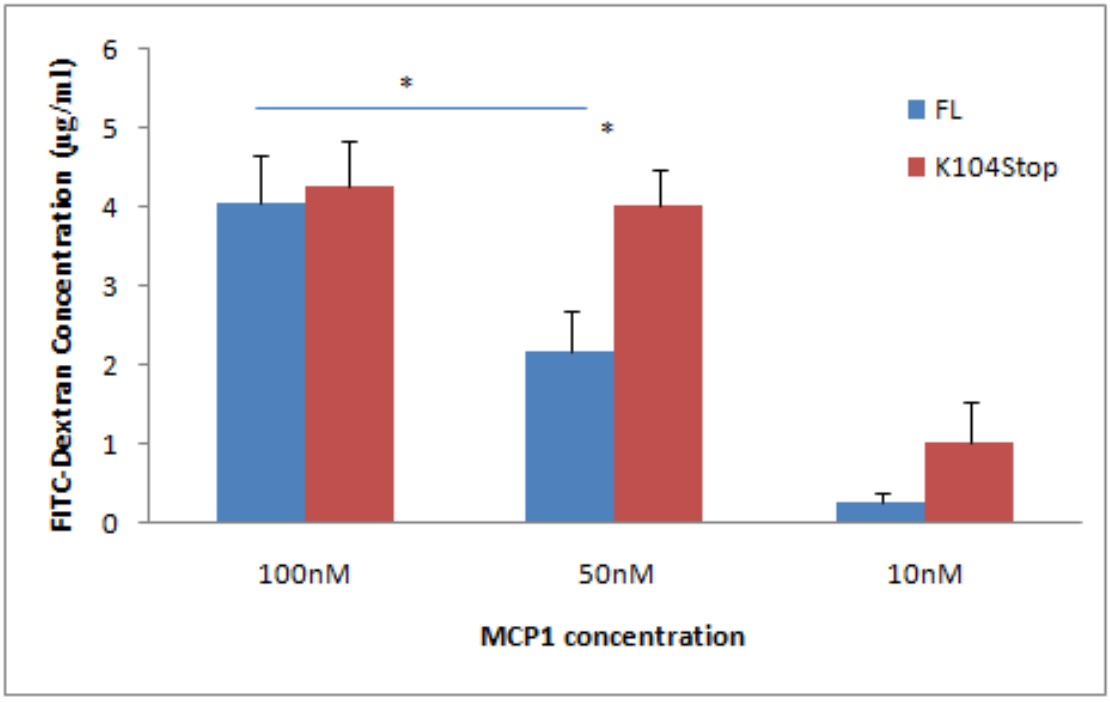

Figure 3-5. Truncated MCP1 compromises BBB integrity. **A**. The indicated form of recombinant MCP1 (100 nM) was added to the lower chamber of the BMEC-astrocyte co-culture system. TEER values were determined over time in the presence of A2AP. Results are means ± s.d. (*n*=3). Ctr, control (saline). **B**. Cells were treated as in A. The leakage of Evans Blue across the co-culture system was determined spectrophotometrically after treatment with A2AP. Results are means ± s.d. (*n*=4). **P*<0.05 (analyzed using one-way ANOVA followed by Newman–Keuls multiple comparison test) compared with results with FL-MCP1. **C**. Infiltration of Evans Blue across the compromised BBB into brain parenchyma was assayed 12 hours after a single injection of MCP1 (1 µg). Mice injected with saline were used as control. Results [OD (optical density; absorbance) per g of body weight] are means + s.d. (*n*=4). **P*<0.05 (analyzed using one-way ANOVA followed by Newman–Keuls multiple comparison test) compared with results with FL-MCP1 without A2AP.

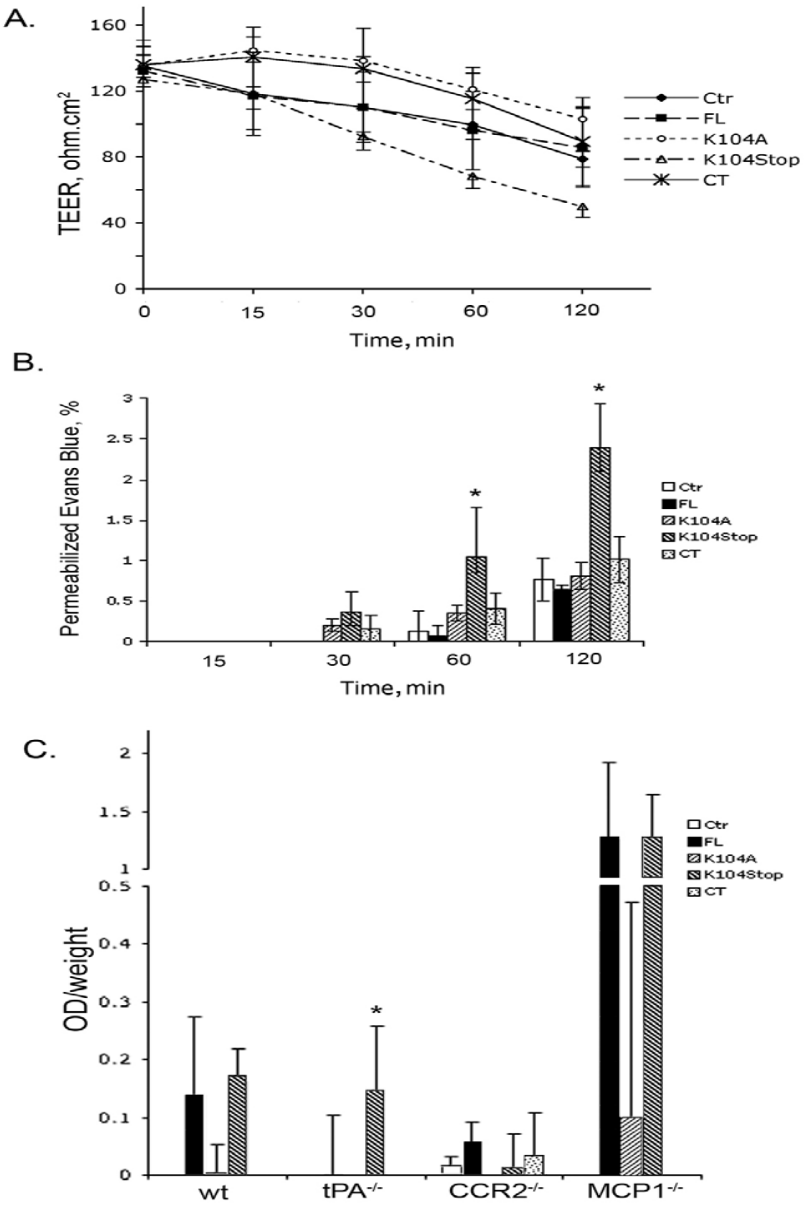

Figure 3-6. Truncated MCP1 induces the redistribution of TJP. **A.** HBMEC were treated with the indicated form of MCP1 (100nM). Ctr, control (saline); WT, wild-type. At 15, 30, 60 and 120 minutes after treatment, the cells were fixed and immunostained for occludin and ZO-1. **B.** Higher magnification of cells incubated with the MCP-1 variants and stained for occludin at the 120-minute timepoint. Scale bar: 15 µm. **C.** Primary mouse BMECs were exposed to the MCP1 variants (100nM) for 2 hours. Then, the cells were fixed and immunostained for ZO-1 and occludin. Blue, DAPI staining.

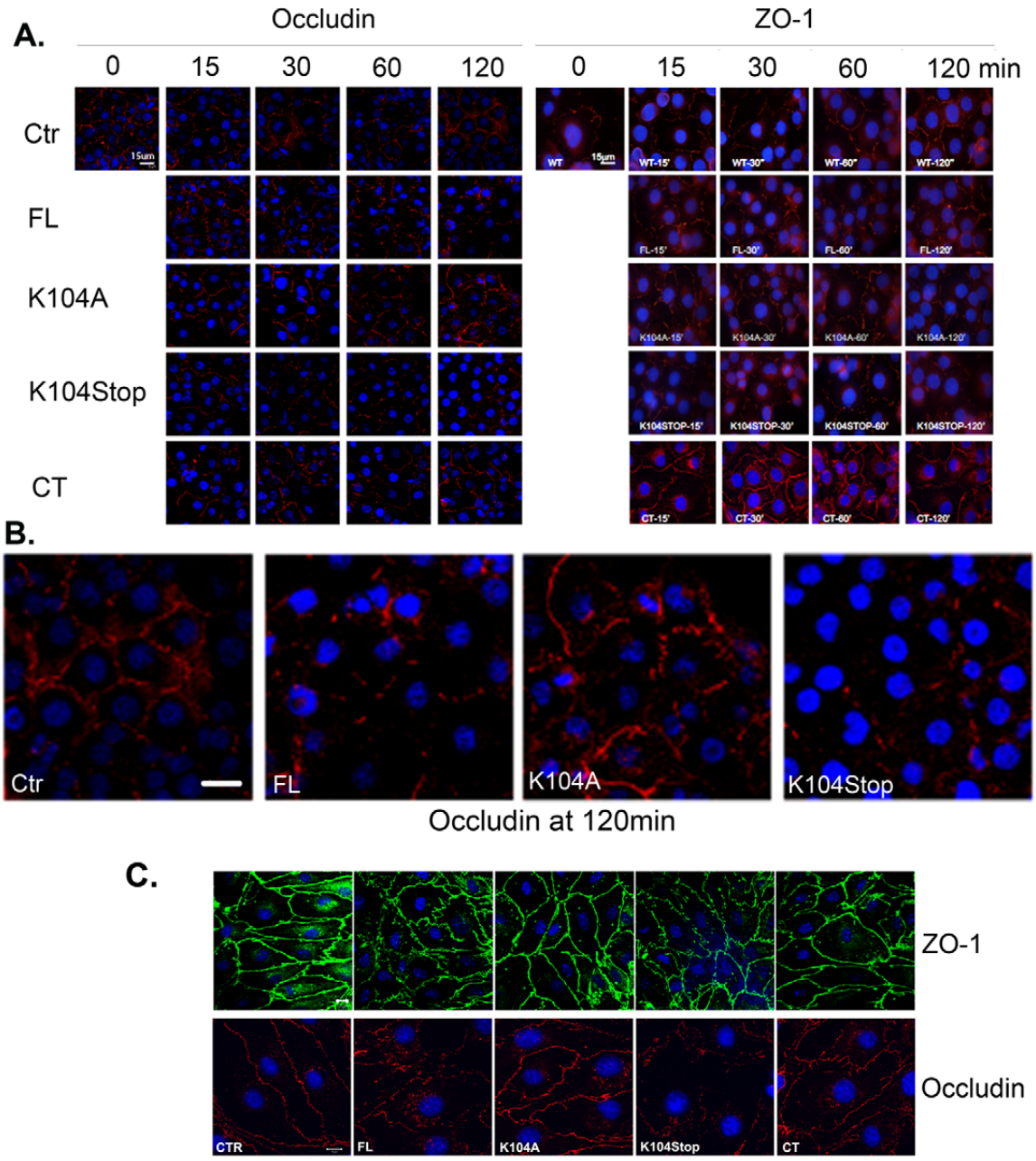

Figure 3-7. Truncated MCP1 shifts TJP from the Triton-X-100-soluble fraction to the Triton-X-100-insoluble fraction. HBMEC were exposed to the indicated form of MCP1 (100nM) for different periods of time in the presence or absence of A2AP. Ctr, control (saline). The shift of occludin and ZO-1 from the Triton-X-100-soluble fraction (S) to the Triton-X-100-insoluble fraction (I) was analyzed by western blotting. Actin was used a loading control. **A.** Representative images of western blots. **B.** Quantitative data from western blots. The intensity of target bands was determined using Scion Image. The intensity of occludin and ZO-1 was normalized to that of actin and the ratios were further normalized to the zero timepoint. Results are means ± s.d. (*n*=3). ***P*<0.01 (analyzed using one-way ANOVA followed by Newman–Keuls multiple comparison test) for K104Stop-MCP1 compared with FL-MCP1 at each timepoint.

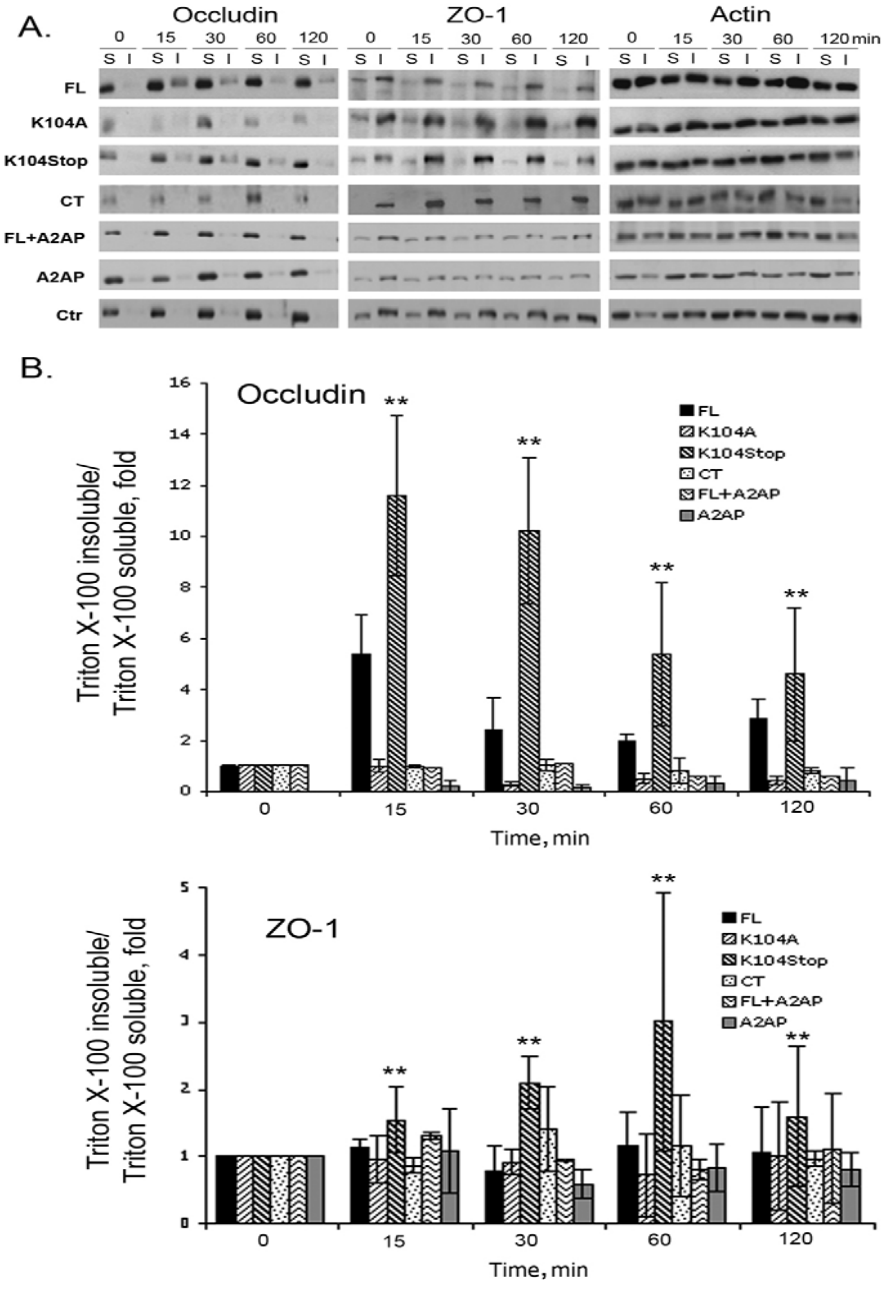

Figure 3-8. Truncated MCP1 promotes reorganization of the actin cytoskeleton. **A.** HBMEC were treated with the indicated form of MCP1 (100nM) for different times, and the actin cytoskeleton was visualized using Alexa-Fluor-647–phalloidin. **B.** Primary mouse BMECs treated with the indicated form of MCP1 (100nM) for 2 hours were immunostained to visualize the actin cytoskeleton. **C.** Quantification of F-actin fluorescence intensity. Values are mean + s.d. (*n*=9). **P*<0.05 (analyzed using Student's *t* tests).

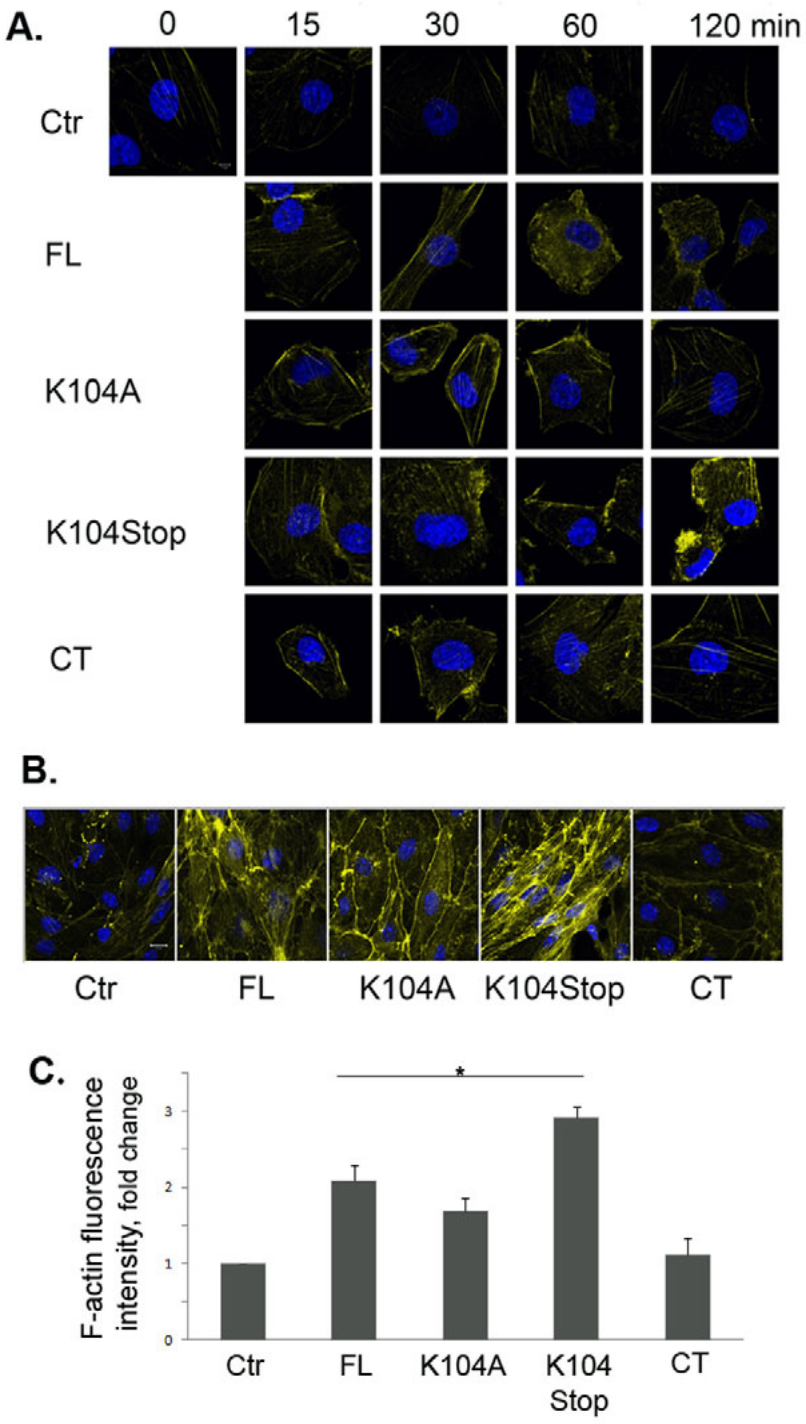

Figure 3-9. Truncated MCP1 induces phosphorylation of ERM proteins. Mouse BMECs were treated with saline (Ctr, control) or the indicated form of recombinant MCP1 proteins (100nM) with or without A2AP over time. The phosphorylated ERM proteins (p-ERM) were determined using a phosphorylation-specific antibody for ERM proteins. The level of total ERM (t-ERM) proteins is also shown. Quantitative data of western blots are shown as mean ± s.d. (*n*=3). **P*<0.05 (compared with the zero timepoint control).

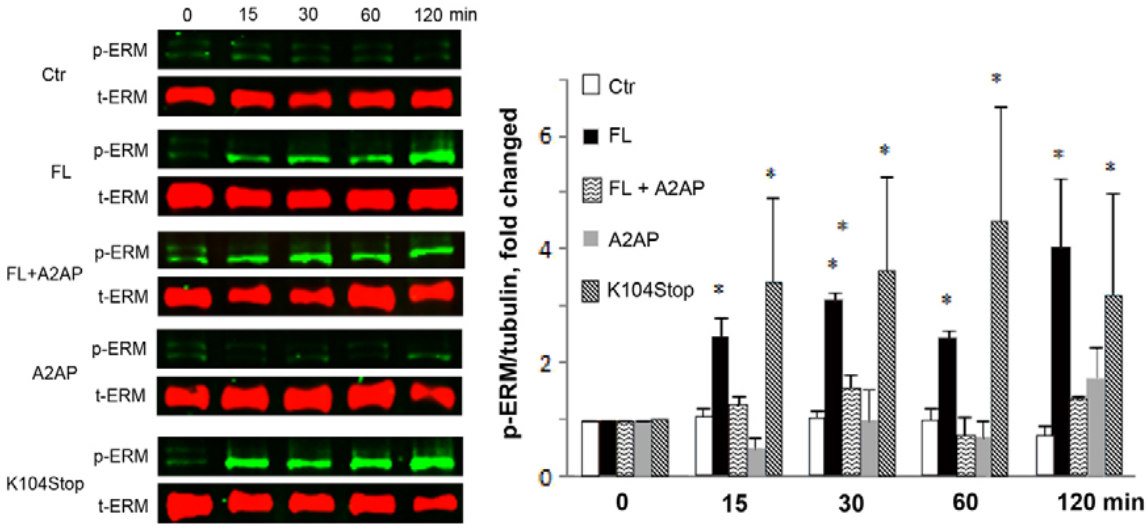

Figure 3-10. Truncated MCP1 promotes interaction between phosphorylated ERM proteins and ZO-1. Mouse BMECs were treated with K104Stop-MCP1 or saline (0 h) for 1 hour. Cell lysates were collected and used for co-immunoprecipitation experiments. **A.** Immunoprecipitation (IP) with an anti-phosphorylated ERM antibody (p-ERM) and immunoblotting (IB) with anti-ZO-1 and anti-occludin antibodies. **B.** Immunoprecipitation with an anti-ZO-1 antibody and immunoblotting with anti-phosphorylated ERM and anti-occludin antibodies. **C.** Immunoprecipitation with an anti-occludin antibody and immunoblotting with anti-phosphorylated ERM and anti-ZO-1 antibodies. Anti-mouse IgG antibody was used as control (Ctr).

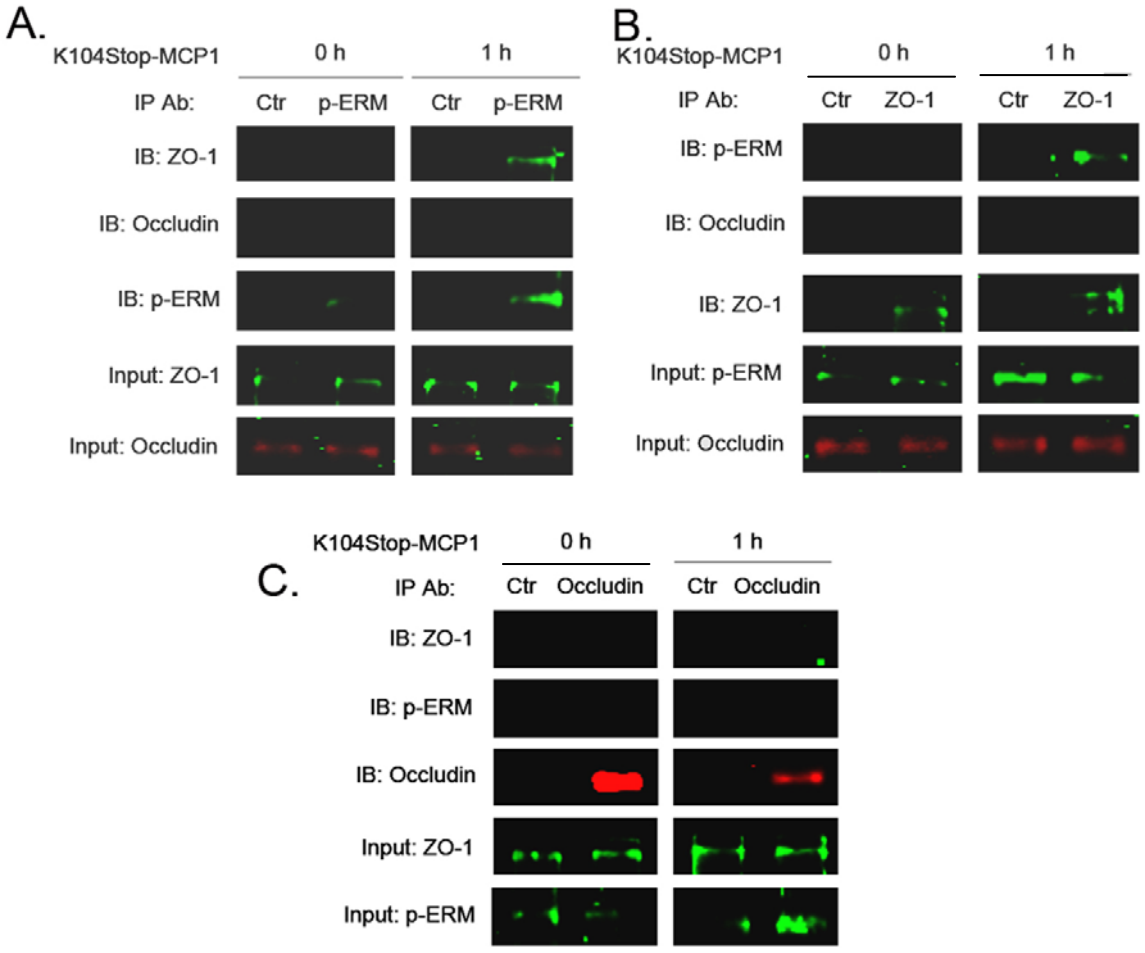

Figure 3-11. Proposed model for MCP1-induced BBB compromise. Upon MCP1 treatment, ERM proteins are phosphorylated by unknown kinases. The phosphorylated ERM proteins then bind to ZO-1 and the actin cytoskeleton. By binding to CCR2, MCP1 also activates RhoA, and Rho-associated kinases, which phosphorylate and inactivate MLCP, leading to enhanced phosphorylation of MLC and thus prolonged actin–myosin contraction. The contractile forces then pull ZO-1 away from the cell-cell border, resulting in a disrupted BBB.

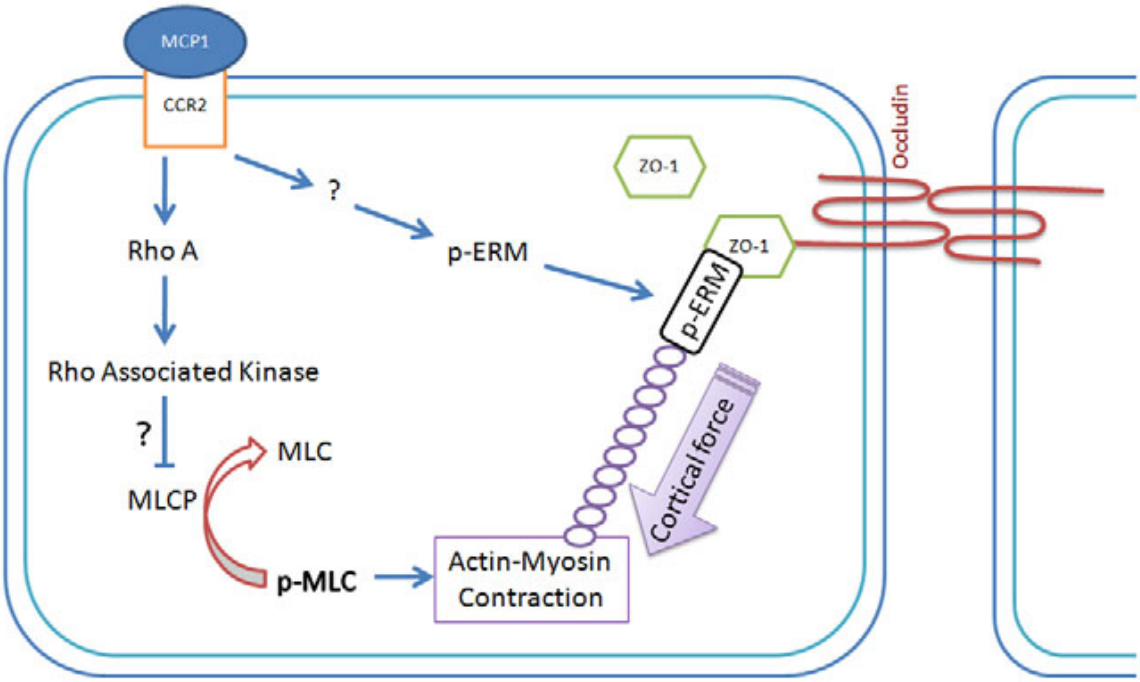

Chapter 4

Mouse MCP1 C-Terminus Inhibits Human MCP1-Induced Chemotaxis And BBB Compromise

INTRODUCTION

When a brain injury occurs, microglia become activated and migrate to the site of injury. The integrity of BBB becomes compromised and peripheral blood cells infiltrate across the disrupted BBB into the brain parenchyma. The activated microglia together with the infiltrated immune cells can affect the outcome of the injury. MCP1 (also known as CCL2) is involved in the chemotaxis of microglia/monocytes (Sheehan et al., 2007, Yao and Tsirka, 2010) and compromise of BBB (Stamatovic et al., 2003, Stamatovic et al., 2005, Dimitrijevic et al., 2006, Stamatovic et al., 2006, Yao and Tsirka, 2011).

Our previous studies revealed that the mouse MCP1 lacking the C-terminus (K104Stop-MCP1) has a much higher chemotactic potency than the full length one (FL-MCP1) (Sheehan et al., 2007, Yao and Tsirka, 2010). Although the C-terminal extension promotes oligomerization of MCP1, it decreases the affinity between MCP1 and its receptor CCR2, inhibits the activation of Rac1 and formation of lamellipodia in microglia (Yao and Tsirka, 2010). In addition, the plasmin-truncated MCP1 disrupted more effectively the integrity of BBB (Yao and Tsirka, 2011). The redistribution of occludin and ZO-1 and reorganization of actin cytoskeleton as well as phosphorylation of ERM proteins are responsible for the compromise of BBB integrity (Stamatovic et al., 2003,

Stamatovic et al., 2006, Yao and Tsirka, 2011). These data suggest that mouse MCP1 is regulated via auto-inhibition by its C-terminus.

In this study we assessed whether the mouse C-terminal extension can exert a regulatory function on human MCP1 by evaluating the functions of a chimeric protein carrying the human N-terminus fused to the mouse C-terminal extension. Our results indicate that such function is indeed mediated by the mouse C-terminal extension, raising the possibility that in the human system another protein or protein complex functions to inhibit a constitutive activity of MCP1.

MATERIALS AND METHODS

Cell Culture

N9 cells (originally provided by Dr. S. Barger at University of Arkansas, Fayetteville and Dr. P. Ricciardi-Castagnoli at University of Milano-Bicocca, Milan) were cultures as described in Chapter 2. CHME3 cells (a human microglial cell line kindly provided by Dr. M. Naghavi, Columbia University, New York) were cultured as described (Haedicke et al., 2009).

Mouse BMEC (CRL2299) and mouse astrocytes (CRL2541) were purchased from ATCC and cultured as in Chapter 3.

Primary microglia were collected from mixed cortical cultures as described previously (Giulian and Baker, 1986, Yao and Tsirka, 2010). The microglia were used immediately (migration assays) or maintained in DMEM with 1% FBS for 2 days (for other experiments).

Primary mouse BMEC were isolated and cultured as described previously (Deli et al., 2003, Calabria et al., 2006, Yao and Tsirka, 2011). The cells were maintained in complete culture medium (DMEM supplemented with 20% bovine pletelet-poor plasma-derived serum (Biomedical Technologies Inc.), 100μg/ml heparin, 1ng/ml basic fibroblast growth factor, 4μg/ml puromycin, 100U/ml penicillin and 100μg/ml streptomycin) and plated on type IV collagen (400μg/ml) and fibronectin (100μg/ml) pre-coated plates or coverslips. The culture medium was changed every 24 h after initial plating. From day 3, complete culture medium without puromycin was used.

Generation of 6xHis-tagged MCP1 proteins

Human-MCP1 (h-MCP1) and human MCP1 with C-terminal extension of mouse MCP1 (hc-MCP1) were subcloned without the signal peptide into pET vectors with an N-terminal 6xHis tag. The constructs were transformed into BL21 cells and expression of the target proteins was induced using IPTG for 5 hours. Recombinant proteins were purified utilizing a cobalt affinity resin (Clontech, Cambridge, UK). The collected fractions were analyzed on 16% Tris-Tricine SDS-PAGE by coomassie blue staining. The purified proteins were confirmed by immunoblotting using 1:1000 anti-MCP1 antibodies (Serotec and Cell Sciences) or 1:1000 anti-6xHis antibody (Santa Cruz Biotechnology).

Western Blot Analysis and Immunoblotting

RIPA buffer (50mM Tris-HCl pH 7.4, 150mM NaCl, 1% NP40, 0.25% sodium deoxycholate, 1mM PMSF, 1x protease inhibitor cocktail, 1x Na3VO4) was used to lyse cells. Lysates containing equal amounts of proteins were resolved in 10% or 15% SDS-PAGE and transferred to Immobilon-P transfer membranes (Millipore). The target proteins were visualized using 1:1000 anti-CCR2, 1:1000 anti-tubulin, 1:1000 anti-Rac1, 1:1000 anti-pERM, 1:1000 anti-pERK, 1:1000 anti-ERK antibodies.

Competitive Binding Assay

The competitive binding assay was performed as previously described (Biber et al, 2003) with minor modifications: CHME3 cells were plated in 96-well plate and incubated with LPS (100ng/ml) for 12 hours. Then, the cells were incubated with 50nM

biotinylated human MCP1 (R&D Fluorokine) with or without increasing concentrations of unlabeled h- or hc-MCP1 for 1 hour at 4℃. This was followed by a 30-minute incubation with FITC-Avidin at 4℃. After extensive wash, the cell-surface FITC signal was captured and quantified by a plate reader (Fluoroskan Ascent, Thermo Electron Corporation). The FITC signaling was then normalized to total protein concentration and expressed as percentage of fluorescence in the absence of unlabeled MCP1.

Rac Activition Assay

Activated Rac was pulled down as previously described (Yao and Tsirka, 2010). Rac activation in stimulated cells was normalized to the amount of activated Rac in control microglia.

Membrane Sheet Assay

This assay was performed as previously described (Yao and Tsirka, 2010).

Immunofluorescent imaging of the F-actin cytoskeleton

To mimic endogenous chemoattractant gradient, a point source of MCP1 was created as previously described (Yao and Tsirka, 2010). In brief, heparin was spotted at the edge of 12-well plates. 15μl of h- or hc-MCP1 was then added directly onto the dried heparin spot. After 1h, primary microglia attached to coverslips were placed in the well. At each time point, the cells were washed and fixed with 4% paraformaldehyde. After washing, the cells were incubated with 1:500 Alexa-488 phalloidin overnight at room

temperature, washed, mounted using FluorMount with DAPI, and imaged using confocal microscopy.

Migration Assay

Migration assays were performed using chemotactic chambers (Boyden; NeuroProbe) as described previously (Yao and Tsirka, 2010). Recombinant h- or hc-MCP1 was suspended in MEM with or without the Rac inhibitor, NSC23766 and added to the bottom chamber. Microglia suspended in MEM (2×10^5/ml) with or without the Rac inhibitor were added to the upper chamber, with a 5.0μm filter inserted between the chemoattractants and microglial cells. Migration was allowed to proceed for 2.5 h at 37℃. After wiping off cells that failed to migrate, the cells that migrated into or through the membrane were fixed and stained with hematoxylin. The membranes were photographed at 100X magnification. Total migration was quantified by counting stained cells. The background for random cell movement (cells responding to MEM only) was subtracted.

TEER Assay

The BMEC-astrocyte co-culture system was constructed as described in Chapter 3 (Stamatovic et al., 2005, Dimitrijevic et al., 2006, Yao and Tsirka, 2011). In brief, astrocytes were seeded on the lower side of the 0.4μm Transwell inserts. After 4 h, the inserts were inverted and BMEC were plated in the upper chamber. 5 days later, 100nM h-, and hc-MCP1 were added to the lower chambers. At each time point, TEER values were measured using the EVOM Epithelial Volt-ohm-meter (World Precision

Instruments). The resistance of empty inserts were also measured and subtracted for calculation of final TEER values ($\Omega \bullet cm^2$).

In vitro Permeability Assay

The leakage of BBB was assessed *in vitro* as described previously in Chapter 3 (Stamatovic et al., 2003, Stamatovic et al., 2005, Stamatovic et al., 2006, Yao and Tsirka, 2011). Briefly, the co-culture system was prepared as described above. Sterile FITC-Dextran (Mw 3000-5000 Dalton) was added into the upper chamber and 100nM h-, and hc-MCP1 were added to the lower chambers. At each time point, 100µl sample from the lower chamber was withdrew and 100µl fresh medium with 100nM MCP1 was added back to the lower chamber. The amount of dextran in the lower chamber was quantified by reading the collected samples at 480nm. The OD values were converted to the concentration of FITC-Dextran in the lower chamber based on a standard curve.

Immunofluorescent Staining

Primary BMEC were plated on coverslips and treated with 100 nM h- or hc-MCP1 for 2 hours. After fixing in 4% formaldehyde for 20min, the cells were incubated with 1:300 rabbit anti-ZO-1 antibody (ZYMED) followed by 1:1000 fluorescent secondary antibodies (Invitrogen). For phalloidin staining, the cells were fixed with 4% formaldehyde and stained with 1:1000 Alexa-488 phalloidin overnight at 4℃. The staining was examined using Zeiss LSM510 confocal microscopy.

Statistics

Results are shown as Mean ± SD. The Student's t-test was used to analyze difference between two groups. *$p<0.05$ was considered significant.

RESULTS

Plasmin cleaves off the mouse MCP1 C-terminus from the chimeric MCP1 protein

A recombinant human MCP1 (h-MCP1) and a chimeric protein consisting of the human MCP1 sequence fused with the C-terminal extension of the mouse MCP1 (hc-MCP1) were generated. To test whether these MCP1 proteins can be cleaved by plasmin, they were incubated with the protease for 2h at 37˚C. Treatment of hc-MCP1 with plasmin led to degradation of the 18kD intact protein and detection of a 13kD fragment corresponding to h-MCP1. h-MCP1 remained intact despite the treatment with plasmin (Figure 4-1).

The mouse MCP1 C-terminus interferes with the interaction between human MCP1 and CCR2.

We have previously reported that the C-terminus of mouse MCP1 affects the interaction of the rodent chemokine with its receptor CCR2 (Yao and Tsirka, 2010). Similarly we explored whether the C-terminus of mouse MCP1 could also affect the interaction of human MCP1 with CCR2. We assessed the chemokine effect on the total cellular level of CCR2 expressed by mouse and human microglial cells. Our data showed that although h-MCP1 or hc-MCP1 treatment did not affect the total cellular CCR2 levels (Figure 4-2), both recombinant proteins decreased membrane bound CCR2 (using the membrane sheet assay); however the effect of h-MCP1 was much more potent than that of hc-MCP1 (Figure 4-3A), suggesting that the C-terminus of mouse MCP1 interferes with the h-MCP1-CCR2 interaction. This is consistent with the

effect of the C-terminus on the affinity between mouse MCP1 and CCR2 (Yao and Tsirka, 2010).

To further examine the affinity of these recombinant MCP1 proteins for CCR2, we performed a competitive binding assay, as previously described (Biber et al., 2003). We found a significant decrease of FITC signaling in the presence of increasing concentration of h-MCP1 (Figure 4-3B), suggesting replacement of biotinylated MCP1 by unlabeled h-MCP1. On the contrary, hc-MCP1, was not able to replace the bound biotinylated MCP1 even at 25μM (500X) (Figure 4-3B). These data reveal that h-MCP1 has a much higher affinity for CCR2 than hc-MCP1.

The mouse MCP1 C-terminal extension decreases the chemotactic potency of human MCP1

To test whether addition of the C-terminus to human MCP1 affects the chemokine's potency, we performed Boyden chamber migration assays using recombinant h- and hc-MCP1. As shown in Figure 4-4A, h-MCP1 elicited a strong chemotactic response (584±101 cells), whereas hc-MCP1 had only a moderate response (98±41 cells), indicating that the C-terminal tail inhibits the chemotaxis initiated by human MCP1. A similar trend was obtained when the human microglial cell line CHME3 was used to assess the chemotactic potency of the two recombinant proteins (Figure 4-4A right panel).

In the presence of NSC23766, a Rac1 specific inhibitor, on the other hand, neither h- or hc-MCP1 was able to induce the migration of microglia (Figure 4-4A left), thus confirming that Rac is a key player in MCP1-induced migration. The effect of h-

MCP1 vs hc-MCP1 on activated Rac was directly assessed using a Rac activation assay. h-MCP1 treatment led to a transient but dramatic activation of Rac (Rac-GTP), whereas hc-MCP1 was slower in activating Rac, and that only to low levels (Figure 4-4B). This piece of data is consistent with our previous data that mouse MCP1 lacking the C-terminus is able to activate Rac whereas intact mouse MCP1 fails to activate Rac (Yao and Tsirka, 2010). When the activation assay was repeated with the human microglia (Figure 4-4C), once again h-MCP1 activated Rac dramatically, although the activation rate appeared to be slower.

Mouse MCP1 C-terminal extension prevents the formation of lamellipodia

The next step in the migration process following activation of Rac is the formation of lamellipodia (Maghazachi, 2000, Pankov et al., 2005, Terashima et al., 2005). Since mouse MCP1 C-terminus affects human MCP1-induced microglial migration and Rac activation, we further investigated its effect on the formation of lamellipodia. Using the method we described before (Yao and Tsirka, 2010), we created a point source of h- and hc-MCP1 and quantified the percentage of unipolar cells (the cells that are able to migrate). Our data showed that h-MCP1 was able to increase the number of unipolar cells since 15 minutes after treatment and up to 2 hours (Figure 4-5A). This effect diminished over time, although it was still significantly higher than Ctr at 2h time point (Figure 4-5A). It should be noted that this pattern is similar to that of commercial human MCP1 (without 6His tag) (Yao and Tsirka, 2010), suggesting that our recombinant MCP1 proteins are biologically active. Unlike h-MCP1, the effect of hc-MCP1 did not decay over time (Figure 4-5A). Although hc-MCP1 had a much lower effect than h-

MCP1 at 15-minute time point, no difference was found at other time points (Figure 4-5A). Similar to h-MCP1, hc-MCP1 significantly enhanced the number of unipolar cells, compared with ctr (Figure 4-5A). The effect of hc-MCP1 is comparable to that of mouse full length-MCP1 (approximately 20% of unipolar cells) (Yao and Tsirka, 2010), suggesting that the C-terminus of mouse MCP1 affects human MCP1 in the same manner as it does in mouse system. These data suggest that human MCP1 may be regulated in the same way as mouse MCP1---by an unknown protein or protein complex functioning just like the C-terminus of mouse MCP1. We tried to pull down the protein or protein complex using anti-human MCP1 antibody or anti-6His antibody via immunoprecipitation, but it did not work, probably due to the sensitivity of the immunoprecipitation method.

Mouse MCP1 C-terminus promotes a delayed but dramatic activation of ERK

Previous studies in our lab have shown that the C-terminal extension affects mouse MCP1-induced activation of MAPK pathway in microglial cells (Yao and Tsirka, 2010). Thus, we further studied whether it was the same case for human MCP1. Similar to K104Stop-MCP1, h-MCP1 promoted an early but fast activation of ERK (Figure 4-5B). Like mouse FL-MCP1, hc-MCP1 induced a prolonged activation of ERK (starting at 30 minutes and up to 2 hours) (Figure 4-5B). Surprisingly, the effect of hc-MCP1 was much higher than that of h-MCP1 or FL-MCP1 (Yao and Tsirka, 2010), suggesting hc-MCP1 and FL-MCP1 have different functions.

Mouse MCP1 C-terminus abrogates the BBB-disrupting activity of human MCP1

In addition to the chemotactic activity, we also investigated the activity of these recombinant MCP1 proteins to compromise BBB integrity. We used an *in vitro* BBB model by co-culturing BMEC and astrocytes as described previously (Yao and Tsirka, 2011). Since BMEC have endogenous plasmin activity and plasmin cleaves the C-terminus off from the chimeric protein, α2-antiplasmin, a specific plasmin inhibitor, is used in our co-culture system to block the endogenous plasmin activity. Our data showed that h-MCP1 significantly lowered the TEER value (Figure 4-6A), indicating a disruption of BBB integrity. hc-MCP1, however, failed to decrease the TEER (Figure 4-6A). Consistently, h-MCP1 dramatically enhanced the permeability of FITC-Dextran across the *in vitro* BBB, whereas hc-MCP1 failed to do so (Figure 4-6B). These data suggest that the C-terminus of mouse MCP1 is inhibitory to MCP1-induce BBB disruption in human system.

Mouse MCP1 C-terminus prevents the redistribution of ZO-1 and reorganization of actin cytoskeleton induced by human MCP1

It has been reported that mouse MCP1 promotes the compromise of BBB through activation of ERM proteins, which bind to ZO-1 and actin cytoskeleton, and reorganization of actin cytoskeleton, which pulls TJP away from cell-cell border (Yao and Tsirka, 2011). Here we showed that h-MCP1 induced disruption of ZO-1 staining at the cell-cell border of primary BMEC, whereas hc-MCP1 did not changed the staining pattern of ZO-1 (Figure 4-6C upper panels). It has been shown that MCP1 treatment promotes the association of TJP with actin cytoskeleton (Stamatovic, et al, 2003, 2005, 2006, Yao and Tsirka, 2011). We thus extracted Triton X-100 soluble (contains free TJP)

and insoluble (includes actin associated TJP) fractions and performed semiquantitative western blot for ZO-1 and occludin. As shown in Figure 4-7, h-MCP1 induced the shift of ZO-1 and occludin from Triton X-100 soluble fraction to insoluble fraction, suggesting increased interaction between TJP and actin cytoskeleton. hc-MCP1, on the other hand, did not change the distribution of TJP. Consistently, h-MCP1 significantly increased the F-actin in primary BMEC, suggesting reorganization of actin cytoskeleton (Figure 4-6C lower panels). hc-MCP1, on the contrary, had no or little effect on F-actin (Figure 4-6C lower panels). The effect of h- and hc-MCP1 was similar to that of K104Stop-MCP1 and K104A-MCP1 (plasmin non-cleavable mouse MCP1), respectively (Yao and Tsirka, 2011), again suggesting that the C-terminus of mouse MCP1 is inhibitory to human MCP1.

Mouse MCP1 C-terminus inhibits the human MCP1-induced phosphorylation of ERM proteins

Phosphorylation of ERM proteins contributes to the redistribution of TJP induced by mouse MCP1. Previous studies in our lab showed that in the mouse system FL-MCP1 and K104Stop-MCP1 significantly promoted the phosphorylation of ERM proteins, whereas full length MCP1 failed to do so in the presence of A2AP (Yao and Tsirka, 2011), suggesting that the C-terminus of mouse MCP1 prevents the activation of ERM proteins induced by mouse MCP1. Here we showed that in the presence of A2AP, h-MCP1 dramatically enhanced the intensity of p-ERM, whereas hc-MCP1 did not change the intensity of p-ERM bands at various time points (Figure 4-6D). Our data suggest that

the C-terminus of mouse MCP1 is inhibitory to human MCP1-induced activation of ERM proteins.

DISCUSSION

In this set of experiments we find that appending the mouse C-terminus to the human MCP1 protein results in a decrease of the chemotactic potency of human MCP1 and an attenuation of all the signaling events and cellular changes that accompany the chemotactic stimulation. Moreover we find that the ability of the chimeric chemokine to compromise the BBB is decreased as well.

It is puzzling why the human MCP1 lacks this highly glycosylated C-terminus Search of the databases reveals that only the mouse and rat MCP1 carry this C-terminal extension. One possibility is that the function that the rodent MCP1 C-terminus exerts is no longer needed in human system. It has been shown that the mouse MCP1 C-terminus promotes the oligomerization of the chemokine and thus formation of chemoattractant gradient (Hoogewerf et al., 1997, Lau et al., 2004, Wang et al., 2005, Yao and Tsirka, 2010). Mouse MCP1 without the C-terminus, however, is unable to oligomerize (Yao and Tsirka, 2010). Human MCP1, on the other hand, has been demonstrated to form homodimers in physiological concentrations (Zhang and Rollins, 1995). This finding that human MCP1 does not need a C-terminal fragment to form oligomers may be the reason of the absence of this fragment in human MCP1.

Previous studies in our lab have shown that plasmin cleaves the C-terminal extension off mouse MCP1 in the proximity of the MCP1-generating neurons, generating a fragment highly homologous to human MCP1. This cleaved protein, lacking the C-terminus, has increased chemotactic potency towards microglia (Yao and Tsirka, 2010), and enhances MCP1-induced BBB disruption (Yao and Tsirka, 2011),

suggesting that MCP1 activities are finely regulated by plasmin-mediated truncation in mouse system. Since the human MCP1 lacks the C-terminus, it is unclear whether regulation of human MCP1 is necessary, or whether another protein or protein complex may be responsible for such regulation of human MCP1 activities.

Studies on the MCP1 receptor, CCR2, reveal that only one isoform of CCR2 is found in rodent, but two alternatively spiced isoforms exist in human. The two isoforms of human CCR2, CCR2A and CCR2B, have different C-terminal tails (Charo et al., 1994), suggesting that they may activate different intracellular signaling pathways and thus have different functions, although the molecular cascades downstream of CCR2A and CCR2B are still elusive. So it is conceivable that the regulation of the human MCP1 chemotactic potency is mediated by the CCR2 receptor, rather than the chemokine.

It is not uncommon for chemotactic ligands and receptors to exist in different isoforms: two alternatively spliced variants of EphA7 receptor have different C-termini and show distinct activities in the regulation of cell adhesion (Holmberg et al., 2000). Splicing variants of Robo3, which are different in the C-terminus, have also been reported to exert distinct functions (Chen et al., 2008). Therefore it is likely that the regulation of MCP1/CCR2 interaction and chemoattraction in humans lies with receptor CCR2 or an as-for-now unknown regulatory factor.

Figure 4-1. Plasmin cleaves hc-MCP1. Recombinant h- and hc-MCP1 were treated with plasmin for 2 hours at 37℃, then the integrity of these proteins were assessed by western blotting. Experiments were performed in triplicate. Representative experiment shown.

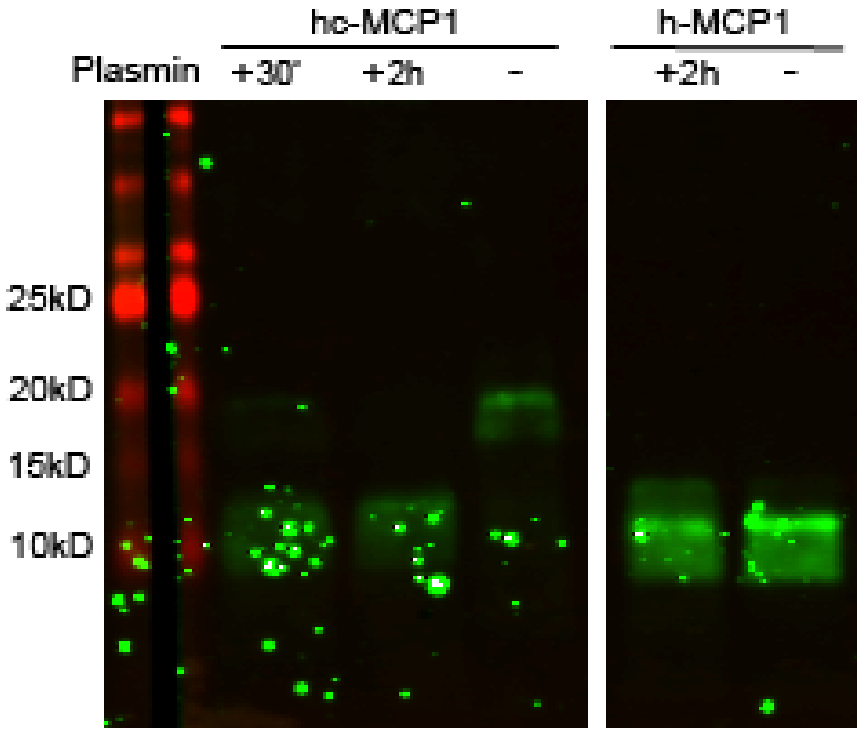

Figure 4-2. Recombinant MCP1 proteins do not change total cellular CCR2 level on microglia over short time periods. Primary microglial cells (top) or the human microglial cell line CHM3 (bottom) were treated with recombinant h- or hc-MCP1 over time and at each time point, cell lysates were collected and assessed for CCR2 and tubulin by western blotting. Experiments were performed in triplicate. Results are shown in the graph for primary microglia as mean ± SD. Representative experiment shown.

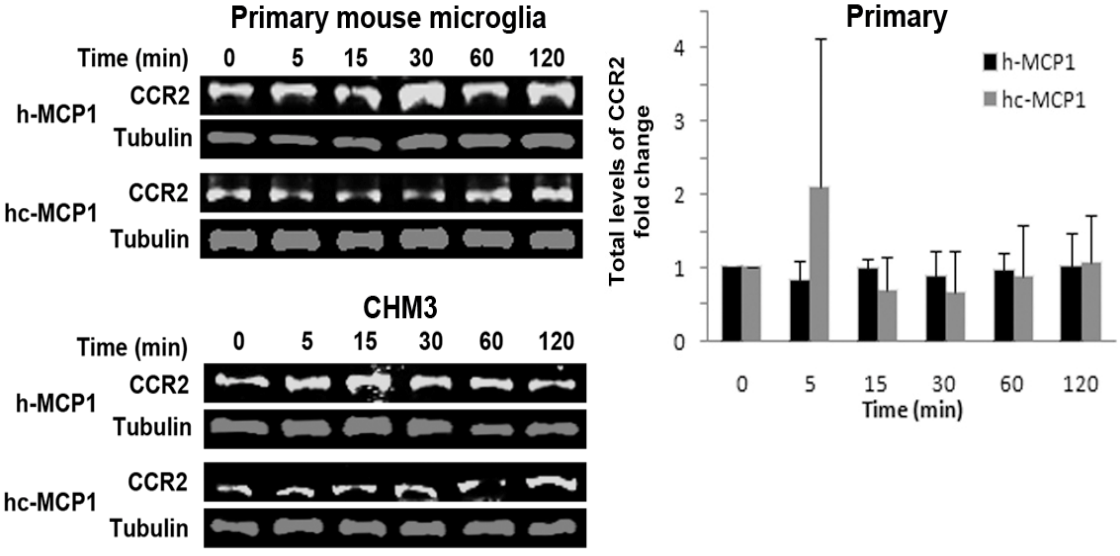

Figure 4-3. **Mouse MCP1 C-terminus decreases the affinity of human MCP1 to CCR2. A.** h-MCP1 decreased membrane-bound CCR2 on microglia. Primary microglia activated overnight with 100ng/ml LPS were treated with saline (Ctr) or 10nM recombinant hMCP1 or hc-MCP1 for 1 h and then swelled in hypotonic buffer for 20 min to cause cell lysis. The plasma membrane sheets that adhered to the coverslips were stained for Mac-2 (Green) to visualize the membrane sheets and CCR2 (Red). Microglia immunostained with secondary antibodies only showed no fluorescence. Scale bar = 5 μm. The fluorescent intensity was quantified using ImageJ program and the fluorescent intensity was normalized to plasma membrane area. 20 cells per condition were used and 3 separate experiments were performed. The results were analyzed using student's *t*-test. *p<0.05. **B.** h-MCP1 has higher affinity for CCR2. Microglia cells (CHME3) were incubated with 50nM biotinylated human MCP1 in the presence or absence of a gradient concentration of unlabeled h- or hc-MCP1 for 1 hour at 4℃. After further incubation with FITC-Avidin for 30 minutes at 4℃, the cells were washed and FITC signal was quantified using a plate reader. Background signal was measured using biotinylated soybean trypsin inhibitor (supplied by R&D) and subtracted from the experimental raw data. Then the FITC signal was normalized to total protein concentration. The final data were expressed as percentage of fluorescence in the absence of unlabeled MCP1. The data were expressed as Mean ± SD (n=4). *p<0.05, compared with Ctr; #p<0.05, comparison between h-MCP1 and hc-MCP1.

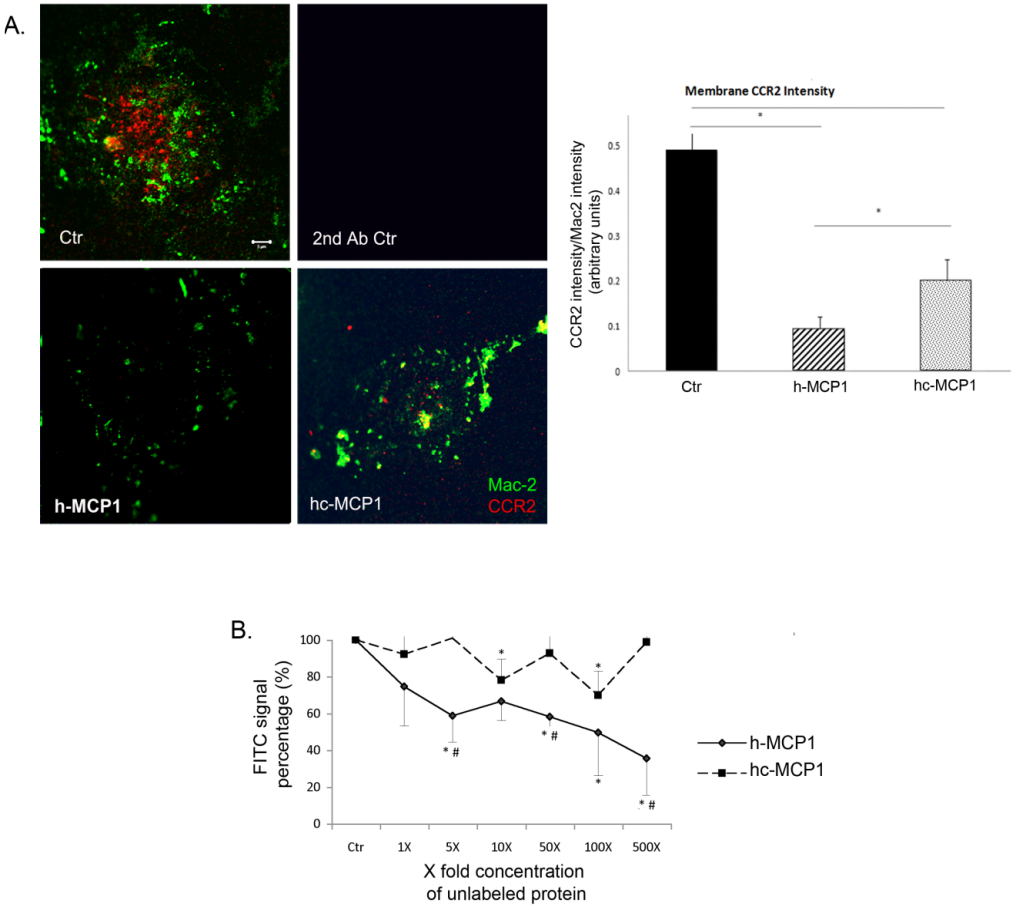

Figure 4-4. Mouse MCP1 C-terminal extension decreases the chemotactic potency of human MCP1 and the chemotactic activity depends on Rac1. A. Primary mouse microglia (left) or the CHME3 human microglial line (right) were plated and evaluated for chemotaxis in response to recombinant hMCP1 or hc-MCP1, in the presence or absence of the Rac1 inhibitor NSC23766. Each experimental condition was assayed in triplicate. Data are expressed as mean ± SD. **, p<0.01. **B.** N9 microglial cells or **C.** CHME3 human microglial cells were treated with 10nM MCP1 over time. The activated Rac1 was immunoprecipitated using GST-PBD beads. At each time point, the activated and total Rac1 were detected by western blotting. Western blots of activated and total Rac1 and quantification of the blots for hMCP1 and hc-MCP1. The blots were normalized to the 0 time point. Each experimental condition was assayed in triplicate and the data were expressed as mean ± SD. *p<0.05, **p<0.01, compared to 0 time point.

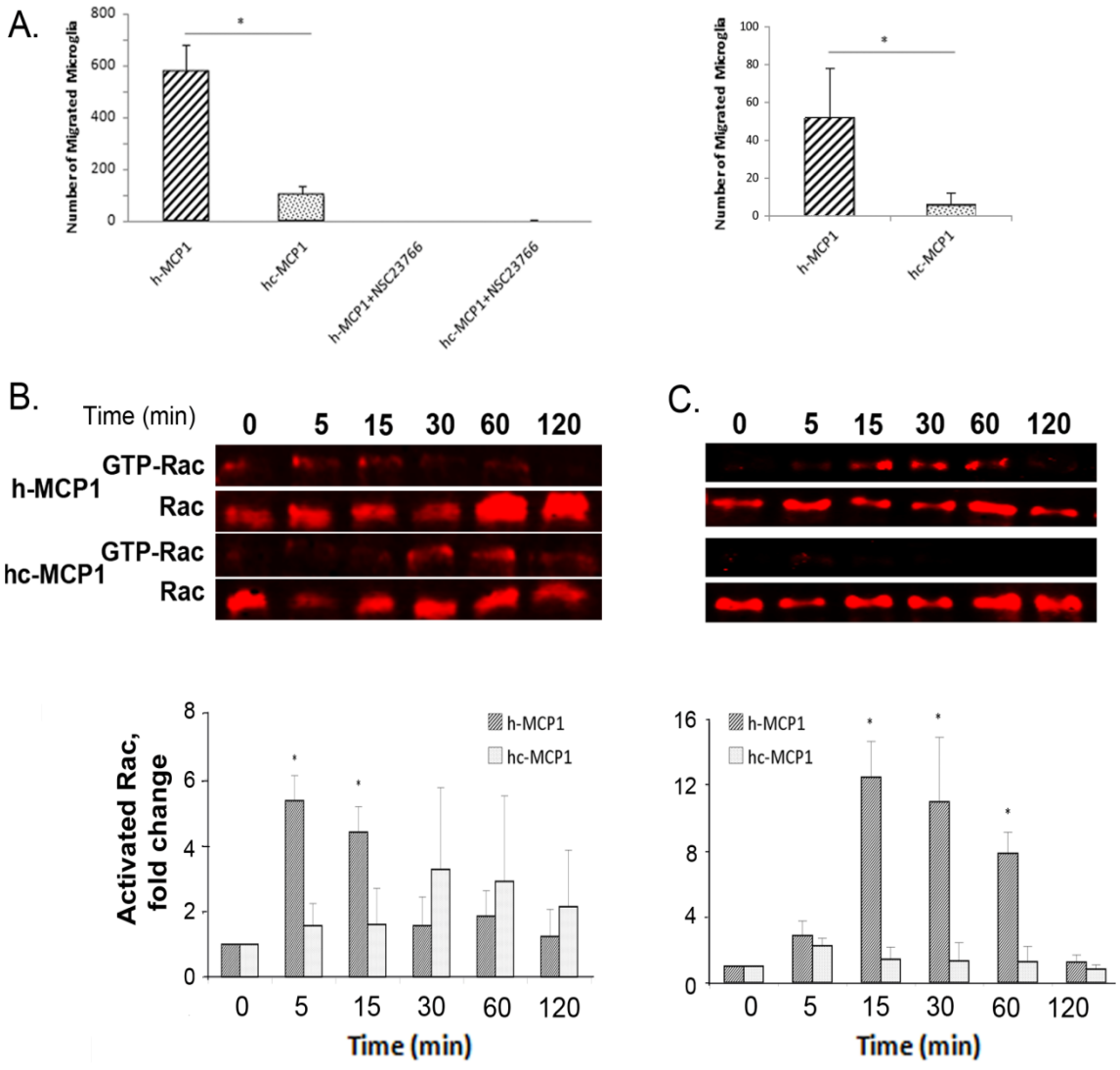

Figure 4-5. Mouse MCP1 C-terminus inhibits the formation of lamellipodia induced by human MCP1. A. Primary microglia plated on coverslips were incubated with a point source of recombinant MCP1 proteins for different periods of time. At each time point, the cells were washed, fixed, and stained for actin cytoskeleton using Alexa-Phalloidin. Scare bar = 10 μm. The percentage of unipolar cells (migrating towards the focal point of MCP1 protein) was quantified. Data are expressed as mean ± SD. N=9. *p<0.05. **B.** Mouse MCP1 C-terminus changes the activation pattern of ERK on microglia. Primary microglial cells were treated with h- or hc-MCP1 over time. At each time point, cell lysates were collected and analyzed for phosphorylated and total ERK1/2 by western blotting. Experiments were performed in triplicate. Representative experiment shown. Data are expressed as mean ± SD. *p<0.05, compared to 0 time point.

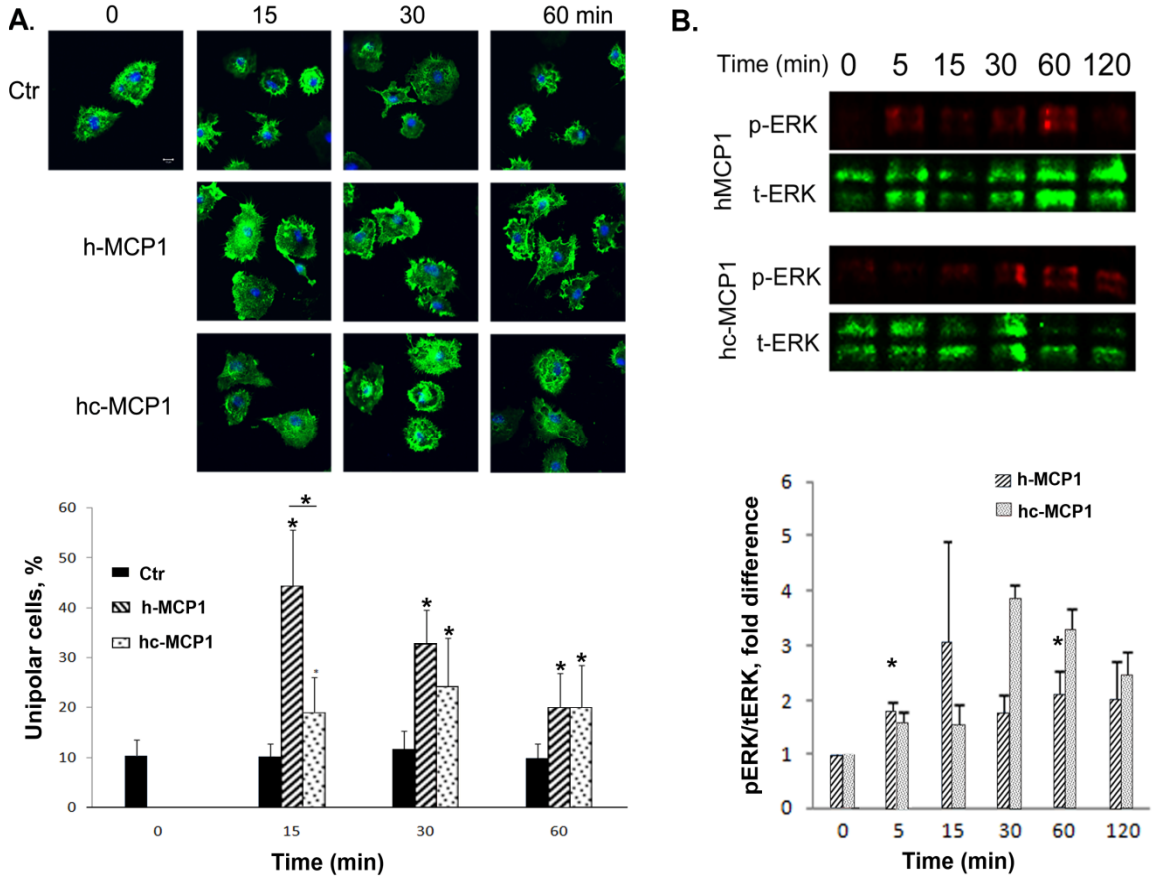

Figure 4-6. Mouse MCP1 C-terminus inhibits human MCP1-induced BBB compromise. **A.** 100 nM h- or hc-MCP1 was added to the lower chamber of the bEND.3-Astrocyte co-culture system. TEER values were determined over time in the presence of A2AP. Values are mean ± SD (n=4). **B.** Cells were treated as in **A**. The leakage of FITC-Dextran across the *in vitro* BBB was determined by a fluorescence plate reader in the presence of A2AP. The concentration of FITC-Dextran in the lower chamber was calculated based on a standard curve. Values are mean ± SD (n=4). Analysis was performed using student's t-test. Comparison with Ctr, *p<0.05 and comparison with hc-MCP1, #p<0.05. **C.** Mouse MCP1 C-terminus inhibits human MCP1-induced redistribution of TJP. Primary BMEC were treated with 100 nM h- or hc-MCP1 for 2 hours in the presence of A2AP. The cells were then fixed and immunostained for ZO-1 (upper panels) and F-actin (lower panels). **D.** Mouse MCP1 C-terminus is inhibitory to human MCP1-induced phosphorylation of ERM proteins. bEND.3 cells were treated with saline or 100nM h- or hc-MCP1 proteins in the presence of A2AP over time. The phosphorylated ERM proteins were determined using anti-phosphor-ERM antibody. Quantitative data of western blots are shown as mean ± SD (n=3). Comparison with control, *p<0.05 and comparison with hc-MCP1, #p<0.05.

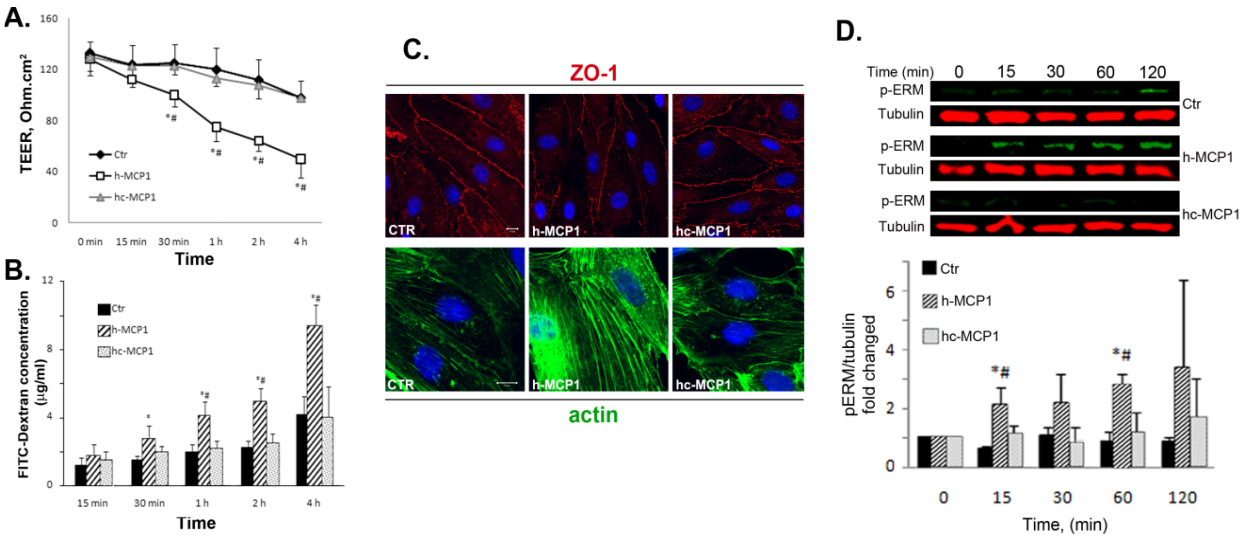

Figure 4-7. h-MCP1 shifts occludin and ZO-1 from Triton X-100 soluble fraction to insoluble fraction. bEnd.3 cells were treated with recombinant h- or hc-MCP1 over time and at each time point, Triton X-100 soluble fraction (S) and insoluble fraction (I) were collected and assessed for occludin and ZO-1 by western blotting. Experiments were performed in triplicate. Representative experiment shown.

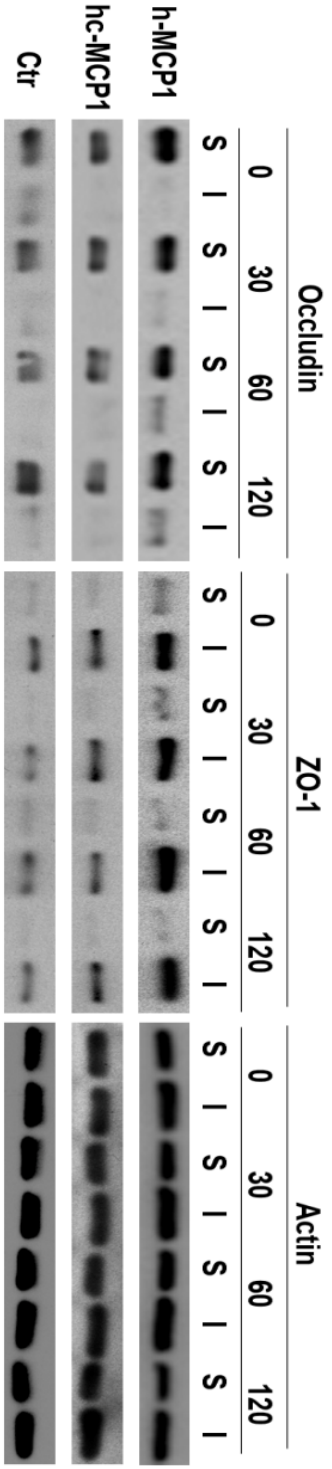

Chapter 5

MCP1-CCR2 Axis Affects The Progress Of Intracerebral Hemorrhage (ICH)

INTRODUCTION

Stroke, the second most common cause of death and a leading cause of disability, includes ischemic stroke and intracerebral hemorrhage (ICH) (Ribo and Grotta, 2006, Wang and Dore, 2007a). ICH is a severe clinical event with poor prognosis, but it has received less research attention than ischemic stroke (2005, Donnan et al., 2010). Although the pathogenesis after ICH is still elusive, accumulating evidence suggests that apoptosis (Matsushita et al., 2000, Gong et al., 2001, Qureshi et al., 2003) and inflammation (Castillo et al., 2002, Wang et al., 2003, Aronowski and Hall, 2005, Xi et al., 2006, Wang and Dore, 2007b, Wang, 2010) play important roles. When ICH occurs, microglia, brain resident immune cells, become activated and secrete inflammatory cytokines and chemokines. In addition, the BBB is also disrupted and peripheral leukocytes infiltrate into the brain parenchyma via chemokine gradients. The activated microglia and infiltrating leukocytes can modulate the disease progression of ICH.

By binding to its receptor CCR2, MCP1 induces the migration and accumulation of monocytes/microglia around lesion sites in many CNS injuries, including excitotoxicity and hemorrhage (Dimitrijevic et al., 2006, Frangogiannis et al., 2007, Hanisch and Kettenmann, 2007, Sheehan et al., 2007, Yan et al., 2007, Capoccia et al., 2008, Kim et al., 2008, Morimoto et al., 2008). In the brain, MCP1 is expressed by neurons,

astrocytes, microglia and BMEC (Ransohoff et al., 1993, Horuk et al., 1997, Andjelkovic et al., 1999a, Andjelkovic et al., 1999b, Boddeke et al., 1999, Mennicken et al., 1999, Andjelkovic and Pachter, 2000, Mahad and Ransohoff, 2003, Dicou et al., 2004, Kalehua et al., 2004, Wittendorp et al., 2004, Banisadr et al., 2005, Mahajan et al., 2005, Meeuwsen et al., 2005, Storer et al., 2005, Zeng et al., 2005) and CCR2 is expressed by microglia, astrocytes and BMEC (Banisadr et al., 2002, Ge et al., 2008). Previous studies in our lab (Sheehan et al., 2007) have suggested MCP1 may contribute to neuronal death via recruitment of microglia. In addition, we and others have shown that MCP1 also promotes BBB compromise (Stamatovic et al., 2003, Stamatovic et al., 2005, Dimitrijevic et al., 2006, Stamatovic et al., 2006, Yao and Tsirka, 2011), which may enhance leukocyte infiltration into the brain. Due to the fact that (1) MCP1 is a potent chemokine for microglia/monocytes, (2) MCP1 promotes the compromise of BBB integrity, (3) inflammation plays an important role in ICH, and (4) BBB is disrupted in ICH, it is interesting to examine the role of MCP1 or CCR2 on the pathogenesis of ICH. We hypothesize that lack of MCP1 or CCR2 may cause either less severe injury resulting from less secreted cytotoxic cytokines or prolonged recovery due to insufficient clearance.

MATERIALS AND METHODS

Animals

C57BL/6 (wild-type) and MCP1$^{-/-}$ and CCR2$^{-/-}$ mice were obtained from the Jackson Laboratories. These mice were maintained in the Department of Laboratory Animal Research at Stony Brook University with free access to water and food ad libitum. MCP1$^{-/-}$ and CCR2$^{-/-}$ mice have already been backcrossed for 12 generations to the C57BL/6 background. All experimental procedures were in accordance to the National Institutes of Health guide for the care and use of laboratory animals and the institutional guidelines established by the Institutional Animal Care and Use Committee at Stony Brook University.

ICH Model

ICH was induced as previously described (Wang et al., 2003, Wang and Tsirka, 2005). Briefly, mice weighting 25-35 g were anesthetized by injecting atropine (0.6ug/g of body weight) and avertin (0.02ml/g of body weight) intraperitoneally. Then, collagenase (0.18U in 500nl saline) with or without recombinant MCP1 proteins (150ng) was injected unilaterally into the caudate putamen at stereotactic coordinates: -0.5mm posterior to bregma, 3.0mm lateral from midline, and 4.0mm in depth. Collagenase was delivered over 3 minutes and the needle was kept in place for 5 minutes to prevent reflux. Mice were put on a warm plate for 3 hours to allow them recover from surgery. At day 1, 3, and 7 post surgery, mice were anesthetized again followed by transcardiac perfusion. The brain were then removed, post fixed in 4% paraformaldehyde over night

at 4℃, and dehydrated in 30% sucrose for 24 hours at room temperature. Next the brains were subjected to serial section.

Histology

H&E staining was performed to visualize the hematoma. Briefly, sections were washed twice in PBS and kept in hematoxylin for 15 min at room temperature. After washed in tap water twice, the slides were washed in 70% ethanol with 1% hydrochloride acid for 3 sec, followed by 3 washes in tap water. Then the slides were stained in eosin for 5 sec and washed in PBS, dehydrated in gradient ethanol and mounted.

Fluoro-Jade C staining was performed according to a standard protocol (Schmued and Hopkins, 2000). Briefly, slides were first incubated in basic alcohol solution (1% sodium hydroxide in 80% ethanol) for 5 min. After washed in 70% ethanol and distilled water for 2 min, the slides were incubated in 0.06% potassium permanganate solution for 10 min. Then the slides were washed in water for 2 min and transferred to 0.0001% Fluoro-Jade C solution (in 0.1% acetic acid) for 10 min. Next, the slides were rinsed in water for 3 times and dried at 56 $^{\circ}C$ for 5 min. After cleared in xylene for 2 min, the slides were mounted with DPX. Fluoro-Jade C positive cells were counted in three fields immediately adjacent to the hematoma at 400X magnification over a microscopic field of 0.01mm^2. Three sections were counted per mouse. Large blood vessels were avoided. The numbers of generating cells were expressed as cells/mm^2.

Hemorrhagic Injury Analysis

The injury volumes were quantified as described previously (Clark et al., 1998, Wang et al., 2003, Thiex et al., 2004, Wang and Tsirka, 2005). Briefly the slides stained with H&E were examined under microscope (Nikon ECLIPSE-E600). The injury volumes from wt, MCP1$^{-/-}$, and CCR2$^{-/-}$ mice were digitally quantified using the NIS-Elements software D 3.0 on 30μm coronal sections. The hemorrhagic injury areas were summed up from the serial coronal slices and the injury volumes (mm^3) were calculated as below: Injury Volume=measured area X slice thickness (30μm).

Immunofluorescence

Activated microglia were visualized by Iba-1 staining as described below. Briefly, after washed in PBS for 5 min, the slides were incubated in 3% H_2O_2 in PBS for 5 min. Then the slides were washed in PBS extensively, followed by incubation with blocking buffer (1% BSA and 0.2% Triton X-100 in PBS) for 1 hour at room temperature. Next, the slides were incubated with 1:500 Iba-1 antibody (Wako) in blocking buffer over night at 4℃. After extensive wash in PBS, the slides were incubated in 1:200 biotinylated anti-Rabbit antibody for 1 hour at room temperature. The slides were then stained with the ABC kit (Vector Labs), followed by incubation in Diaminobenzidine (DAB) solution (0.05% DAB and 0.02% H_2O_2 in PBS) for 10 min. Finally, the slides were rinsed in PBS, dehydrated in gradient ethanol, cleared in xylene, and mounted.

Infiltration of leukocytes were visualized by CD45 immunohistochemistry. Briefly, the slides were blocked with blocking buffer for 1 hour at room temperature, followed by incubation with 1:1000 anti-CD45 antibody (BD Pharmingen) overnight. Then, the slides

were incubated with 1:200 Alexa-488 anti-rat secondary antibody for 1 hour at room temperature and mounted with FluorMount.

Brain Edema Measurement

Brain edema was measured as described previously (Wang 2003, Wang 2007). Briefly, mice were injected with collagenase as described above. At days 1 and 7 post injection, the mice were euthanized by cervical dislocation. The brains were collected and cut into two hemispheres. Cerebellum was also collected and used to serve as the internal control. The wet weights were obtained by weighting the two hemispheres and cerebellum using an analytical balance (Denver Instrument Co) immediately after collecting the samples. Then, the samples were dried using the speed vacuum concentrator (Savant Instruments) for 24 hours and weighted (dry weight). Brain edema was calculated using the equation below: Brain Edema=(Wet Weight-Dry Weight)/Wet Weight X100.

Neurological Deficit

All mice were scored for neurological deficit 1, 3, and 7 days after collagenase injection using a modified 28 point neurological scoring system as described previously (Clark et al., 1998, Wang et al., 2003, Thiex et al., 2004, Wang and Tsirka, 2005). This system includes 6 aspects: body symmetry, gait, climbing, circling behavior, front limb symmetry, and compulsory circling. Each aspect can be graded from 0 to 4, establishing a maximum score of 24. The investigator scoring the deficit was blinded to the genotypes.

RESULTS

Effects of MCP1-CCR2 axis on hematoma volume

Because the MCP1-CCR2 axis plays an important role in microglia recruitment (Sheehan et al., 2007, Yao and Tsirka, 2010) and microglia exhibit both detrimental and beneficial roles during ICH (Wang et al., 2003, Wang and Tsirka, 2005, Wang and Dore, 2007b), we first examined whether lack of MCP1 or CCR2 affected the size of hematoma. We induced hemorrhage in wt mice and mice deficient for MCP1 or CCR2 by injecting collagenase into the caudate putamen and examined the outcome at day 1, 3, and 7 post injury. As shown in Figure 5-1, for wt mice the hematoma reached its maximal size (28.42mm^3) at 1 day post injury (1 dpi) and started decreasing at 3 dpi (22.2 mm^3). By 7 dpi, the hematoma was almost resolved (4.26 mm^3). On the contrary, for MCP1$^{-/-}$ and CCR2$^{-/-}$ mice, the hematoma size followed a different course: The volumes of hematoma were much smaller at 1 dpi in these knockout mice (9.22 and 7.27 mm^3, respectively). They peaked at 3 dpi (14.73 and 20.2 mm^3) and maintained at a similar size at 7 dpi (10.78 and 16.24 mm^3). These data suggested that MCP1-CCR2 signaling contributes to the pathological development/clearance of ICH.

Effects of MCP1-CCR2 axis on microglia recruitment and leukocyte infiltration during ICH

One of the major functions of MCP1 is to recruit mononuclear cells (Mennicken et al., 1999, Sheehan et al., 2007, Yao and Tsirka, 2010). It has been shown that MCP1 induces microglial migration *in vitro* and recruits microglia in kainate-induced

excitotoxicity (Sheehan et al., 2007, Yao and Tsirka, 2010), but its chemotactic effect has not been studied in ICH. Here, we visualized the recruitment of microglia to the injury site by immunostaining against Iba-1, a microglia marker. As shown in Figure 5-2A, there is no difference in baseline microglia staining among different genotypes. Consistent with previous reports (Wang et al., 2003, Wang and Tsirka, 2005, Wang and Dore, 2007b), collagenase-induced hemorrhage significantly recruited microglia to the injury site 1 dpi in wt mice and these microglia had large cell bodies and short processes (Figure 5-2B), indicating that they were activated. As expected, mice deficient for MCP1 or CCR2 presented lower numbers of microglia around the hematoma 1dpi (Figure 5-2B), suggesting that MCP1-CCR2 axis was a major signaling pathway that recruits microglia at early time point after ICH. The density of Iba-1-positive cells increased at 3 dpi in wt mice (Figure 5-2B). Surprisingly, in $MCP^{-/-}$ or $CCR2^{-/-}$ mice, there were more activated microglia accumulated in the hematoma border 3 dpi (Figure 5-2B), suggesting that alternative (MCP1 and CCR2 independent) signaling cascades were responsible for the accumulation of microglia. By 7 dpi, wt mice had decreased numbers of microglia in the penumbra, and the Iba-1 signal was weaker (Figure 5-2B), reminiscent of microglia in a recovering state. Mice deficient for MCP1 or CCR2 by 7 dpi, on the contrary, showed high density and strong staining of microglia (Figure 5-2B), suggesting the alternative signaling pathway(s) activated in 3 dpi was still functional by 7 dpi. Together with the injury size data, our Iba-1 staining suggests that microglia may play a detrimental role at early time point (1 day after injury in collagenase induced ICH model), although their role at later time point is unclear due to the activation of alternative signaling cascades.

Another function of MCP1 is to compromise the integrity of BBB (Stamatovic et al., 2003, Stamatovic et al., 2005, Dimitrijevic et al., 2006, Stamatovic et al., 2006, Yao and Tsirka, 2011). We examined the extent of infiltration of leukocytes into the brain by immunostaining against CD45, a pan leukocyte marker. As shown in Figure 5-3, wt mice had similar numbers of infiltrating CD45-positive cells around the hematoma at early time points (1 and 3 dpi) as MCP1$^{-/-}$ and CCR2$^{-/-}$ animals. By 7 dpi, there was an increase of CD45-positive signals, although the hematoma size was smaller, suggesting the presence of a compromised BBB and infiltration of peripheral blood cells. MCP1$^{-/-}$ and CCR2$^{-/-}$ mice, however, displayed CD45 level comparable to the previous timepoints, suggesting an intact BBB and very limited infiltration of leukocytes. These data are consistent with our previous observation that MCP1 compromises the integrity of BBB in a CCR2-dependent manner (Yao and Tsirka, 2011). We have shown that there is no difference in baseline BBB leakage among wt mice and mice deficient for MCP1 or CCR2 under physiological conditions (Yao and Tsirka, 2011). Here, we reported that MCP1$^{-/-}$ and/or CCR2$^{-/-}$ mice had a relatively intact BBB even in pathological conditions, at least as evident in the collagenase-induced ICH model. Together with the injury volume and Iba-1 data, the CD45 staining indicated that the prolonged recovery time in MCP1$^{-/-}$ and CCR2$^{-/-}$ mice may be due to the lack of infiltrating leukocytes at later times after ICH.

Effects of MCP1-CCR2 axis on edema, neuronal death, and neurobehavial deficits

Brain edema, as an important clinical complication, significantly affects the outcome of ICH. Thus, we quantified the water content in the collagenase-induced ICH

model. As shown in Figure 5-4A, collagenase injection induced a significant increase of brain water in the ipsilateral hemisphere in wt mice 1 dpi. Mirrored by the hematoma volume, the water content in the ipsilateral side decreased at later time points (3 and 7 dpi), suggesting the recovery of ICH. Compared to wt mice, MCP1$^{-/-}$ and CCR2$^{-/-}$ mice showed a reverse pattern of water content in the ipsilateral side. The water content was high (77.87% for MCP1$^{-/-}$ mice and 78.11% for CCR2$^{-/-}$ mice) in the ipsilateral hemisphere at 1 dpi. These numbers increased to 78.52% and 78.63% at 3 dpi and reached 78.90% and 79.73% at 7 dpi for MCP1$^{-/-}$ and CCR2$^{-/-}$ mice, respectively, floowing the progression of ICH. Water content in the contralateral hemisphere, however, was not changed dramatically. Water content in the cerebellum, the internal control, was not affected by collagenase injection, indicating that the difference in the ipsilateral side was not due to different genotypes nor the experimental procedures.

Next we quantified the extent of neuronal death at the site of hemorrhage using Fluoro-Jade C histological staining, which specifically labels degenerating neurons (Bian et al., 2007). We found that wt mice had a large number of FJC-positive cells (387/mm^2) at 1 dpi and the number decreased to 142/mm^2 at 7 dpi (Figure 5-4B and C), suggesting that neurons were degenerating early after injury and but were recovering later. MCP1$^{-/-}$ mice, on the contrary, exhibited less cell death (229/mm^2) at 1 dpi, but more death (295/mm^2) at 7 dpi (Figure 5-4B and C), indicative of the progression of disease. Similarly to MCP1$^{-/-}$ mice, CCR2$^{-/-}$ mice followed the same trend. We measured 200 and 303 FJC-positive cells per mm^2 at 1 dpi and 7 dpi, respectively, in CCR2$^{-/-}$ mice (Figure 5-4B and C). These data suggested that neuronal death was evident at the ICH site and that the number of degenerating neurons correlated with the size of hematoma.

ICH is classically followed by behavioral deficits. To study whether the observed pathological events were accompanied by neurobehavioral changes, we performed a a battery of behavior tests on these animals. For wt mice, the neuronal deficit score was high early after injury (10.9 and 10.1 at 1 and 3 dpi, respectively). It decreased to 4.7 at 7 dpi (Figure 5-4D), correlating with recovery after injury. MCP1$^{-/-}$ mice, on the other hand, showed low neuronal deficit score at 1 dpi (7.3) and high scores at 3 dpi (9) and 7 dpi (10.2) (Figure 5-4D), indicating a mild injury early after collagenase injection and continuous progression of disease. Like MCP1$^{-/-}$ mice, CCR2$^{-/-}$ mice showed the same trend (Figure 5-4D). When comparing the neuronal deficit scores among different genotypes at the same time points after injury, we found that both knockout mice had smaller score at 1 dpi and larger score at 7 dpi (Figure 5-4D). These data suggested that the progress of disease was delayed in mice lacking MCP1 or CCR2.

Infusion of plasmin-truncated MCP1 restores wt-phenotype in MCP1$^{-/-}$ mice

To investigate whether plasmin-mediated truncation of MCP1 plays a role in pathological conditions, specifically collagenase-induced ICH model, we infused different recombinant MCP1 proteins into the brains of MCP1$^{-/-}$ mice and examined the outcome. First, we incubated recombinant FL-MCP1 with collagenase at 37℃ for 24 hours and performed a western blot against MCP1 on tissue extracts from these animals. We found only one 18kD band corresponding to FL-MCP1 (Figure 5-5), suggesting that collagenase does not cleave MCP1. To evaluate whether the effect of MCP1 could last for 7 days, we incubated recombinant FL- and K104Stop-MCP1 at 37℃ for 0, 3, and 7 days and quantified their chemot actic activity for MCP1$^{-/-}$ primary

microglia using the Boyden chamber assay. These proteins maintained their chemotactic potency (Figure 5-6), suggesting that one single injection of MCP1 would be sufficient during the course of the experiment. Thus we injected MCP1 together with collagenase into the brains at day 0 and studied the pathological changes at 1, 3, and 7 days post injury. As shown in Figure 5-7, infusion of K104Stop-MCP1 (the constitutively active MCP1) into $MCP1^{-/-}$ mice reversed the progression of the hematoma size shown in $MCP1^{-/-}$ mice. We observed a larger hematoma at 1 dpi (34.35mm^3) and smaller hematoma at 3 and 7 dpi (6.08 and 3.21mm^3, respectively), similar to wt mice after collagenase injection. Infusion of K104A-MCP1 (MCP1 non-cleavable by plasmin) into $MCP1^{-/-}$ brains, on the contrary, did not affect the hematoma pattern found in $MCP1^{-/-}$ mice---gradual increase of the injury volume. Like K104Stop-MCP1, FL-MCP1 infusion induced a large hematoma (12.98mm^3) at 1 dpi and the volume decreased to 1.01mm^3 at 7 dpi. It should be noticed that FL-MCP1-infused mice resulted in a much smaller hematoma at 1 dpi, compared to K104Stop-MCP1-induced mice, suggesting a higher potency of K104Stop-MCP1 than FL-MCP1. These data suggest that the truncated MCP1 is responsible for change of pathological progress of ICH in $MCP1^{-/-}$ mice, indicating that plasmin-mediated truncation of MCP1 is a necessary step to activate MCP1 *in vivo*.

Infusion of FL- or K104Stop-MCP1 changes the pattern of microglia recruitment and enhances leukocyte infiltration

Next, we also examined how infusion of the recombinant MCP1 proteins would affect the activation of microglia after ICH. Infusion of FL-MCP1 significantly increased

the density of microglia in the peri-injury site at 1 dpi (Figure 5-8). The microglia presented morphology characterized by long processes and lightly stained cell body (Figure 5-8), indicating that the majority of the cells were at resting state. Infusion of K104Stop-MCP1, as expected, led to even higher density of microglia immediately adjacent to the hematoma at 1 dpi (Figure 5-8). Although not showing an amoeboid morphology, the cells had an intensely $Iba1^{+}$ cell body, indicating a semi-activated state. K104A-MCP1, however, did not significantly change the density of microglia in the peri-hematoma region at 1 dpi (Figure 5-8). 3 days after injury, microglia became fully activated (amoeboid morphology with short processes and intensity cell body) and the density of activated microglia increased significantly, no matter which MCP1 was infused (Figure 5-8). This is consistent with our previous observation that microglia were fully activated in $MCP1^{-/-}$ or $CCR2^{-/-}$ at 3 dpi (Figure 5-8). By 7 dpi, mice infused with K104A-MCP1 showed consistent activation of microglia and high density of microglia around the injury site (Figure 5-8). Mice injected with FL- and K104Stop-MCP1, on the other hand, showed dramatic drop of microglia number at site of injury and the morphology of microglial cells returned to a resting or semi-activated state (Figure 5-8), indicating recovery. Together with our previous findings that $MCP1^{-/-}$ mice showed continuous activation of microglia 7 day after collagenase injection (Figure 5-2B), these data suggested that infusion of FL- or K104Stop-MCP1, but not K104A-MCP1, was able to restore the phenotype noted in mice deficient for MCP1 or CCR2. These data further indicate that plasmin-mediated truncation of MCP1 may be an indispensable step to fully activate MCP1 *in vivo*.

Since MCP1$^{-/-}$ or CCR2$^{-/-}$ mice exhibited very limited leukocyte infiltration after ICH (Figure 5-3), we also examined the infiltration of leukocytes in MCP1$^{-/-}$ after recombinant MCP1 infusion. As shown in Figure 5-9, infusion of FL-MCP1 led to infiltration of CD45-positive cells at 7 dpi in MCP1$^{-/-}$ mice. Mice injected with K104Stop-MCP1 showed leukocyte infiltration at 3 dpi and the effect was more dramatic at 7 dpi, suggesting a higher activity of K104Stop-MCP1 than FL-MCP1. K104A-MCP1, on the other hand, did not induce the infiltration of CD45-positive cells at any time point examined, suggesting that K104A-MCP1 is inactive in leukocyte infiltration *in vivo* in our experimental system.

Infusion of plasmin-truncated MCP1 changes edema, neuronal death, and neurobehavior patterns

Because infusion of K104Stop-MCP1 reversed the pattern /size of hematoma formed in MCP1$^{-/-}$ mice, we further explored whether this change was paralleled by edema, neuronal death and neurobehavior. We found the water content in the ipsilateral hemisphere correlated well with the hematoma volume. Infusion of FL- or K104Stop-MCP1 into the brains of MCP1$^{-/-}$ mice led to a significant increase of water content in the ipsilateral hemisphere at 1 and 3 dpi and the water content decreased to level comparable to contralateral at 7 dpi (Figure 5-10A). On the contrary, we found that the water content continuously increased with time and peaked at 7 dpi in K104A-MCP1 infused mice (Figure 8A), confirming that the edema also contributed to disease progression after ICH.

Similarly, we also examined the death of neurons at the border of hematoma after injection of recombinant MCP1 proteins. Compared with MCP1$^{-/-}$ mice, infusion of FL- or K104Stop-MCP1 significantly enhanced the number of degenerating neurons at 1 dpi but not at 7 dpi (Figure 5-10B and C). It should be noted that the effect of K104Stop-MCP1 was more dramatic than that of FL-MCP1 at 1 dpi (Figure 5-10B and C), suggesting a higher activity of K104Stop-MCP1. Infusion of K104A-MCP1, however, did not change the number of degenerating neurons significantly at either time point (Figure 5-10B and C), suggesting that K104A-MCP1 was inactive. These data indicated that plasmin-mediated truncation of MCP1 is a necessary step, and it is the truncated fully active MCP1 that rescued the phenotype found in MCP1$^{-/-}$ mice.

In addition, we found K104Stop-MCP1-infused mice showed a higher neural deficit score (11.73) at 1dpi and the score decreased to 8.67 and 4.33 at 3 and 7 dpi, respectively (Figure 5-10D). FL-MCP1 infusion also led to a high neural deficit score at early time points (10.25 at 1 dpi) after injury and low score at later time point (5.67 at 7 dpi) (Figure 5-10D). K104A-MCP1, on the contrary, did not change the neural deficit score found on MCP1$^{-/-}$ mice. The score was low at 1 dpi (5.78) and increased to 7.67 at 3 dpi and peaked at 7 dpi (9.75) (Figure 5-10D). Collectively, our data suggested that the infusion of FL- or K104Stop-MCP1 reversed the behaviors of MCP1$^{-/-}$ mice to those of wt mice after ICH, again underscoring the crucial role of plasmin-mediated truncation of MCP1 on its biological activities *in vivo*.

DISCUSSION

Hemorrhagic stroke, which represents about 10-20% of all strokes (Qureshi et al., 2001, Ribo and Grotta, 2006), is an acute clinical event. Accumulating evidence shows that inflammation is critical in the pathogenesis of this disease (Gong et al., 2001, Wang et al., 2003, Wang and Tsirka, 2005, Xi et al., 2006, Wang, 2010). Activated microglia and infiltrated macrophages have been shown to accumulate in the peri-hematoma region (Wang et al., 2003, Wang and Tsirka, 2005). Although the MCP1-CCR2 system has been shown to induce the migration of microglia/macrophages and regulate the integrity of BBB *in vitro* and *in vivo* (Sheehan et al., 2007, Yao and Tsirka, 2010, 2011), its role in ICH has not been investigated. In the experiments described in this chapter we find that lack of MCP1 or CCR2 significantly decreased hematoma size at early time points but delayed the recovery of the animals from ICH. The size of hematoma was paralleled by the water content in the ipsilateral hemisphere and neuronal death at peri-hematoma region. Consistently, neurobehavioral deficit score was mirrored by hematoma size. These data suggest that mice deficient for MCP1 or CCR2 have a milder but long-lasting injury after ICH. This is, to our understanding, the first evidence showing the role of MCP1-CCR2 axis on ICH.

Microglia have been shown to play a dual role during brain injury. On one hand, they can promote neuronal death by secreting a variety of cytotoxic factors, such as TNF-α and IL-1β (Aloisi, 2001, Kim and de Vellis, 2005, Hanisch and Kettenmann, 2007). On the other hand, they can also phagocytose cell debris and injured neurons to enhance recovery (Elkabes et al., 1996, Rabchevsky and Streit, 1997, Nakajima et al.,

2002, Nakajima and Kohsaka, 2004). Which role they take after ICH is dependent on the time after injury, and this temporal pattern is unknown. The immunochemistry staining revealed decreased numbers of microglia around the hematoma at 1 dpi in MCP1$^{-/-}$ or CCR2$^{-/-}$ mice, suggesting that microglia may play a detrimental role at 1 dpi in collegenase-induced ICH. Unexpectedly, at 3 and 7 dpi, the knockout mice showed higher density of microglia in the peri-hematoma region, suggesting that other signaling pathways may function to attract microglia. It is thus unclear whether microglia are beneficial or neurotoxic at 3 or 7 dpi after ICH. Consistent with our previous report that mice lacking MCP1 or CCR2 have a tighter BBB, infiltration of leukocytes was not detectable in mice lacking MCP1 or CCR2 at any time point examined. Ongoing projects in the lab involve the identification of chemokines or chemokine receptors that are upregulated at 3 and 7 dpi in the knockout mice.

Our rescue experiment showed that FL- and K104Stop-MCP1 proteins were able to restore the wt phenotype in MCP1$^{-/-}$ mice, whereas plasmin-resistant K104A-MCP1 failed to do so, suggesting that plasmin-mediated truncation may be an indispensable step to fully activate MCP1 *in vivo*. This is consistent with the *in vitro* data that plasmin-truncated MCP1 has higher biological activities (Yao and Tsirka, 2010, 2011). Collectively, our data indicate that inhibiting plasmin activity may be an alternative way to regulate the MCP1-CCR2 system and microglia/monocyte activities after injury. In addition, our data also support a beneficial role of inhibiting MCP1-CCR2 axis early after ICH. However, it should be noted that complete or long-lasting inhibition of MCP1-CCR2 activity may be detrimental, because MCP1$^{-/-}$ or CCR2$^{-/-}$ mice showed delayed recovery.

Future research should focus on methods to detect ICH right after its onset and to inhibit the MCP1-CCR2 system transiently.

Figure 5-1. The effect of MCP1 or CCR2 on injury volume. A. Wild-type, MCP1$^{-/-}$, and CCR2$^{-/-}$ mice were co-injected with collagenase into the brain and the injury volume was examined by H&E staining 1, 3, 7 days after injection. **B.** Quantitative data of injury volume are shown as mean ± SD (n=3-7). Comparison with day 1 within the same genotype, *p<0.05 and comparison with wild-type at the same time points, #p<0.05.

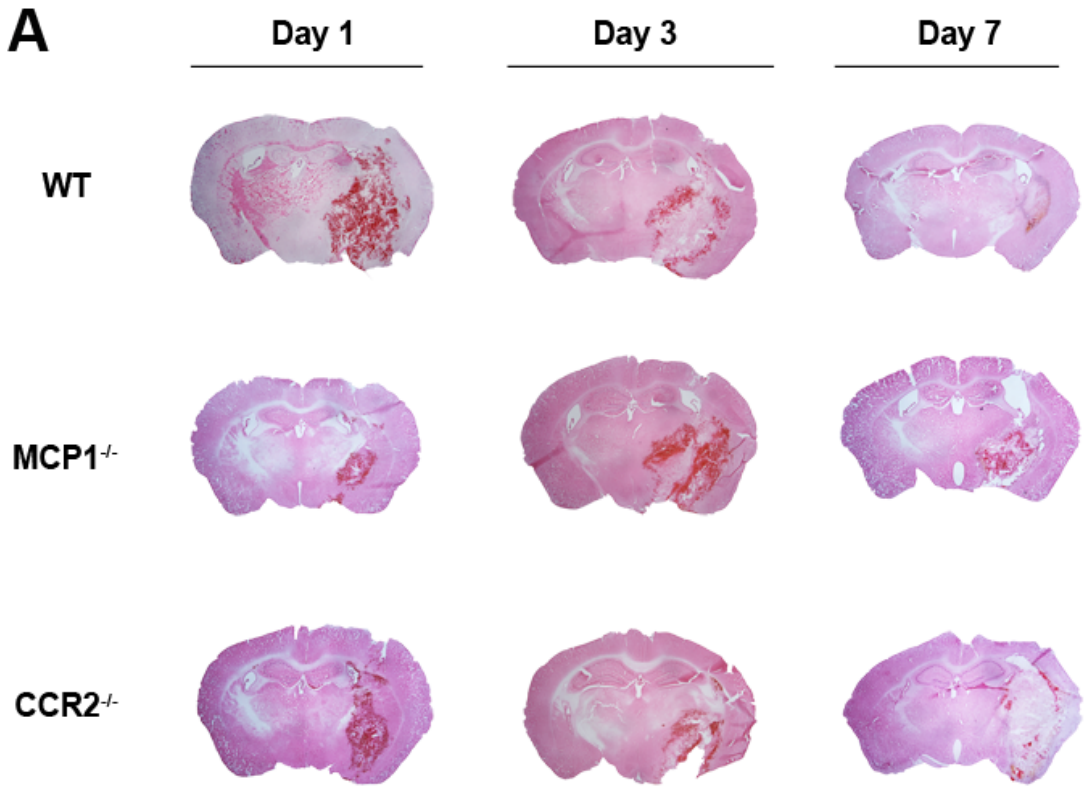

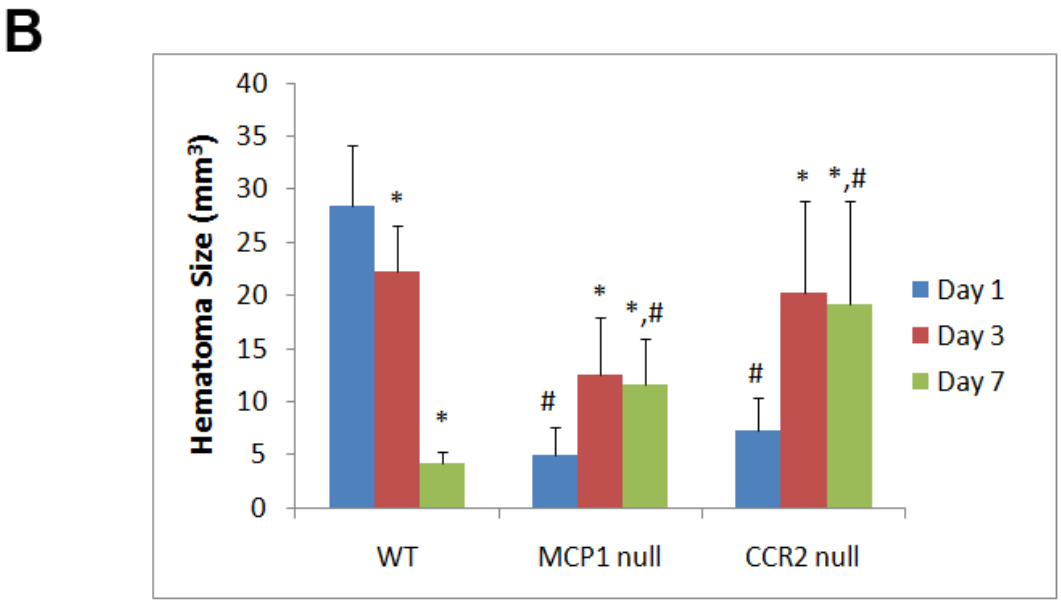

Figure 5-2. The effect of MCP1 or CCR2 on microglia activation. A. Wild-type, MCP1$^{-/-}$, and CCR2$^{-/-}$ mice without collagenase injection were perfused and the activation of microglia was examined by Iba-1 DAB-staining. **B.** Wild-type, MCP1$^{-/-}$, and CCR2$^{-/-}$ mice were injected with collagenase into the brain and the activation of microglia was examined by Iba-1 DAB-staining 1, 3, 7 days after injection.

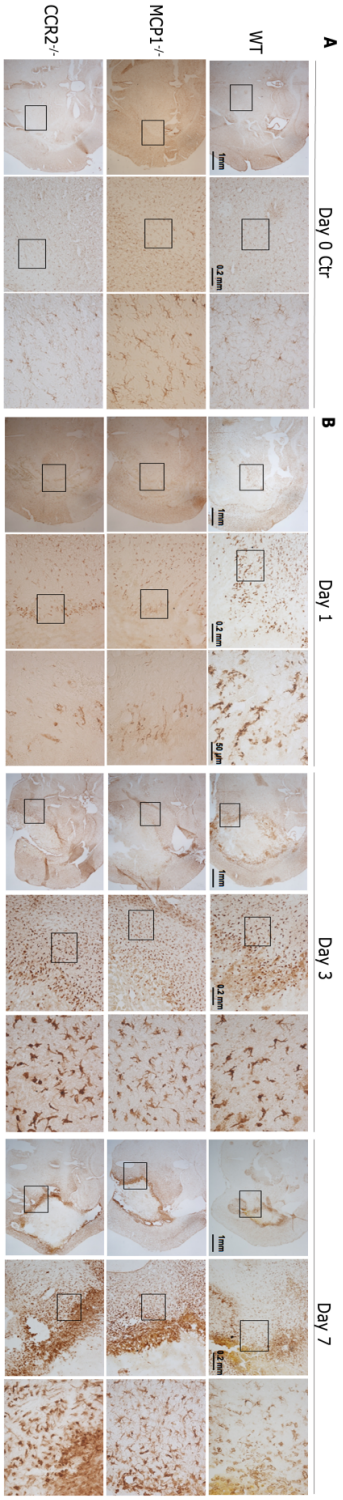

Figure 5-3. The effect of MCP1 or CCR2 on leukocyte infiltration. A. Wild-type, MCP1$^{-/-}$, and CCR2$^{-/-}$ mice were injected with collagenase into the brain and the infiltration of leukocytes was examined using CD45 immunostaining 1, 3, 7 days after injection. **B.** The infiltration of leukocytes was expressed as mean pixel intensity (the ratio of CD45 intensity over the area). Data are shown as mean ± SD (n=3-7). Comparison with day 1 within the same genotype, *p<0.05.

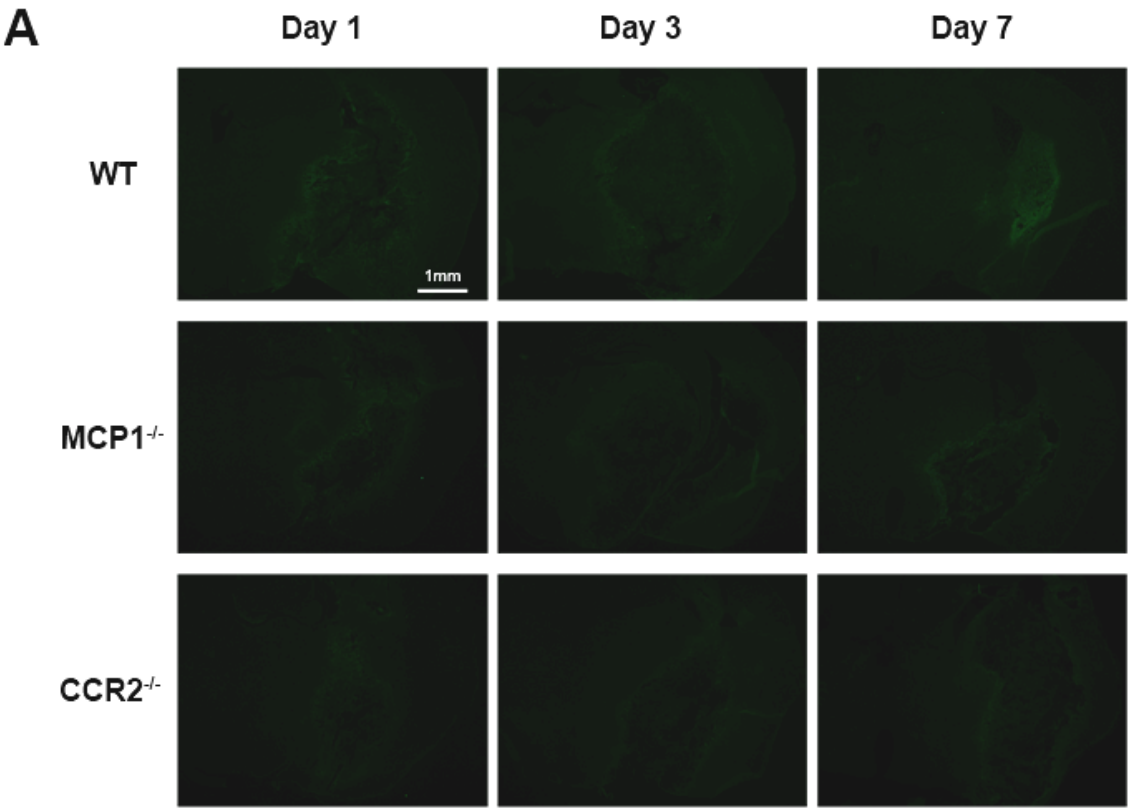

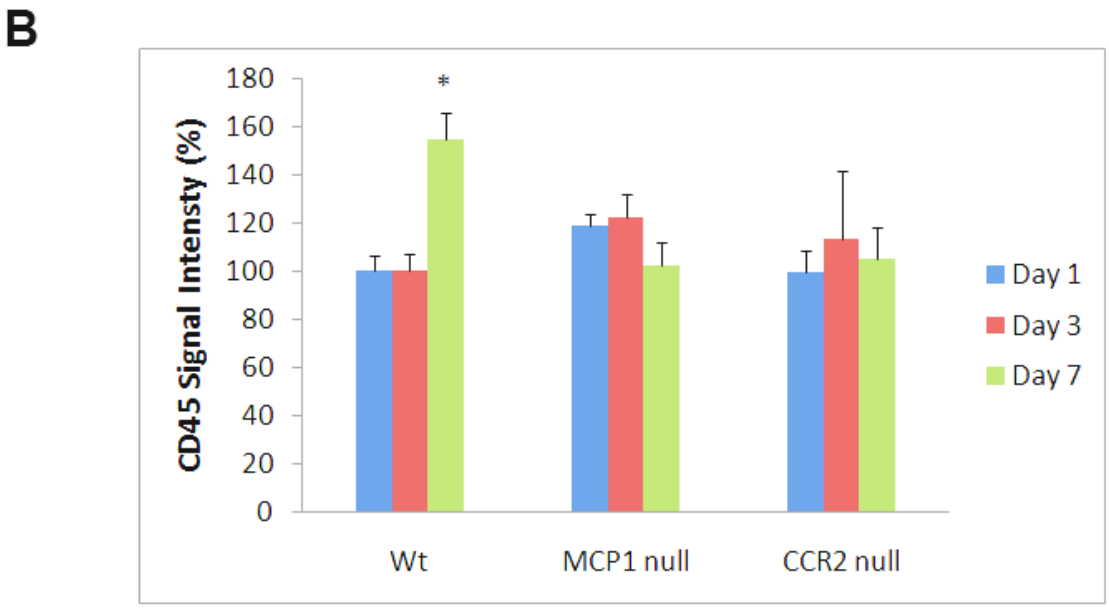

Figure 5-4. The effect of MCP1 or CCR2 on brain edema, neuronal death, and neurobehavior. A. Wild-type, MCP1$^{-/-}$, and CCR2$^{-/-}$ mice were injected with collagenase into the brain and water content was calculated as described in Materials and Methods. Data are shown as mean ± SD (n=6). **B.** Mice were treated as described above. Degenerating neurons were visualized using Fluoro-Jade C staining on day 1 and day 7 post injury. **C.** Quantification of the number of degenerating neurons on day 1 and day 7 post injury in these mice. Data are shown as mean ± SD (n=3-4). **D.** Mice were treated as described above. Neurological scores were evaluated at 1, 3, and 7 days after injury. Values are shown as mean ± SD (n=5-17). For **A, C,** and **D,** comparison with day 1 within the same genotype, *p<0.05 and comparison with wild-type at the same time points, #p<0.05.

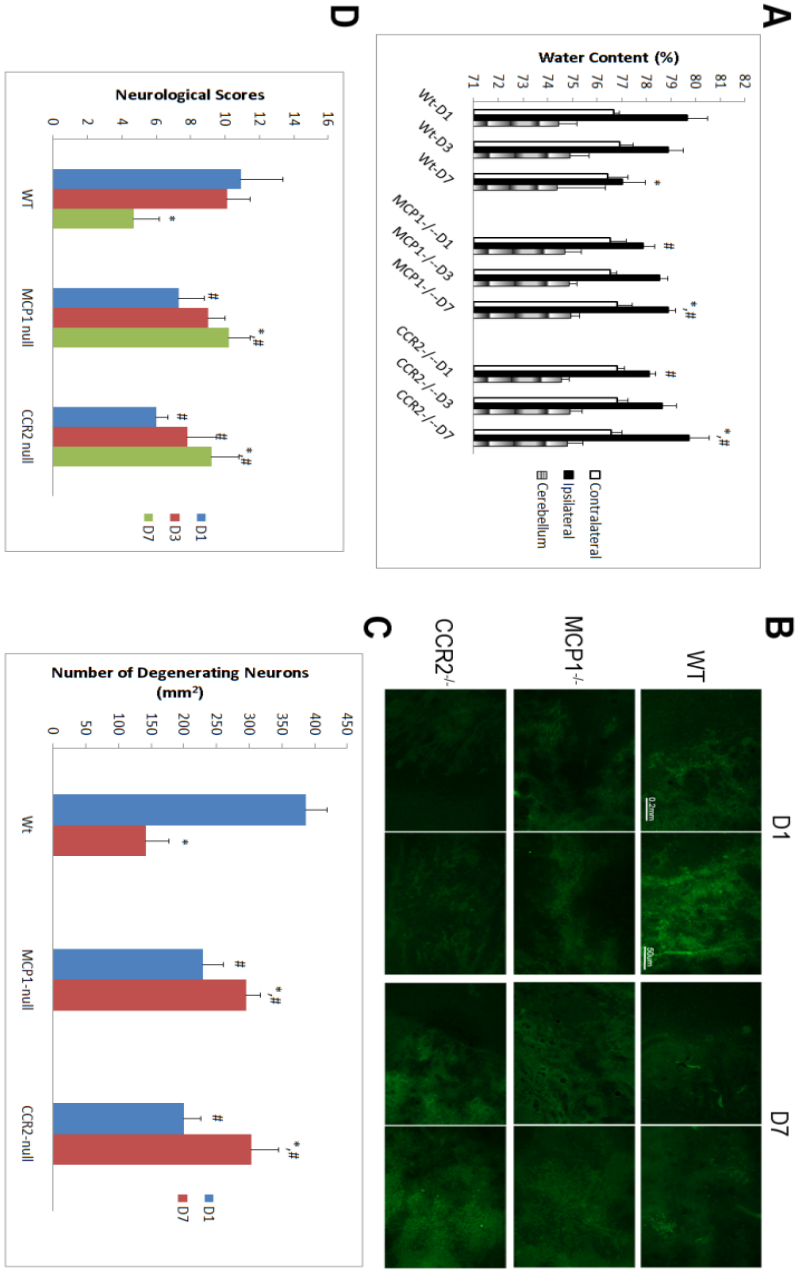

Figure 5-5. Collagenase does not cleave mouse MCP1. Recombinant FL-MCP1 was incubated with collagenase for 24 hours at 37℃. The mixture was then resolved on 15% SDS-PAGE and visualized using anti-6His and anti-MCP1 antibodies.

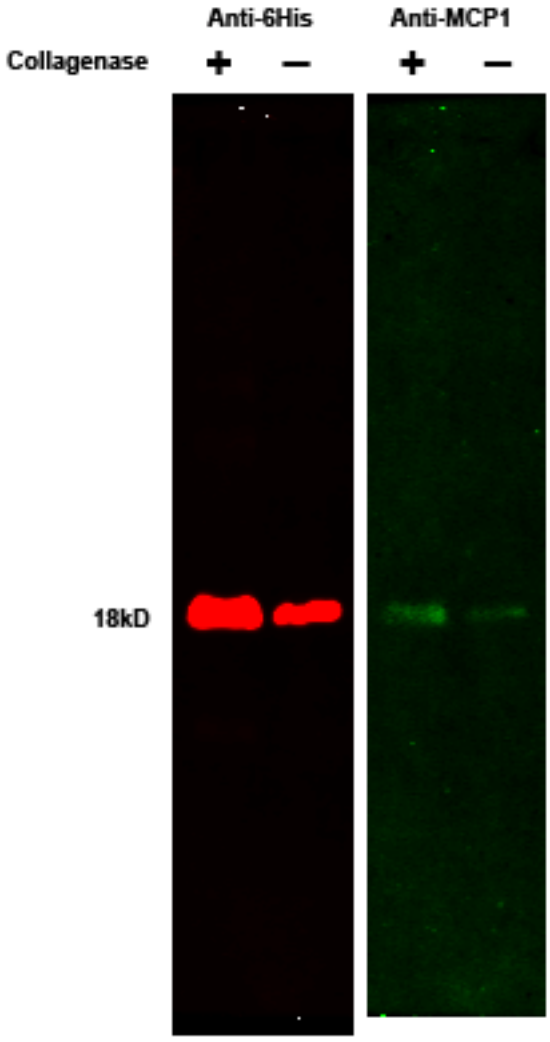

Figure 5-6. Recombinant MCP1 proteins are still active after 7 days at 37℃. A. FL- and K104Stop-MCP1 were incubated at 37℃ for 0, 3, and 7 days. Then, a Boyden chamber migration assay was performed. **B.** Quantification of migrated microglia. Data are shown as mean ± SD (n=3).

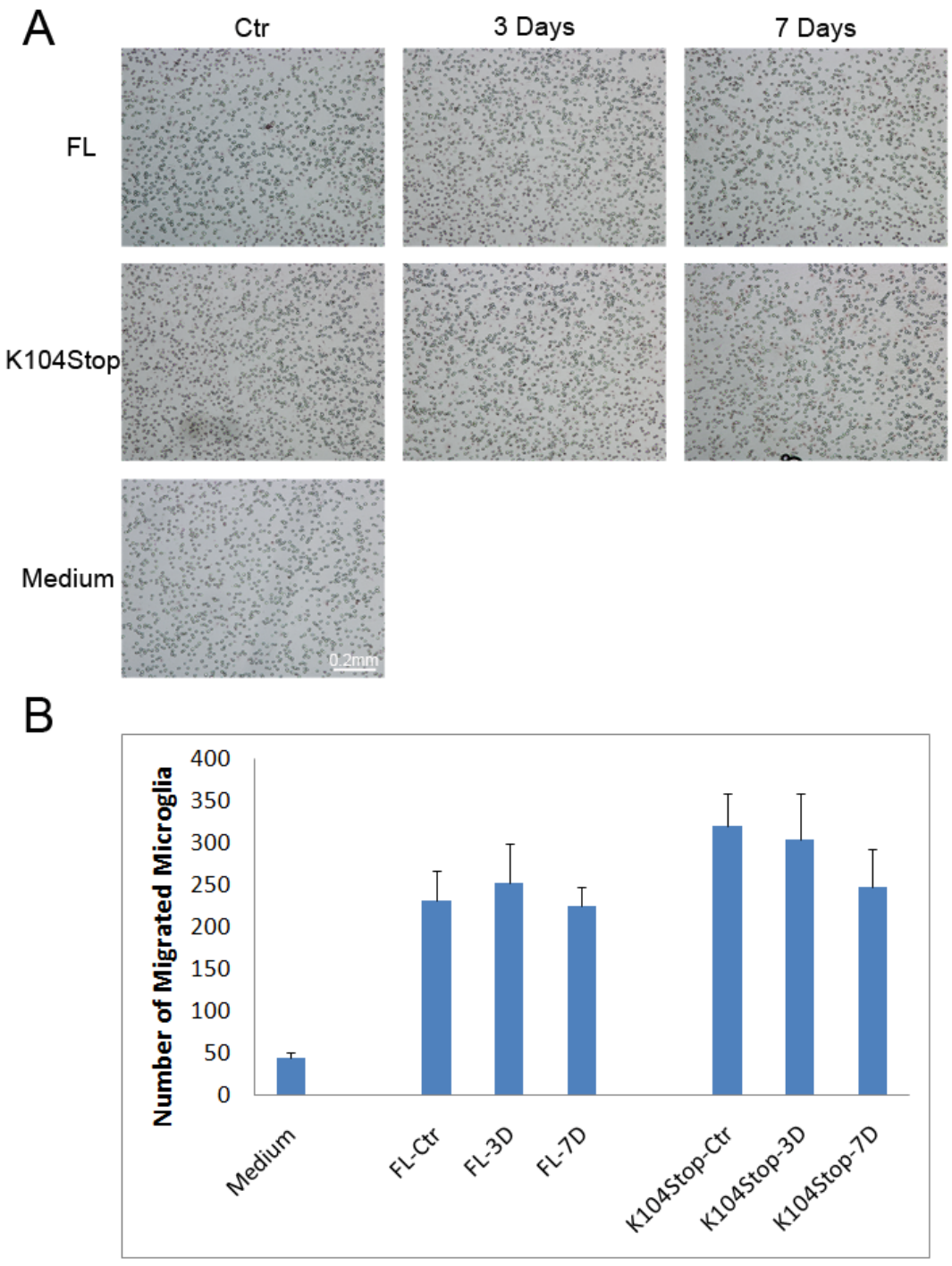

Figure 5-7. The effect of recombinant MCP1 proteins on injury volume. A. MCP1$^{-/-}$ mice were injected with collagenase together with FL-, K104A-, or K104Stop-MCP1 and the injury volume was examined by H&E staining 1, 3, 7 days after injection. **B.** Quantitative data of injury volume are shown as mean ± SD (n=3-4). Comparison with day 1 within the same genotype, *p<0.05 and comparison with MCP1$^{-/-}$ mice injected with FL-MCP1 at the same time points, #p<0.05.

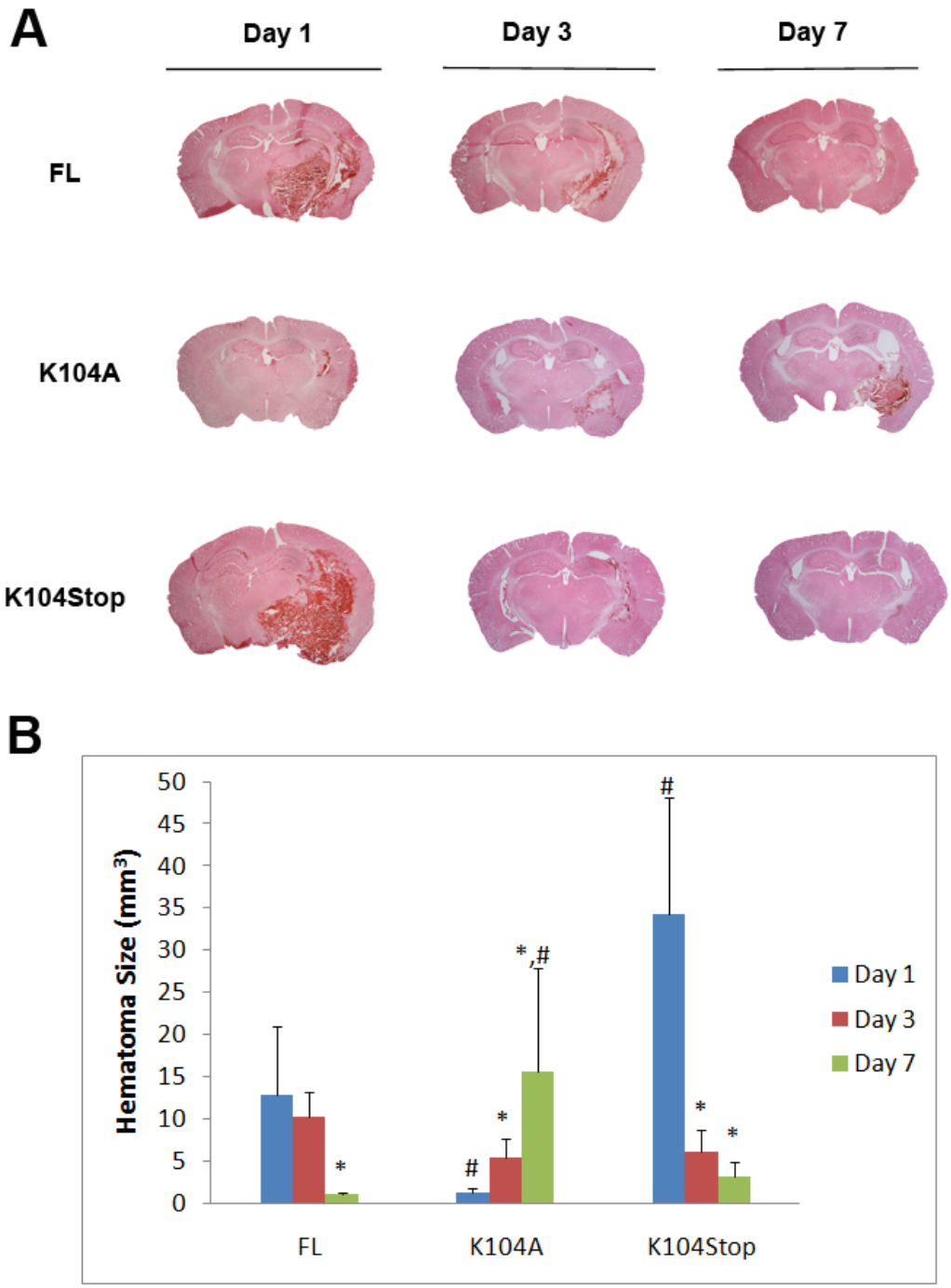

Figure 5-8. The effect of different recombinant MCP1 proteins on microglia activation in MCP1$^{-/-}$ mice. MCP1$^{-/-}$ mice were injected with collagenase and FL-, K104A-, or K104Stop-MCP1. 1, 3, 7 days after injection, the brains were collected and DAB-stained with Iba-1 antibody.

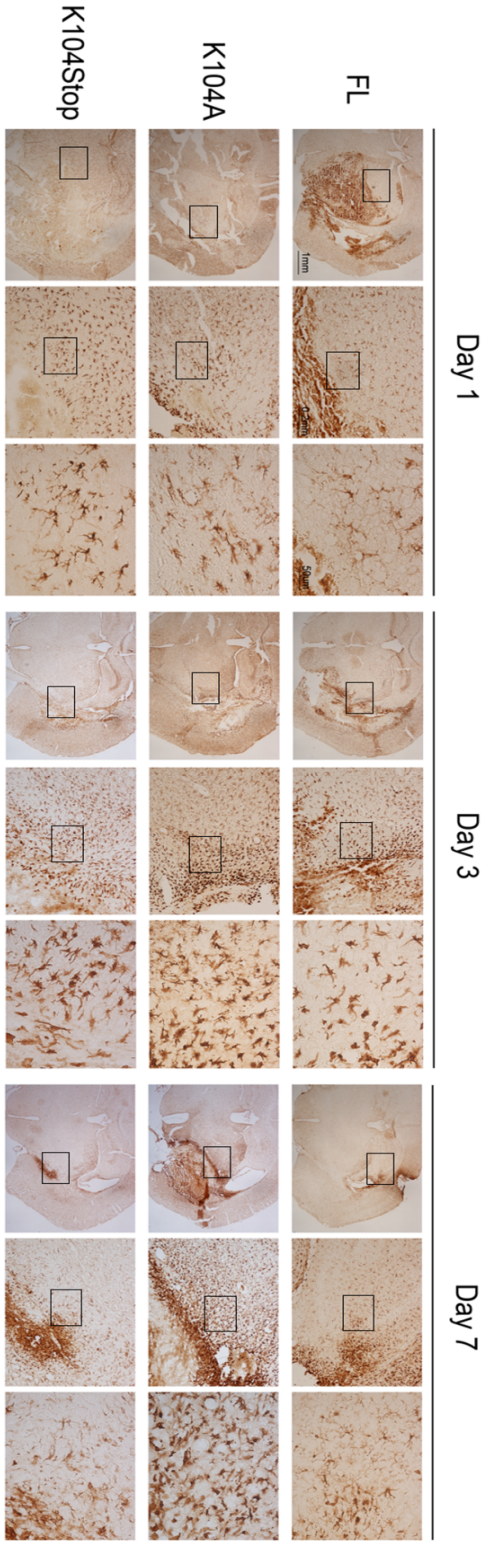

Figure 5-9. The effect of different recombinant MCP1 proteins on leukocyte infiltration in MCP1$^{-/-}$ mice. **A.** MCP1$^{-/-}$ mice were injected with collagenase and FL-, K104A-, or K104Stop-MCP1. 1, 3, 7 days after injection, the infiltration of leukocytes was examined using CD45 immunostaining. **B.** The infiltration of leukocytes is expressed by mean pixel intensity (the ratio of CD45 intensity over the area). Data are shown as mean ± SD (n=3-4). Comparison with day 1 within the same genotype, *p<0.05 and comparison with MCP1$^{-/-}$ mice injected with FL-MCP1 at the same time points, #p<0.05.

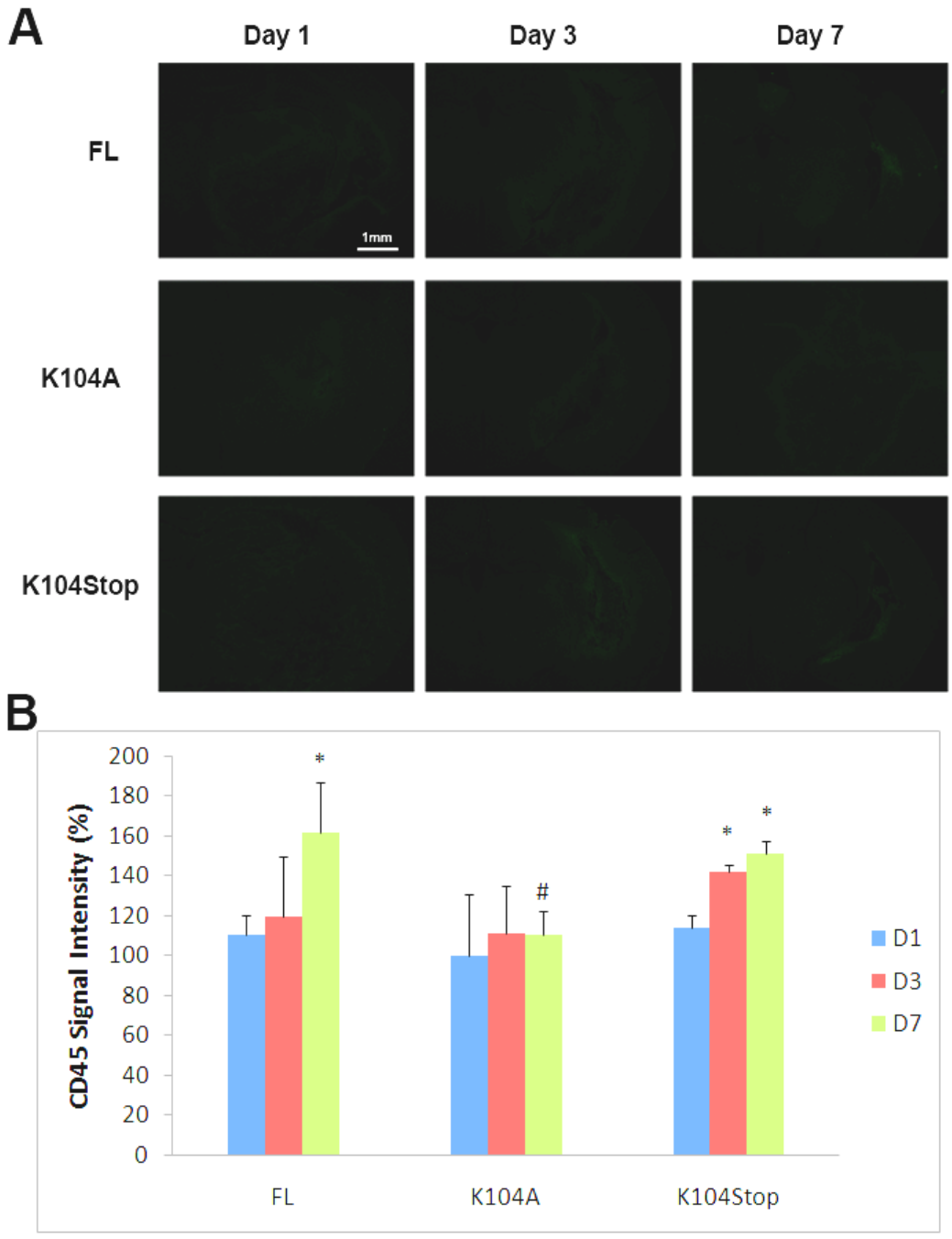

Figure 5-10. The effect of recombinant MCP1 proteins on brain edema, neuronal death, and neurobehavior in MCP1$^{-/-}$ mice. A. MCP1$^{-/-}$ mice were injected with collagenase and FL-, K104A-, or K104Stop-MCP1. The water content was calculated at days 1, 3 and 7 post injury. Data are shown as mean ± SD (n=3). **B.** Mice were treated as described above. Degenerating neurons were visualized using Fluoro-Jade C staining on days 1 and 7 post injury. **C.** Quantification of the number of degenerating neurons on days 1 and 7 post injury. Data are shown as mean ± SD (n=3). **D.** Mice were treated as described above. Neurological scores were evaluated at 1, 3, and 7 days after injury. Values are shown as mean ± SD (n=3-11). For **A, C,** and **D,** comparison with day 1 within the same genotype, *p<0.05 and comparison with MCP1$^{-/-}$ mice injected with FL-MCP1 at the same time points, #p<0.05.

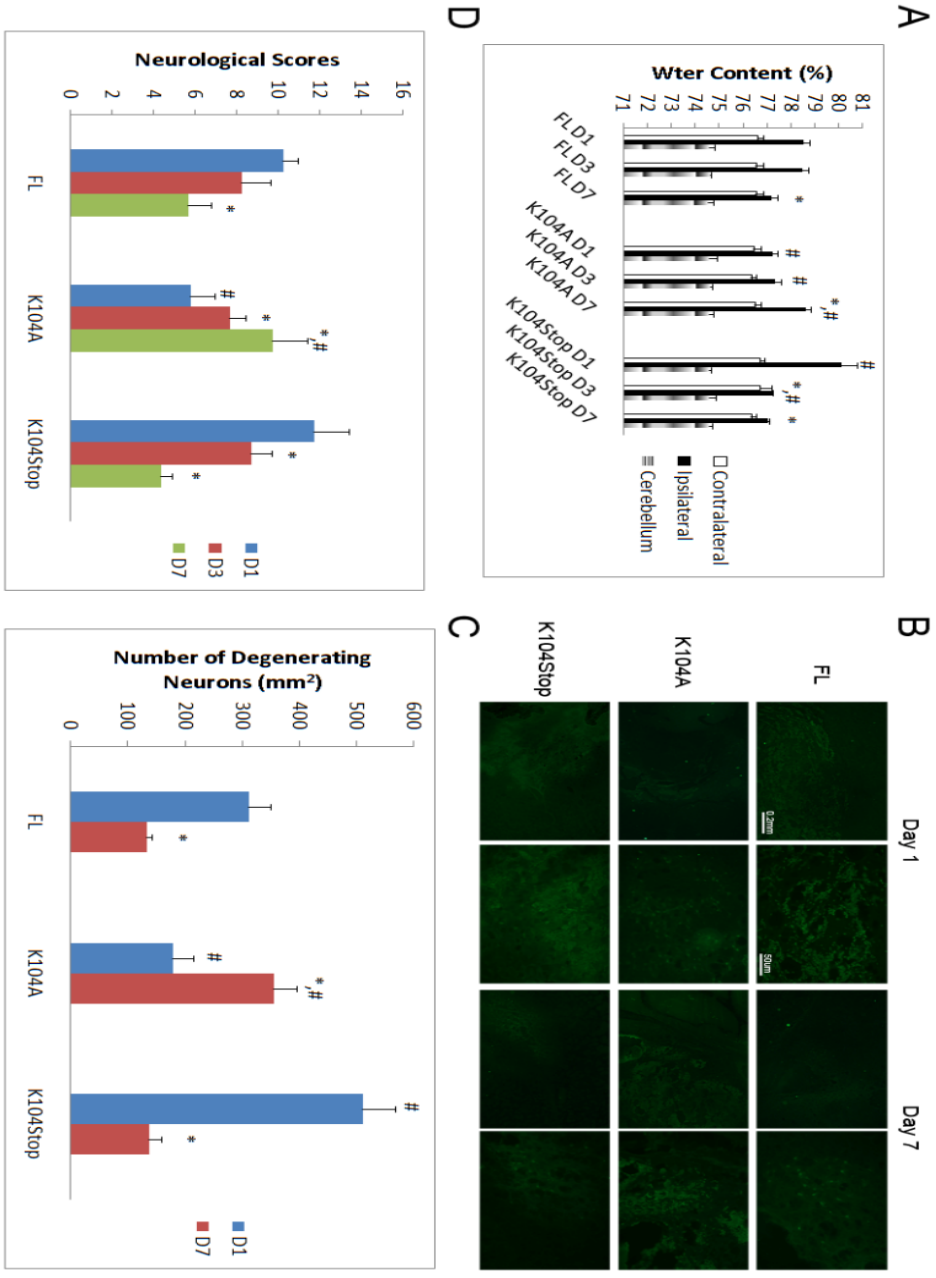

Chapter 6

Conclusions And Future Directions

CONCLUSIONS

We found that plasmin-mediated cleavage of MCP1 enhanced its chemotactic potency by increasing MCP1-CCR2 interaction, activating Rac1 and promoting formation of lamellipodia in microglia.

In addition, we also showed that plasmin-mediated truncation of MCP1 was indispensable for MCP1-induced BBB disruption. The mechanisms underlying the compromise of BBB included activation of ERM proteins, which connected TJP to actin, and reorganization of actin cytoskeleton, which pulled TJP away from the cell-cell borders.

Next, we also found that the extra C-terminal fragment of mouse MCP was inhibitory when appended to the human MCP1 protein, which lacks the heavily glycosylated C-terminus.

Last, using the collagenase-induced ICH model, we demonstrated that lack of MCP1 or CCR2 decreased hematoma size, water content, neuronal death at peri-hematoma region and neurobehavioral deficit score early after injury, but prolonged the disease progression, leading to a delay in recovery. Consistent with our previous studies, we found that the K104Stop-MCP1 was more active than FL-MCP1 in this model.

The work shown here not only broadens our knowledge on glia biology, but also

paves the way to the development of novel inhibitors to MCP1-CCR2 axis, which could be of clinical values in treating inflammatory diseases.

FUTURE DIRECTIONS

Because human MCP1 lacks the heavily glycosylated C-terminus, which is inhibitory to MCP1's functions, future studies should focus on how human MCP1 (always active) is regulated. The first hypothesis is that another protein or protein complex inhibits its activity, just as the C-terminus does. I tried to pull down proteins that interact with human MCP1, however, I was not successful, probably due to the sensitivity of the pull-down assay. An alternative hypothesis is that human MCP1 is regulated at other levels, such as protein turnover rate, binding affinity for CCR2, and signaling diversity. It should be noted that mouse MCP1 has only one CCR2 receptor, whereas the human MCP1 interacts with two receptors, CCR2A and CCR2B, which differ only in the intracellular C-terminus. It is thus likely that the signaling of MCP1 is tight regulated at the receptor-binding/signaling level. It would be interesting to investigate the differential expression of these receptors on different cells and the intracellular signaling cascades following receptor activation. In addition, it is also very interesting to examine the turnover rate of human MCP1 and mouse MCP1 as well as their affinity for CCR2 *in vivo*.

Next, the role of glycosylation should also be investigated. We have shown that absence of the heavily glycosylated C-terminus abrogated the homodimerization/ oligomerization of MCP1. However, how glycosylation affects the functions of MCP1 *in vivo* is still elusive.

We and others have shown that MCP1 disrupts the BBB integrity and BMEC is the major target of MCP1. Does MCP1 affect the integrity of BBB through cells other

than BMEC, such as pericytes, neurons, and microglia? I believe the answer is yes. However, due to underestimated roles of these cells, there are very limited research data on the roles of these cells. Recent studies suggest that pericytes play very important roles in regulation of BBB integrity (Armulik et al., 2010, Daneman et al., 2010). Thus, further studies on BBB should include these cells, such as using BMEC-Astrocyte-Pericyte triple co-culture or BMEC-Astrocyte-Pericyte-Microglia tetra co-culture, instead of BMEC-Astrocyte double co-culture.

We found that MCP1$^{-/-}$ or CCR2$^{-/-}$ mice have more activated microglia accumulated in the peri-hematoma region 3 or 7 days after collagenase injection, suggesting that other signaling pathways, besides MCP1-CCR2, may be responsible for the recruitment of microglia. Using a chemokine-chemokine receptor PCR array, I found that three genes were upregulated in both knockout mice at 3 dpi. The up-regulation of these genes was confirmed by RT-PCR. Thus, future studies should concentrate on the roles of these genes in the recruitment of microglia both *in vitro* and *in vivo*. Additionally, our data also showed that mice deficient for MCP1 or CCR2 had lower numbers of microglia at the peri-hematoma region and these mice had smaller hematoma, lower edema and neuronal death, and smaller neurobehavioral deficit score, suggesting that microglial activation/accumulation at 1 dpi may be neurotoxic. It is, however, unclear what role they have at later time points, probably due to the activation of alternative signaling pathways, which lead to accumulation of microglia in MCP1$^{-/-}$ or CCR2$^{-/-}$ mice at 3 or 7 dpi. To answer this question, it would be necessary to knockdown or knockout the genes that attract microglia to the hematoma. Once we figure out when and at what condition microglial activation is neurotoxic or neuroprotective, we could manipulate the

activation or inhibition of microglial activation (using specific agonists/antagonists of microglia activation (Zhai et al., 2011) or MCP1-CCR2 axis) at specific time and conditions to achieve better recovery.

Another interesting point to work on in the future is to screen for specific plasmin inhibitors. It has been shown that plasmin-mediated truncation of MCP1 is critical for its biological activities. Thus, inhibiting plasmin activity could be a potential therapeutic target. However, it should be noted that this type of inhibitors may not be functional in humans, because plasmin does not cleave human MCP1, the constitutively active MCP1.

REFERENCES

(2005) Priorities for clinical research in intracerebral hemorrhage: report from a National Institute of Neurological Disorders and Stroke workshop. Stroke 36:e23-41.

Abbott NJ, Ronnback L, Hansson E (2006) Astrocyte-endothelial interactions at the blood-brain barrier. Nat Rev Neurosci 7:41-53.

Abbruscato TJ, Lopez SP, Mark KS, Hawkins BT, Davis TP (2002) Nicotine and cotinine modulate cerebral microvascular permeability and protein expression of ZO-1 through nicotinic acetylcholine receptors expressed on brain endothelial cells. J Pharm Sci 91:2525-2538.

Abromson-Leeman S, Hayashi M, Martin C, Sobel R, al-Sabbagh A, Weiner H, Dorf ME (1993) T cell responses to myelin basic protein in experimental autoimmune encephalomyelitis-resistant BALB/c mice. J Neuroimmunol 45:89-101.

Ahdieh M, Vandenbos T, Youakim A (2001) Lung epithelial barrier function and wound healing are decreased by IL-4 and IL-13 and enhanced by IFN-gamma. Am J Physiol Cell Physiol 281:C2029-C2038.

Aloisi F (2001) Immune function of microglia. Glia 36:165-179.

Alter A, Duddy M, Hebert S, Biernacki K, Prat A, Antel JP, Yong VW, Nuttall RK, Pennington CJ, Edwards DR, Bar-Or A (2003) Determinants of human B cell migration across brain endothelial cells. J Immunol 170:4497-4505.

Andersson PB, Perry VH, Gordon S (1991) The kinetics and morphological characteristics of the macrophage-microglial response to kainic acid-induced neuronal degeneration. Neuroscience 42:201-214.

Andjelkovic AV, Kerkovich D, Shanley J, Pulliam L, Pachter JS (1999a) Expression of binding sites for beta chemokines on human astrocytes. Glia 28:225-235.

Andjelkovic AV, Pachter JS (2000) Characterization of binding sites for chemokines MCP-1 and MIP-1alpha on human brain microvessels. J Neurochem 75:1898-1906.

Andjelkovic AV, Spencer DD, Pachter JS (1999b) Visualization of chemokine binding sites on human brain microvessels. J Cell Biol 145:403-412.

Andreeva AY, Krause E, Muller EC, Blasig IE, Utepbergenov DI (2001) Protein kinase C regulates the phosphorylation and cellular localization of occludin. J Biol Chem 276:38480-38486.

Armulik A, Genove G, Mae M, Nisancioglu MH, Wallgard E, Niaudet C, He L, Norlin J, Lindblom P, Strittmatter K, Johansson BR, Betsholtz C (2010) Pericytes regulate the blood-brain barrier. Nature.

Aronowski J, Hall CE (2005) New horizons for primary intracerebral hemorrhage treatment: experience from preclinical studies. Neurol Res 27:268-279.

Balda MS, Matter K (2000) The tight junction protein ZO-1 and an interacting transcription factor regulate ErbB-2 expression. EMBO J 19:2024-2033.

Banisadr G, Gosselin RD, Mechighel P, Kitabgi P, Rostene W, Parsadaniantz SM (2005) Highly regionalized neuronal expression of monocyte chemoattractant protein-1 (MCP-1/CCL2) in rat brain: evidence for its colocalization with neurotransmitters and neuropeptides. J Comp Neurol 489:275-292.

Banisadr G, Queraud-Lesaux F, Boutterin MC, Pelaprat D, Zalc B, Rostene W, Haour F, Parsadaniantz SM (2002) Distribution, cellular localization and functional role of CCR2 chemokine receptors in adult rat brain. J Neurochem 81:257-269.

Bartoli C, Civatte M, Pellissier JF, Figarella-Branger D (2001) CCR2A and CCR2B, the two isoforms of the monocyte chemoattractant protein-1 receptor are up-regulated and expressed by different cell subsets in idiopathic inflammatory myopathies. Acta Neuropathol 102:385-392.

Bazzoni G, Dejana E (2004) Endothelial cell-to-cell junctions: molecular organization and role in vascular homeostasis. Physiol Rev 84:869-901.

Ben-Menachem E, Johansson BB, Svensson TH (1982) Increased vulnerability of the blood-brain barrier to acute hypertension following depletion of brain noradrenaline. J Neural Transm 53:159-167.

Bian GL, Wei LC, Shi M, Wang YQ, Cao R, Chen LW (2007) Fluoro-Jade C can specifically stain the degenerative neurons in the substantia nigra of the 1-methyl-4-phenyl-1,2,3,6-tetrahydro pyridine-treated C57BL/6 mice. Brain Res 1150:55-61.

Blamire A, Anthony D, Rajagopalan B, Sibson N, Perry V, Styles P (2000a) Interleukin-1beta -induced changes in blood-brain barrier permeability, apparent diffusion coefficient, and cerebral blood volume in the rat brain: a magnetic resonance study. J Neurosci 20:8153-8159.

Blamire AM, Anthony DC, Rajagopalan B, Sibson NR, Perry VH, Styles P (2000b) Interleukin-1beta -induced changes in blood-brain barrier permeability, apparent diffusion coefficient, and cerebral blood volume in the rat brain: a magnetic resonance study. J Neurosci 20:8153-8159.

Boddeke EW, Meigel I, Frentzel S, Gourmala NG, Harrison JK, Buttini M, Spleiss O, Gebicke-Harter P (1999) Cultured rat microglia express functional beta-chemokine receptors. J Neuroimmunol 98:176-184.

Bolton SJ, Anthony DC, Perry VH (1998) Loss of the tight junction proteins occludin and zonula occludens-1 from cerebral vascular endothelium during neutrophil-induced blood-brain barrier breakdown in vivo. Neuroscience 86:1245-1257.

Bretscher A, Gary R, Berryman M (1995) Soluble ezrin purified from placenta exists as stable monomers and elongated dimers with masked C-terminal ezrin-radixin-moesin association domains. Biochemistry 34:16830-16837.

Brown RC, Davis TP (2005) Hypoxia/aglycemia alters expression of occludin and actin in brain endothelial cells. Biochem Biophys Res Commun 327:1114-1123.

Calabria AR, Weidenfeller C, Jones AR, de Vries HE, Shusta EV (2006) Puromycin-purified rat brain microvascular endothelial cell cultures exhibit improved barrier properties in response to glucocorticoid induction. J Neurochem 97:922-933.

Capoccia BJ, Gregory AD, Link DC (2008) Recruitment of the inflammatory subset of monocytes to sites of ischemia induces angiogenesis in a monocyte chemoattractant protein-1-dependent fashion. J Leukoc Biol 84:760-768.

Castillo J, Davalos A, Alvarez-Sabin J, Pumar JM, Leira R, Silva Y, Montaner J, Kase CS (2002) Molecular signatures of brain injury after intracerebral hemorrhage. Neurology 58:624-629.

Chan WY, Kohsaka S, Rezaie P (2007) The origin and cell lineage of microglia: new concepts. Brain Res Rev 53:344-354.

Charo IF, Myers SJ, Herman A, Franci C, Connolly AJ, Coughlin SR (1994) Molecular cloning and functional expression of two monocyte chemoattractant protein 1 receptors reveals alternative splicing of the carboxyl-terminal tails. Proc Natl Acad Sci U S A 91:2752-2756.

Chen BP, Kuziel WA, Lane TE (2001) Lack of CCR2 results in increased mortality and impaired leukocyte activation and trafficking following infection of the central nervous system with a neurotropic coronavirus. J Immunol 167:4585-4592.

Chen YL, Chang YJ, Jiang MJ (1999) Monocyte chemotactic protein-1 gene and protein expression in atherogenesis of hypercholesterolemic rabbits. Atherosclerosis 143:115-123.

Chen Z, Gore BB, Long H, Ma L, Tessier-Lavigne M (2008) Alternative splicing of the Robo3 axon guidance receptor governs the midline switch from attraction to repulsion. Neuron 58:325-332.

Choi YK, Kim KW (2008) Blood-neural barrier: its diversity and coordinated cell-to-cell communication. BMB Rep 41:345-352.

Citi S, Cordenonsi M (1998) Tight junction proteins. Biochim Biophys Acta 1448:1-11.

Clark W, Gunion-Rinker L, Lessov N, Hazel K (1998) Citicoline treatment for experimental intracerebral hemorrhage in mice. Stroke 29:2136-2140.

Clarke H, Marano CW, Peralta Soler A, Mullin JM (2000a) Modification of tight junction function by protein kinase C isoforms. Adv Drug Deliv Rev 41:283-301.

Clarke H, Soler AP, Mullin JM (2000b) Protein kinase C activation leads to dephosphorylation of occludin and tight junction permeability increase in LLC-PK1 epithelial cell sheets. J Cell Sci 113 (Pt 18):3187-3196.

Cohen Z, Bonvento G, Lacombe P, Hamel E (1996) Serotonin in the regulation of brain microcirculation. Prog Neurobiol 50:335-362.

Cohen Z, Molinatti G, Hamel E (1997) Astroglial and vascular interactions of noradrenaline terminals in the rat cerebral cortex. J Cereb Blood Flow Metab 17:894-904.

Coyne C, Vanhook M, Gambling T, Carson J, Boucher R, Johnson L (2002) Regulation of airway tight junctions by proinflammatory cytokines. Mol Biol Cell 13:3218-3234.

Daneman R, Zhou L, Kebede AA, Barres BA (2010) Pericytes are required for blood-brain barrier integrity during embryogenesis. Nature.

Davalos D, Grutzendler J, Yang G, Kim JV, Zuo Y, Jung S, Littman DR, Dustin ML, Gan WB (2005) ATP mediates rapid microglial response to local brain injury in vivo. Nature neuroscience 8:752-758.

Dean RA, Cox JH, Bellac CL, Doucet A, Starr AE, Overall CM (2008) Macrophage-specific metalloelastase (MMP-12) truncates and inactivates ELR+ CXC chemokines and generates CCL2, -7, -8, and -13 antagonists: potential role of the macrophage in terminating polymorphonuclear leukocyte influx. Blood 112:3455-3464.

del Pozo MA, Price LS, Alderson NB, Ren XD, Schwartz MA (2000) Adhesion to the extracellular matrix regulates the coupling of the small GTPase Rac to its effector PAK. Embo J 19:2008-2014.

Deli MA, Abraham CS, Niwa M, Falus A (2003) N,N-diethyl-2-[4-(phenylmethyl)phenoxy]ethanamine increases the permeability of primary mouse cerebral endothelial cell monolayers. Inflamm Res 52 Suppl 1:S39-40.

Dente CJ, Steffes CP, Speyer C, Tyburski JG (2001) Pericytes augment the capillary barrier in in vitro cocultures. J Surg Res 97:85-91.

Dicou E, Vincent JP, Mazella J (2004) Neurotensin receptor-3/sortilin mediates neurotensin-induced cytokine/chemokine expression in a murine microglial cell line. J Neurosci Res 78:92-99.

Dimitrijevic OB, Stamatovic SM, Keep RF, Andjelkovic AV (2006) Effects of the chemokine CCL2 on blood-brain barrier permeability during ischemia-reperfusion injury. J Cereb Blood Flow Metab 26:797-810.

Dohgu S, Takata F, Yamauchi A, Nakagawa S, Egawa T, Naito M, Tsuruo T, Sawada Y, Niwa M, Kataoka Y (2005) Brain pericytes contribute to the induction and up-regulation of blood-brain barrier functions through transforming growth factor-beta production. Brain Res 1038:208-215.

Donnan GA, Hankey GJ, Davis SM (2010) Intracerebral haemorrhage: a need for more data and new research directions. Lancet Neurol 9:133-134.

Dore-Duffy P, Owen C, Balabanov R, Murphy S, Beaumont T, Rafols JA (2000) Pericyte migration from the vascular wall in response to traumatic brain injury. Microvasc Res 60:55-69.

Edelman DA, Jiang Y, Tyburski J, Wilson RF, Steffes C (2006) Pericytes and their role in microvasculature homeostasis. J Surg Res 135:305-311.

El Khoury J, Toft M, Hickman SE, Means TK, Terada K, Geula C, Luster AD (2007) Ccr2 deficiency impairs microglial accumulation and accelerates progression of Alzheimer-like disease. Nat Med 13:432-438.

Elkabes S, DiCicco-Bloom EM, Black IB (1996) Brain microglia/macrophages express neurotrophins that selectively regulate microglial proliferation and function. J Neurosci 16:2508-2521.

Ernst CA, Zhang YJ, Hancock PR, Rutledge BJ, Corless CL, Rollins BJ (1994) Biochemical and biologic characterization of murine monocyte chemoattractant protein-1. Identification of two functional domains. J Immunol 152:3541-3549.

Fanning AS, Jameson BJ, Jesaitis LA, Anderson JM (1998) The tight junction protein ZO-1 establishes a link between the transmembrane protein occludin and the actin cytoskeleton. J Biol Chem 273:29745-29753.

Farshori P, Kachar B (1999) Redistribution and phosphorylation of occludin during opening and resealing of tight junctions in cultured epithelial cells. J Membr Biol 170:147-156.

Favre N, Camps M, Arod C, Chabert C, Rommel C, Pasquali C (2008) Chemokine receptor CCR2 undergoes transportin1-dependent nuclear translocation. Proteomics 8:4560-4576.

Fenstermacher J, Gross P, Sposito N, Acuff V, Pettersen S, Gruber K (1988) Structural and functional variations in capillary systems within the brain. Ann N Y Acad Sci 529:21-30.

Fey EG, Wan KM, Penman S (1984) Epithelial cytoskeletal framework and nuclear matrix-intermediate filament scaffold: three-dimensional organization and protein composition. J Cell Biol 98:1973-1984.

Fischer S, Wobben M, Marti HH, Renz D, Schaper W (2002) Hypoxia-induced hyperpermeability in brain microvessel endothelial cells involves VEGF-mediated changes in the expression of zonula occludens-1. Microvasc Res 63:70-80.
Forster C (2008) Tight junctions and the modulation of barrier function in disease. Histochem Cell Biol 130:55-70.
Frangogiannis NG, Dewald O, Xia Y, Ren G, Haudek S, Leucker T, Kraemer D, Taffet G, Rollins BJ, Entman ML (2007) Critical role of monocyte chemoattractant protein-1/CC chemokine ligand 2 in the pathogenesis of ischemic cardiomyopathy. Circulation 115:584-592.
Galasso JM, Liu Y, Szaflarski J, Warren JS, Silverstein FS (2000) Monocyte chemoattractant protein-1 is a mediator of acute excitotoxic injury in neonatal rat brain. Neuroscience 101:737-744.
Ge S, Song L, Serwanski DR, Kuziel WA, Pachter JS (2008) Transcellular transport of CCL2 across brain microvascular endothelial cells. J Neurochem 104:1219-1232.
Ginhoux F, Greter M, Leboeuf M, Nandi S, See P, Gokhan S, Mehler MF, Conway SJ, Ng LG, Stanley ER, Samokhvalov IM, Merad M (2010) Fate Mapping Analysis Reveals That Adult Microglia Derive from Primitive Macrophages. Science.
Giulian D, Baker TJ (1986) Characterization of ameboid microglia isolated from developing mammalian brain. J Neurosci 6:2163-2178.
Glabinski AR, Balasingam V, Tani M, Kunkel SL, Strieter RM, Yong VW, Ransohoff RM (1996) Chemokine monocyte chemoattractant protein-1 is expressed by astrocytes after mechanical injury to the brain. J Immunol 156:4363-4368.
Glynn SL, Yazdanian M (1998) In vitro blood-brain barrier permeability of nevirapine compared to other HIV antiretroviral agents. J Pharm Sci 87:306-310.
Gong C, Boulis N, Qian J, Turner DE, Hoff JT, Keep RF (2001) Intracerebral hemorrhage-induced neuronal death. Neurosurgery 48:875-882; discussion 882-873.
Gong JH, Clark-Lewis I (1995) Antagonists of monocyte chemoattractant protein 1 identified by modification of functionally critical NH2-terminal residues. J Exp Med 181:631-640.
Gong JH, Ratkay LG, Waterfield JD, Clark-Lewis I (1997) An antagonist of monocyte chemoattractant protein 1 (MCP-1) inhibits arthritis in the MRL-lpr mouse model. J Exp Med 186:131-137.
Gonul E, Duz B, Kahraman S, Kayali H, Kubar A, Timurkaynak E (2002) Early pericyte response to brain hypoxia in cats: an ultrastructural study. Microvasc Res 64:116-119.
Gottardi CJ, Arpin M, Fanning AS, Louvard D (1996) The junction-associated protein, zonula occludens-1, localizes to the nucleus before the maturation and during the remodeling of cell-cell contacts. Proc Natl Acad Sci U S A 93:10779-10784.
Gouwy M, Struyf S, Catusse J, Proost P, Van Damme J (2004) Synergy between proinflammatory ligands of G protein-coupled receptors in neutrophil activation and migration. J Leukoc Biol 76:185-194.
Guillemin GJ, Brew BJ (2004) Microglia, macrophages, perivascular macrophages, and pericytes: a review of function and identification. J Leukoc Biol 75:388-397.

Hailer NP, Heppner FL, Haas D, Nitsch R (1997) Fluorescent dye prelabelled microglial cells migrate into organotypic hippocampal slice cultures and ramify. Eur J Neurosci 9:863-866.
Handel TM, Johnson Z, Crown SE, Lau EK, Proudfoot AE (2005) Regulation of protein function by glycosaminoglycans--as exemplified by chemokines. Annu Rev Biochem 74:385-410.
Hanisch UK (2002) Microglia as a source and target of cytokines. Glia 40:140-155.
Hanisch UK, Kettenmann H (2007) Microglia: active sensor and versatile effector cells in the normal and pathologic brain. Nat Neurosci 10:1387-1394.
Harhaj NS, Barber AJ, Antonetti DA (2002) Platelet-derived growth factor mediates tight junction redistribution and increases permeability in MDCK cells. J Cell Physiol 193:349-364.
Hart MN, VanDyk LF, Moore SA, Shasby DM, Cancilla PA (1987) Differential opening of the brain endothelial barrier following neutralization of the endothelial luminal anionic charge in vitro. J Neuropathol Exp Neurol 46:141-153.
Hawkins BT, Abbruscato TJ, Egleton RD, Brown RC, Huber JD, Campos CR, Davis TP (2004) Nicotine increases in vivo blood-brain barrier permeability and alters cerebral microvascular tight junction protein distribution. Brain Res 1027:48-58.
Hawkins BT, Davis TP (2005) The blood-brain barrier/neurovascular unit in health and disease. Pharmacol Rev 57:173-185.
Helander TS, Carpen O, Turunen O, Kovanen PE, Vaheri A, Timonen T (1996) ICAM-2 redistributed by ezrin as a target for killer cells. Nature 382:265-268.
Hemmerich S, Paavola C, Bloom A, Bhakta S, Freedman R, Grunberger D, Krstenansky J, Lee S, McCarley D, Mulkins M, Wong B, Pease J, Mizoue L, Mirzadegan T, Polsky I, Thompson K, Handel TM, Jarnagin K (1999) Identification of residues in the monocyte chemotactic protein-1 that contact the MCP-1 receptor, CCR2. Biochemistry 38:13013-13025.
Hicks K, O'Neil RG, Dubinsky WS, Brown RC (2010) TRPC-mediated actin-myosin contraction is critical for BBB disruption following hypoxic stress. Am J Physiol Cell Physiol 298:C1583-1593.
Hirase T, Kawashima S, Wong EY, Ueyama T, Rikitake Y, Tsukita S, Yokoyama M, Staddon JM (2001) Regulation of tight junction permeability and occludin phosphorylation by Rhoa-p160ROCK-dependent and -independent mechanisms. J Biol Chem 276:10423-10431.
Holmberg J, Clarke DL, Frisen J (2000) Regulation of repulsion versus adhesion by different splice forms of an Eph receptor. Nature 408:203-206.
Hoogewerf AJ, Kuschert GS, Proudfoot AE, Borlat F, Clark-Lewis I, Power CA, Wells TN (1997) Glycosaminoglycans mediate cell surface oligomerization of chemokines. Biochemistry 36:13570-13578.
Horuk R, Martin AW, Wang Z, Schweitzer L, Gerassimides A, Guo H, Lu Z, Hesselgesser J, Perez HD, Kim J, Parker J, Hadley TJ, Peiper SC (1997) Expression of chemokine receptors by subsets of neurons in the central nervous system. J Immunol 158:2882-2890.
Huang D, Wujek J, Kidd G, He TT, Cardona A, Sasse ME, Stein EJ, Kish J, Tani M, Charo IF, Proudfoot AE, Rollins BJ, Handel T, Ransohoff RM (2005) Chronic expression of monocyte chemoattractant protein-1 in the central nervous system

causes delayed encephalopathy and impaired microglial function in mice. FASEB J 19:761-772.
Huber JD, Egleton RD, Davis TP (2001) Molecular physiology and pathophysiology of tight junctions in the blood-brain barrier. Trends Neurosci 24:719-725.
Huber JD, Hau VS, Borg L, Campos CR, Egleton RD, Davis TP (2002) Blood-brain barrier tight junctions are altered during a 72-h exposure to lambda-carrageenan-induced inflammatory pain. Am J Physiol Heart Circ Physiol 283:H1531-1537.
Hulkower K, Brosnan CF, Aquino DA, Cammer W, Kulshrestha S, Guida MP, Rapoport DA, Berman JW (1993) Expression of CSF-1, c-fms, and MCP-1 in the central nervous system of rats with experimental allergic encephalomyelitis. J Immunol 150:2525-2533.
Janzer RC, Raff MC (1987) Astrocytes induce blood-brain barrier properties in endothelial cells. Nature 325:253-257.
Jimenez-Sainz MC, Fast B, Mayor F, Jr., Aragay AM (2003) Signaling pathways for monocyte chemoattractant protein 1-mediated extracellular signal-regulated kinase activation. Mol Pharmacol 64:773-782.
Jung H, Bhangoo S, Banisadr G, Freitag C, Ren D, White FA, Miller RJ (2009) Visualization of chemokine receptor activation in transgenic mice reveals peripheral activation of CCR2 receptors in states of neuropathic pain. J Neurosci 29:8051-8062.
Kacem K, Lacombe P, Seylaz J, Bonvento G (1998) Structural organization of the perivascular astrocyte endfeet and their relationship with the endothelial glucose transporter: a confocal microscopy study. Glia 23:1-10.
Kale G, Naren AP, Sheth P, Rao RK (2003) Tyrosine phosphorylation of occludin attenuates its interactions with ZO-1, ZO-2, and ZO-3. Biochem Biophys Res Commun 302:324-329.
Kalehua AN, Nagel JE, Whelchel LM, Gides JJ, Pyle RS, Smith RJ, Kusiak JW, Taub DD (2004) Monocyte chemoattractant protein-1 and macrophage inflammatory protein-2 are involved in both excitotoxin-induced neurodegeneration and regeneration. Exp Cell Res 297:197-211.
Kataoka K, Asai T, Taneda M, Ueshima S, Matsuo O, Kuroda R, Kawabata A, Carmeliet P (2000) Roles of urokinase type plasminogen activator in a brain stab wound. Brain Res 887:187-190.
Kawedia JD, Nieman ML, Boivin GP, Melvin JE, Kikuchi K, Hand AR, Lorenz JN, Menon AG (2007) Interaction between transcellular and paracellular water transport pathways through Aquaporin 5 and the tight junction complex. Proc Natl Acad Sci U S A 104:3621-3626.
Kim GH, Kellner CP, Hahn DK, Desantis BM, Musabbir M, Starke RM, Rynkowski M, Komotar RJ, Otten ML, Sciacca R, Schmidt JM, Mayer SA, Connolly ES, Jr. (2008) Monocyte chemoattractant protein-1 predicts outcome and vasospasm following aneurysmal subarachnoid hemorrhage. J Neurosurg 109:38-43.
Kim JA, Tran ND, Li Z, Yang F, Zhou W, Fisher MJ (2006) Brain endothelial hemostasis regulation by pericytes. J Cereb Blood Flow Metab 26:209-217.
Kim SU, de Vellis J (2005) Microglia in health and disease. J Neurosci Res 81:302-313.
Kitamoto S, Egashira K (2003) Anti-monocyte chemoattractant protein-1 gene therapy for cardiovascular diseases. Expert Rev Cardiovasc Ther 1:393-400.

Kniesel U, Wolburg H (2000) Tight junctions of the blood-brain barrier. Cell Mol Neurobiol 20:57-76.
Koch AE, Kunkel SL, Harlow LA, Johnson B, Evanoff HL, Haines GK, Burdick MD, Pope RM, Strieter RM (1992) Enhanced production of monocyte chemoattractant protein-1 in rheumatoid arthritis. The Journal of clinical investigation 90:772-779.
Kowala MC, Recce R, Beyer S, Gu C, Valentine M (2000) Characterization of atherosclerosis in LDL receptor knockout mice: macrophage accumulation correlates with rapid and sustained expression of aortic MCP-1/JE. Atherosclerosis 149:323-330.
Krum JM, Kenyon KL, Rosenstein JM (1997) Expression of blood-brain barrier characteristics following neuronal loss and astroglial damage after administration of anti-Thy-1 immunotoxin. Exp Neurol 146:33-45.
Kunkel SL, Lukacs N, Kasama T, Strieter RM (1996) The role of chemokines in inflammatory joint disease. Journal of leukocyte biology 59:6-12.
Kuschert GS, Coulin F, Power CA, Proudfoot AE, Hubbard RE, Hoogewerf AJ, Wells TN (1999) Glycosaminoglycans interact selectively with chemokines and modulate receptor binding and cellular responses. Biochemistry 38:12959-12968.
Lahrtz F, Piali L, Spanaus KS, Seebach J, Fontana A (1998) Chemokines and chemotaxis of leukocytes in infectious meningitis. J Neuroimmunol 85:33-43.
Lai CH, Kuo KH (2005) The critical component to establish in vitro BBB model: Pericyte. Brain Res Brain Res Rev 50:258-265.
Lamkhioued B, Garcia-Zepeda EA, Abi-Younes S, Nakamura H, Jedrzkiewicz S, Wagner L, Renzi PM, Allakhverdi Z, Lilly C, Hamid Q, Luster AD (2000) Monocyte chemoattractant protein (MCP)-4 expression in the airways of patients with asthma. Induction in epithelial cells and mononuclear cells by proinflammatory cytokines. American journal of respiratory and critical care medicine 162:723-732.
Lau EK, Paavola CD, Johnson Z, Gaudry JP, Geretti E, Borlat F, Kungl AJ, Proudfoot AE, Handel TM (2004) Identification of the glycosaminoglycan binding site of the CC chemokine, MCP-1: implications for structure and function in vivo. J Biol Chem 279:22294-22305.
Ling EA (1979) Transformation of monocytes into amoeboid microglia in the corpus callosum of postnatal rats, as shown by labelling monocytes by carbon particles. J Anat 128:847-858.
Louvet-Vallee S (2000) ERM proteins: from cellular architecture to cell signaling. Biol Cell 92:305-316.
Maghazachi AA (2000) Intracellular signaling events at the leading edge of migrating cells. Int J Biochem Cell Biol 32:931-943.
Mahad DJ, Ransohoff RM (2003) The role of MCP-1 (CCL2) and CCR2 in multiple sclerosis and experimental autoimmune encephalomyelitis (EAE). Semin Immunol 15:23-32.
Mahajan SD, Schwartz SA, Aalinkeel R, Chawda RP, Sykes DE, Nair MP (2005) Morphine modulates chemokine gene regulation in normal human astrocytes. Clin Immunol 115:323-332.
Marinissen MJ, Gutkind JS (2001) G-protein-coupled receptors and signaling networks: emerging paradigms. Trends Pharmacol Sci 22:368-376.

Mark KS, Davis TP (2002) Cerebral microvascular changes in permeability and tight junctions induced by hypoxia-reoxygenation. Am J Physiol Heart Circ Physiol 282:H1485-1494.
Matsui T, Maeda M, Doi Y, Yonemura S, Amano M, Kaibuchi K, Tsukita S (1998) Rho-kinase phosphorylates COOH-terminal threonines of ezrin/radixin/moesin (ERM) proteins and regulates their head-to-tail association. J Cell Biol 140:647-657.
Matsushita K, Meng W, Wang X, Asahi M, Asahi K, Moskowitz MA, Lo EH (2000) Evidence for apoptosis after intercerebral hemorrhage in rat striatum. J Cereb Blood Flow Metab 20:396-404.
McCarthy KM, Skare IB, Stankewich MC, Furuse M, Tsukita S, Rogers RA, Lynch RD, Schneeberger EE (1996) Occludin is a functional component of the tight junction. J Cell Sci 109 (Pt 9):2287-2298.
McQuibban GA, Gong JH, Wong JP, Wallace JL, Clark-Lewis I, Overall CM (2002) Matrix metalloproteinase processing of monocyte chemoattractant proteins generates CC chemokine receptor antagonists with anti-inflammatory properties in vivo. Blood 100:1160-1167.
Meeuwsen S, Bsibsi M, Persoon-Deen C, Ravid R, van Noort JM (2005) Cultured human adult microglia from different donors display stable cytokine, chemokine and growth factor gene profiles but respond differently to a pro-inflammatory stimulus. Neuroimmunomodulation 12:235-245.
Mennicken F, Maki R, de Souza EB, Quirion R (1999) Chemokines and chemokine receptors in the CNS: a possible role in neuroinflammation and patterning. Trends Pharmacol Sci 20:73-78.
Michel CC, Curry FE (1999) Microvascular permeability. Physiol Rev 79:703-761.
Middleton J, Neil S, Wintle J, Clark-Lewis I, Moore H, Lam C, Auer M, Hub E, Rot A (1997) Transcytosis and surface presentation of IL-8 by venular endothelial cells. Cell 91:385-395.
Middleton J, Patterson AM, Gardner L, Schmutz C, Ashton BA (2002) Leukocyte extravasation: chemokine transport and presentation by the endothelium. Blood 100:3853-3860.
Miller RJ, Meucci O (1999) AIDS and the brain: is there a chemokine connection? Trends Neurosci 22:471-479.
Minnis JG, Patierno S, Kohlmeier SE, Brecha NC, Tonini M, Sternini C (2003) Ligand-induced mu opioid receptor endocytosis and recycling in enteric neurons. Neuroscience 119:33-42.
Mitic LL, Anderson JM (1998) Molecular architecture of tight junctions. Annu Rev Physiol 60:121-142.
Morimoto H, Hirose M, Takahashi M, Kawaguchi M, Ise H, Kolattukudy PE, Yamada M, Ikeda U (2008) MCP-1 induces cardioprotection against ischaemia/reperfusion injury: role of reactive oxygen species. Cardiovasc Res 78:554-562.
Murphy PM (1994) The molecular biology of leukocyte chemoattractant receptors. Annu Rev Immunol 12:593-633.
Nakagawa S, Deli MA, Kawaguchi H, Shimizudani T, Shimono T, Kittel A, Tanaka K, Niwa M (2009) A new blood-brain barrier model using primary rat brain endothelial cells, pericytes and astrocytes. Neurochem Int 54:253-263.

Nakajima K, Kohsaka S (2004) Microglia: neuroprotective and neurotrophic cells in the central nervous system. Curr Drug Targets Cardiovasc Haematol Disord 4:65-84.
Nakajima K, Tohyama Y, Kohsaka S, Kurihara T (2002) Ceramide activates microglia to enhance the production/secretion of brain-derived neurotrophic factor (BDNF) without induction of deleterious factors in vitro. J Neurochem 80:697-705.
Nakamura F, Amieva MR, Furthmayr H (1995) Phosphorylation of threonine 558 in the carboxyl-terminal actin-binding domain of moesin by thrombin activation of human platelets. J Biol Chem 270:31377-31385.
Neuhaus J, Risau W, Wolburg H (1991) Induction of blood-brain barrier characteristics in bovine brain endothelial cells by rat astroglial cells in transfilter coculture. Ann N Y Acad Sci 633:578-580.
Ni W, Egashira K, Kitamoto S, Kataoka C, Koyanagi M, Inoue S, Imaizumi K, Akiyama C, Nishida KI, Takeshita A (2001) New anti-monocyte chemoattractant protein-1 gene therapy attenuates atherosclerosis in apolipoprotein E-knockout mice. Circulation 103:2096-2101.
Nimmerjahn A, Kirchhoff F, Helmchen F (2005) Resting microglial cells are highly dynamic surveillants of brain parenchyma in vivo. Science 308:1314-1318.
Ogunrinade O, Kameya GT, Truskey GA (2002) Effect of fluid shear stress on the permeability of the arterial endothelium. Ann Biomed Eng 30:430-446.
Ohno K, Chiueh CC, Burns EM, Pettigrew KD, Rapoport SI (1980) Cerebrovascular integrity in protein-deprived rats. Brain Res Bull 5:251-255.
Oldendorf WH, Cornford ME, Brown WJ (1977) The large apparent work capability of the blood-brain barrier: a study of the mitochondrial content of capillary endothelial cells in brain and other tissues of the rat. Ann Neurol 1:409-417.
Ono K, Takii T, Onozaki K, Ikawa M, Okabe M, Sawada M (1999) Migration of exogenous immature hematopoietic cells into adult mouse brain parenchyma under GFP-expressing bone marrow chimera. Biochem Biophys Res Commun 262:610-614.
Oshima T, Laroux FS, Coe LL, Morise Z, Kawachi S, Bauer P, Grisham MB, Specian RD, Carter P, Jennings S, Granger DN, Joh T, Alexander JS (2001) Interferon-gamma and interleukin-10 reciprocally regulate endothelial junction integrity and barrier function. Microvasc Res 61:130-143.
Paavola CD, Hemmerich S, Grunberger D, Polsky I, Bloom A, Freedman R, Mulkins M, Bhakta S, McCarley D, Wiesent L, Wong B, Jarnagin K, Handel TM (1998) Monomeric monocyte chemoattractant protein-1 (MCP-1) binds and activates the MCP-1 receptor CCR2B. J Biol Chem 273:33157-33165.
Pankov R, Endo Y, Even-Ram S, Araki M, Clark K, Cukierman E, Matsumoto K, Yamada KM (2005) A Rac switch regulates random versus directionally persistent cell migration. J Cell Biol 170:793-802.
Paolini JF, Willard D, Consler T, Luther M, Krangel MS (1994) The chemokines IL-8, monocyte chemoattractant protein-1, and I-309 are monomers at physiologically relevant concentrations. J Immunol 153:2704-2717.
Parathath S, Parathath S, Tsirka S (2006) Nitric oxide mediates neurodegeneration and breakdown of the blood-brain barrier in tPA-dependent excitotoxic injury in mice.

. J Cell Sci 119:339-349.

Paul R, Koedel U, Winkler F, Kieseier B, Fontana A, Kopf M, Hartung H, Pfister H (2003) Lack of IL-6 augments inflammatory response but decreases vascular permeability in bacterial meningitis. Brain 126:1873-1882.

Pearson MA, Reczek D, Bretscher A, Karplus PA (2000) Structure of the ERM protein moesin reveals the FERM domain fold masked by an extended actin binding tail domain. Cell 101:259-270.

Pedram A, Razandi M, Levin ER (2002) Deciphering vascular endothelial cell growth factor/vascular permeability factor signaling to vascular permeability. Inhibition by atrial natriuretic peptide. J Biol Chem 277:44385-44398.

Peppiatt CM, Howarth C, Mobbs P, Attwell D (2006) Bidirectional control of CNS capillary diameter by pericytes. Nature 443:700-704.

Persidsky Y, Ramirez SH, Haorah J, Kanmogne GD (2006) Blood-brain barrier: structural components and function under physiologic and pathologic conditions. J Neuroimmune Pharmacol 1:223-236.

Pestonjamasp K, Amieva MR, Strassel CP, Nauseef WM, Furthmayr H, Luna EJ (1995) Moesin, ezrin, and p205 are actin-binding proteins associated with neutrophil plasma membranes. Mol Biol Cell 6:247-259.

Proost P, Struyf S, Couvreur M, Lenaerts JP, Conings R, Menten P, Verhaert P, Wuyts A, Van Damme J (1998) Posttranslational modifications affect the activity of the human monocyte chemotactic proteins MCP-1 and MCP-2: identification of MCP-2(6-76) as a natural chemokine inhibitor. J Immunol 160:4034-4041.

Qureshi AI, Ali Z, Suri MF, Shuaib A, Baker G, Todd K, Guterman LR, Hopkins LN (2003) Extracellular glutamate and other amino acids in experimental intracerebral hemorrhage: an in vivo microdialysis study. Crit Care Med 31:1482-1489.

Qureshi AI, Tuhrim S, Broderick JP, Batjer HH, Hondo H, Hanley DF (2001) Spontaneous intracerebral hemorrhage. N Engl J Med 344:1450-1460.

Rabchevsky AG, Streit WJ (1997) Grafting of cultured microglial cells into the lesioned spinal cord of adult rats enhances neurite outgrowth. J Neurosci Res 47:34-48.

Ransohoff RM (2002) The chemokine system in neuroinflammation: an update. J Infect Dis 186 Suppl 2:S152-156.

Ransohoff RM, Hamilton TA, Tani M, Stoler MH, Shick HE, Major JA, Estes ML, Thomas DM, Tuohy VK (1993) Astrocyte expression of mRNA encoding cytokines IP-10 and JE/MCP-1 in experimental autoimmune encephalomyelitis. FASEB J 7:592-600.

Rao RK, Basuroy S, Rao VU, Karnaky Jr KJ, Gupta A (2002) Tyrosine phosphorylation and dissociation of occludin-ZO-1 and E-cadherin-beta-catenin complexes from the cytoskeleton by oxidative stress. Biochem J 368:471-481.

Ray E, Samanta AK (1996) Dansyl cadaverine regulates ligand induced endocytosis of interleukin-8 receptor in human polymorphonuclear neutrophils. FEBS letters 378:235-239.

Reijerkerk A, Kooij G, van der Pol SM, Leyen T, van Het Hof B, Couraud PO, Vivien D, Dijkstra CD, de Vries HE (2008) Tissue-type plasminogen activator is a regulator of monocyte diapedesis through the brain endothelial barrier. J Immunol 181:3567-3574.

Ribo M, Grotta JC (2006) Latest advances in intracerebral hemorrhage. Curr Neurol Neurosci Rep 6:17-22.
Rickert P, Weiner OD, Wang F, Bourne HR, Servant G (2000) Leukocytes navigate by compass: roles of PI3Kgamma and its lipid products. Trends in cell biology 10:466-473.
Ridley AJ, Schwartz MA, Burridge K, Firtel RA, Ginsberg MH, Borisy G, Parsons JT, Horwitz AR (2003) Cell migration: integrating signals from front to back. Science (New York, NY 302:1704-1709.
Riesen FK, Rothen-Rutishauser B, Wunderli-Allenspach H (2002) A ZO1-GFP fusion protein to study the dynamics of tight junctions in living cells. Histochem Cell Biol 117:307-315.
Robatzek S, Chinchilla D, Boller T (2006) Ligand-induced endocytosis of the pattern recognition receptor FLS2 in Arabidopsis. Genes & development 20:537-542.
Robinson LJ, Pang S, Harris DS, Heuser J, James DE (1992) Translocation of the glucose transporter (GLUT4) to the cell surface in permeabilized 3T3-L1 adipocytes: effects of ATP insulin, and GTP gamma S and localization of GLUT4 to clathrin lattices. J Cell Biol 117:1181-1196.
Rogove AD, Siao C, Keyt B, Strickland S, Tsirka SE (1999) Activation of microglia reveals a non-proteolytic cytokine function for tissue plasminogen activator in the central nervous system. Journal of cell science 112 (Pt 22):4007-4016.
Rollins BJ (1997) Chemokines. Blood 90:909-928.
Romero IA, Radewicz K, Jubin E, Michel CC, Greenwood J, Couraud PO, Adamson P (2003) Changes in cytoskeletal and tight junctional proteins correlate with decreased permeability induced by dexamethasone in cultured rat brain endothelial cells. Neurosci Lett 344:112-116.
Ross D, Joyner W (1997) Resting distribution and stimulated translocation of protein kinase C isoforms alpha, epsilon and zeta in response to bradykinin and TNF in human endothelial cells. Endothelium 5:321-332.
Rot A (1992) Endothelial cell binding of NAP-1/IL-8: role in neutrophil emigration. Immunol Today 13:291-294.
Rot A (1993) Neutrophil attractant/activation protein-1 (interleukin-8) induces in vitro neutrophil migration by haptotactic mechanism. Eur J Immunol 23:303-306.
Ruffini PA, Morandi P, Cabioglu N, Altundag K, Cristofanilli M (2007) Manipulating the chemokine-chemokine receptor network to treat cancer. Cancer 109:2392-2404.
Sakakibara A, Furuse M, Saitou M, Ando-Akatsuka Y, Tsukita S (1997) Possible involvement of phosphorylation of occludin in tight junction formation. J Cell Biol 137:1393-1401.
Schmued LC, Hopkins KJ (2000) Fluoro-Jade B: a high affinity fluorescent marker for the localization of neuronal degeneration. Brain Res 874:123-130.
Schulze C, Firth JA (1993) Immunohistochemical localization of adherens junction components in blood-brain barrier microvessels of the rat. J Cell Sci 104 (Pt 3):773-782.
Sedlakova R, Shivers RR, Del Maestro RF (1999) Ultrastructure of the blood-brain barrier in the rabbit. J Submicrosc Cytol Pathol 31:149-161.
Serrador JM, Alonso-Lebrero JL, del Pozo MA, Furthmayr H, Schwartz-Albiez R, Calvo J, Lozano F, Sanchez-Madrid F (1997) Moesin interacts with the cytoplasmic

region of intercellular adhesion molecule-3 and is redistributed to the uropod of T lymphocytes during cell polarization. J Cell Biol 138:1409-1423.
Sheehan JJ, Zhou C, Gravanis I, Rogove AD, Wu YP, Bogenhagen DF, Tsirka SE (2007) Proteolytic activation of monocyte chemoattractant protein-1 by plasmin underlies excitotoxic neurodegeneration in mice. J Neurosci 27:1738-1745.
Simard M, Arcuino G, Takano T, Liu QS, Nedergaard M (2003) Signaling at the gliovascular interface. J Neurosci 23:9254-9262.
Stamatovic SM, Dimitrijevic OB, Keep RF, Andjelkovic AV (2006) Protein kinase Calpha-RhoA cross-talk in CCL2-induced alterations in brain endothelial permeability. J Biol Chem 281:8379-8388.
Stamatovic SM, Keep RF, Kunkel SL, Andjelkovic AV (2003) Potential role of MCP-1 in endothelial cell tight junction 'opening': signaling via Rho and Rho kinase. J Cell Sci 116:4615-4628.
Stamatovic SM, Shakui P, Keep RF, Moore BB, Kunkel SL, Van Rooijen N, Andjelkovic AV (2005) Monocyte chemoattractant protein-1 regulation of blood-brain barrier permeability. J Cereb Blood Flow Metab 25:593-606.
Stephan CC, Brock TA (1996) Vascular endothelial growth factor, a multifunctional polypeptide. P R Health Sci J 15:169-178.
Stevenson BR, Siliciano JD, Mooseker MS, Goodenough DA (1986) Identification of ZO-1: a high molecular weight polypeptide associated with the tight junction (zonula occludens) in a variety of epithelia. J Cell Biol 103:755-766.
Stewart PA, Wiley MJ (1981) Developing nervous tissue induces formation of blood-brain barrier characteristics in invading endothelial cells: a study using quail--chick transplantation chimeras. Dev Biol 84:183-192.
Storer PD, Xu J, Chavis J, Drew PD (2005) Peroxisome proliferator-activated receptor-gamma agonists inhibit the activation of microglia and astrocytes: implications for multiple sclerosis. J Neuroimmunol 161:113-122.
Suzumura A, Mezitis SG, Gonatas NK, Silberberg DH (1987) MHC antigen expression on bulk isolated macrophage-microglia from newborn mouse brain: induction of Ia antigen expression by gamma-interferon. J Neuroimmunol 15:263-278.
Tao-Cheng JH, Nagy Z, Brightman MW (1987) Tight junctions of brain endothelium in vitro are enhanced by astroglia. J Neurosci 7:3293-3299.
Terashima Y, Onai N, Murai M, Enomoto M, Poonpiriya V, Hamada T, Motomura K, Suwa M, Ezaki T, Haga T, Kanegasaki S, Matsushima K (2005) Pivotal function for cytoplasmic protein FROUNT in CCR2-mediated monocyte chemotaxis. Nat Immunol 6:827-835.
Thiex R, Mayfrank L, Rohde V, Gilsbach JM, Tsirka SA (2004) The role of endogenous versus exogenous tPA on edema formation in murine ICH. Exp Neurol 189:25-32.
Tillie-Leblond I, Hammad H, Desurmont S, Pugin J, Wallaert B, Tonnel AB, Gosset P (2000) CC chemokines and interleukin-5 in bronchial lavage fluid from patients with status asthmaticus. Potential implication in eosinophil recruitment. American journal of respiratory and critical care medicine 162:586-592.
Tong XK, Hamel E (1999) Regional cholinergic denervation of cortical microvessels and nitric oxide synthase-containing neurons in Alzheimer's disease. Neuroscience 92:163-175.

Tran PB, Miller RJ (2003) Chemokine receptors: signposts to brain development and disease. Nat Rev Neurosci 4:444-455.
Tsirka SE, Gualandris A, Amaral DG, Strickland S (1995) Excitotoxin-induced neuronal degeneration and seizure are mediated by tissue plasminogen activator. Nature 377:340-344.
Tsirka SE, Rogove AD, Bugge TH, Degen JL, Strickland S (1997) An extracellular proteolytic cascade promotes neuronal degeneration in the mouse hippocampus. J Neurosci 17:543-552.
Tsukamoto T, Nigam S (1997a) Tight junction proteins form large complexes and associate with the cytoskeleton in an ATP depletion model for reversible junction assembly. J Biol Chem 272:16133-16139.
Tsukamoto T, Nigam S (1999a) Role of tyrosine phosphorylation in the reassembly of occludin and other tight junction proteins. Am J Physiol 276:F737-750.
Tsukamoto T, Nigam SK (1997b) Tight junction proteins form large complexes and associate with the cytoskeleton in an ATP depletion model for reversible junction assembly. J Biol Chem 272:16133-16139.
Tsukamoto T, Nigam SK (1999b) Role of tyrosine phosphorylation in the reassembly of occludin and other tight junction proteins. Am J Physiol 276:F737-750.
Tsukita S, Oishi K, Sato N, Sagara J, Kawai A (1994) ERM family members as molecular linkers between the cell surface glycoprotein CD44 and actin-based cytoskeletons. J Cell Biol 126:391-401.
Turunen O, Wahlstrom T, Vaheri A (1994) Ezrin has a COOH-terminal actin-binding site that is conserved in the ezrin protein family. J Cell Biol 126:1445-1453.
Ulvestad E, Williams K, Bjerkvig R, Tiekotter K, Antel J, Matre R (1994) Human microglial cells have phenotypic and functional characteristics in common with both macrophages and dendritic antigen-presenting cells. J Leukoc Biol 56:732-740.
Van Der Voorn P, Tekstra J, Beelen RH, Tensen CP, Van Der Valk P, De Groot CJ (1999) Expression of MCP-1 by reactive astrocytes in demyelinating multiple sclerosis lesions. Am J Pathol 154:45-51.
van Nieuw Amerongen GP, van Delft S, Vermeer MA, Collard JG, van Hinsbergh VW (2000) Activation of RhoA by thrombin in endothelial hyperpermeability: role of Rho kinase and protein tyrosine kinases. Circ Res 87:335-340.
Vaucher E, Hamel E (1995) Cholinergic basal forebrain neurons project to cortical microvessels in the rat: electron microscopic study with anterogradely transported Phaseolus vulgaris leucoagglutinin and choline acetyltransferase immunocytochemistry. J Neurosci 15:7427-7441.
Vaucher E, Tong XK, Cholet N, Lantin S, Hamel E (2000) GABA neurons provide a rich input to microvessels but not nitric oxide neurons in the rat cerebral cortex: a means for direct regulation of local cerebral blood flow. J Comp Neurol 421:161-171.
Vorbrodt AW, Dobrogowska DH (2003) Molecular anatomy of intercellular junctions in brain endothelial and epithelial barriers: electron microscopist's view. Brain Res Brain Res Rev 42:221-242.

Wachtel M, Frei K, Ehler E, Fontana A, Winterhalter K, Gloor SM (1999) Occludin proteolysis and increased permeability in endothelial cells through tyrosine phosphatase inhibition. J Cell Sci 112 (Pt 23):4347-4356.
Wagner L, Yang OO, Garcia-Zepeda EA, Ge Y, Kalams SA, Walker BD, Pasternack MS, Luster AD (1998) Beta-chemokines are released from HIV-1-specific cytolytic T-cell granules complexed to proteoglycans. Nature 391:908-911.
Wain JH, Kirby JA, Ali S (2002) Leucocyte chemotaxis: Examination of mitogen-activated protein kinase and phosphoinositide 3-kinase activation by Monocyte Chemoattractant Proteins-1, -2, -3 and -4. Clin Exp Immunol 127:436-444.
Wang J (2010) Preclinical and clinical research on inflammation after intracerebral hemorrhage. Prog Neurobiol 92:463-477.
Wang J, Dore S (2007a) Heme oxygenase-1 exacerbates early brain injury after intracerebral haemorrhage. Brain 130:1643-1652.
Wang J, Dore S (2007b) Inflammation after intracerebral hemorrhage. J Cereb Blood Flow Metab 27:894-908.
Wang J, Rogove AD, Tsirka AE, Tsirka SE (2003) Protective role of tuftsin fragment 1-3 in an animal model of intracerebral hemorrhage. Ann Neurol 54:655-664.
Wang J, Tsirka SE (2005) Tuftsin fragment 1-3 is beneficial when delivered after the induction of intracerebral hemorrhage. Stroke 36:613-618.
Wang L, Fuster M, Sriramarao P, Esko JD (2005) Endothelial heparan sulfate deficiency impairs L-selectin- and chemokine-mediated neutrophil trafficking during inflammatory responses. Nat Immunol 6:902-910.
Ward PD, Klein RR, Troutman MD, Desai S, Thakker DR (2002) Phospholipase C-gamma modulates epithelial tight junction permeability through hyperphosphorylation of tight junction proteins. J Biol Chem 277:35760-35765.
Willis CL, Nolan CC, Reith SN, Lister T, Prior MJ, Guerin CJ, Mavroudis G, Ray DE (2004) Focal astrocyte loss is followed by microvascular damage, with subsequent repair of the blood-brain barrier in the apparent absence of direct astrocytic contact. Glia 45:325-337.
Wittendorp MC, Boddeke HW, Biber K (2004) Adenosine A3 receptor-induced CCL2 synthesis in cultured mouse astrocytes. Glia 46:410-418.
Wojciak-Stothard B, Entwistle A, Garg R, Ridley A (1998a) Regulation of TNF-alpha-induced reorganization of the actin cytoskeleton and cell-cell junction by Rho, Rac and Cdc42 in human endothelial cells. J Cell Physiol 176:150-165.
Wojciak-Stothard B, Entwistle A, Garg R, Ridley AJ (1998b) Regulation of TNF-alpha-induced reorganization of the actin cytoskeleton and cell-cell junctions by Rho, Rac, and Cdc42 in human endothelial cells. J Cell Physiol 176:150-165.
Wolburg H, Lippoldt A (2002) Tight junctions of the blood-brain barrier: development, composition and regulation. Vascul Pharmacol 38:323-337.
Wu M, Tsirka S (2009) Endothelial NOS-deficient mice reveal dual roles for nitric oxide during experimental autoimmune encephalomyelitis. Glia 57:1204-1215.
Wu VY, Walz DA, McCoy LE (1977) Purification and characterization of human and bovine platelet factor 4. Prep Biochem 7:479-493.
Wu YP, McMahon E, Kraine MR, Tisch R, Meyers A, Frelinger J, Matsushima GK, Suzuki K (2000) Distribution and characterization of GFP(+) donor

hematogenous cells in Twitcher mice after bone marrow transplantation. Am J Pathol 156:1849-1854.
Xi G, Keep RF, Hoff JT (2006) Mechanisms of brain injury after intracerebral haemorrhage. Lancet Neurol 5:53-63.
Yan YP, Sailor KA, Lang BT, Park SW, Vemuganti R, Dempsey RJ (2007) Monocyte chemoattractant protein-1 plays a critical role in neuroblast migration after focal cerebral ischemia. J Cereb Blood Flow Metab 27:1213-1224.
Yang G, Gong C, Qin Z, Liu X, Betz L (1999a) Tumor necrosis factor alpha expression produces increased blood−brain barrier permeability following temporary focal cerebral ischemia in mice. Brain Res Mol Brain Res 69:135-143.
Yang GY, Gong C, Qin Z, Liu XH, Lorris Betz A (1999b) Tumor necrosis factor alpha expression produces increased blood-brain barrier permeability following temporary focal cerebral ischemia in mice. Brain Res Mol Brain Res 69:135-143.
Yao Y, Tsirka SE (2010) The C terminus of mouse monocyte chemoattractant protein 1 (MCP1) mediates MCP1 dimerization while blocking its chemotactic potency. J Biol Chem 285:31509-31516.
Yao Y, Tsirka SE (2011) Truncation of monocyte chemoattractant protein 1 by plasmin promotes blood-brain barrier disruption. J Cell Sci.
Yepes M, Sandkvist M, Moore E, Bugge T, Strickland D, Lawrence D (2003) Tissue-type plasminogen activator induces opening of the blood-brain barrier via the LDL receptor-related protein. J Clin Invest 112:1533-1540.
Yonemura S, Nagafuchi A, Sato N, Tsukita S (1993) Concentration of an integral membrane protein, CD43 (leukosialin, sialophorin), in the cleavage furrow through the interaction of its cytoplasmic domain with actin-based cytoskeletons. J Cell Biol 120:437-449.
Yoshie O, Imai T, Nomiyama H (1997) Novel lymphocyte-specific CC chemokines and their receptors. J Leukoc Biol 62:634-644.
Yoshimura T, Yuhki N, Moore SK, Appella E, Lerman MI, Leonard EJ (1989) Human monocyte chemoattractant protein-1 (MCP-1). Full-length cDNA cloning, expression in mitogen-stimulated blood mononuclear leukocytes, and sequence similarity to mouse competence gene JE. FEBS Lett 244:487-493.
Youakim A, Ahdieh M (1999) Interferon-gamma decreases barrier function in T84 cells by reducing ZO-1 levels and disrupting apical actin. Am J Physiol 276:G1279-1288.
Zeng HY, Zhu XA, Zhang C, Yang LP, Wu LM, Tso MO (2005) Identification of sequential events and factors associated with microglial activation, migration, and cytotoxicity in retinal degeneration in rd mice. Invest Ophthalmol Vis Sci 46:2992-2999.
Zhai H, Heppner FL, Tsirka SE (2011) Microglia/macrophages promote glioma progression. Glia 59:472-485.
Zhang Y, Ernst CA, Rollins BJ (1996) MCP-1: Structure/Activity Analysis. Methods 10:93-103.
Zhang Y, Rollins BJ (1995) A dominant negative inhibitor indicates that monocyte chemoattractant protein 1 functions as a dimer. Mol Cell Biol 15:4851-4855.
Zimmermann KW. 1923. Der feinere Bau der Blutkapillaren. Z Anat Entwicklungsgesch 68:29−109.